UNIVERSITE D'ABOMEY - CALAVI (UAC)

INSTITUT NATIONAL DE L'EAU

Registered under N°: ***1974-21/UAC/VR -AA/SA***

A DISSERTATION

Submitted

In partial fulfillment of the requirements for the degree of

DOCTOR of Philosophy (PhD) of the University of Abomey-Calavi (Benin Republic)

In the framework of the

Graduate Research Program on Climate Change and Water Resources (GRP-CCWR)

By

Abdou Boko BOUBACAR

Public defense on: 06/03/2020

======

INTEGRATED HYDROLOGICAL MODELLING OF CLIMATE CHANGE IMPACTS IN SEMI-ARID URBAN WATERSHED OF NIAMEY, NIGER

======

Supervisors:

Nicaise YALO, Full Professor, Université D'Abomey Calavi, Cotonou, Benin
Moussa KONATE Full Professor, Université Abdou Moumouni, Niamey, Niger

======

Reviewers:

Serigne FAYE, Full Professor Université Cheick Anta Diop, Sénégal
Masamaéya GNAZOU, Associate Professor, Université de Lomé, Togo
Julien G. ADOUNKPE, Associate Professor, Université d'Abomey Calavi, Benin

======

JURY

Mama DAOUDA, Full Professor, University of Abomey Calavi, Benin	President
Serigne FAYE, Full Professor, University Cheick Anta Diop, Senegal	Reviewer
Masamaéya D.T GNAZOU, Associate Professor, University of Lomé, Togo	Reviewer
Julien G. ADOUNKPE, Associate Professor, University of Abomey Calavi, Benin	Reviewer
Moussa BOUKARI, Full Professor, University of Abomey Calavi, Benin	Examiner
Nicaise YALO, Full Professor, University of Abomey Calavi, Benin	Supervisor
Moussa KONATE, Full Professor, Abdou Moumouni University, Niger	Co-Supervisor

Dedication

I would like to dedicate this P.hD work for all my family.

Special dedication to my Wonderful wife, Dr. Idi Souley Reyanatou who has fully supported me, and for her patience during my long absence abroad and during my extended fieldwork.

Acknowledgments

This PhD work is realized in the framework of the West African Science Service Center on Climate Change and Adapted Land use (WASCAL) and funded by the **German Ministry of Education and Research (BMBF) in collaboration with the Benin Ministry of High Education and Scientific Research** (MESRS).

This Ph.D. thesis represents three years of work achievement, and many people have provided support and helped me, I would like to gratefully thank them.

Special thanks to Pr Moussa Konaté and Pr Yalo Nicaise who supervised this work. Pr Moussa Konaté has been teaching me since my undergraduate and was available to accompan me in the fields. Thanks for all the advice and fieldwork experience gained from you. Dr. Yalo Nicaise was available for me every time and I have learned a lot from scientific discussions during these three years.

Special thanks to Pr Walter Illman and Pr Edward. A Sudicky for accepting me at the University of Waterloo as a visiting graduate student, and providing state of the art scientific guidance on integrated hydrological modeling and fractured aquifer modeling in collaboration with Aquanty where I met special people. Dr. Steve Berg, you have provided full support in using HydroGeoSphere, and given a chance and beleive on my potential. Steve Berg, special thanks for all you did, knowing you as a mentor was a great opportunity for me.

At Aquanty, many people supported me, Dr. Andre Erler, for interesting discussions on climate and hydrological modeling. Thanks to Dr. Hyoun-Tae Hwang, Dr. Alaba Boluwade, Dr. Omar Khader, Dr. Michael Callaghan, Dr. Steven Frey, Amanda Taylor, Diana Zhang, and Graham Stonebridge. Thanks for the helping hands provided in using HydroGeoSphere and processing complex binary data.

Pr Ousmane Seydou, at the University of Ottawa, thanks for the climate data and review of the modeling you provided.

At the University of Abomey Calavi, I would like to thank Pr Moussa Boukari, Dr. Julien Adounkpe and Pr. Emmanuel LAWIN for their help and support during this Ph.D. thesis. Mr. Salem Kore and Imelda Djagoun, thanks for the administrative support you have provided.

At Abdou Moumouni University, special thanks to Pr Ousmane Boureima, Dr. Yahaya Nazouma, Dr. Moussa Harouna, Dr. Soumaila Amadou, and all the teacher of the Departement of Geology.

At AGRHMET Regional center, Dr. Pigbigna Bazié and Dr. Abdou Ali have contributed a lot to this work through interesting discussions we have had. They have also provided logistics support at AGRHYMET, where I have performed my office work and research.

Special thanks to Pr Adamaou Rabani for all the support provided to me.

Dr. Albachir Seyou and Prof Keith Schimmel at College of Science & Technology North Carolina A&T State University, have provided mentorship and a thorough review of some chapters in this Thesis. Thanks for all.

Finally, I will address my sincere thanks to all the third bach students of WASCAL GRP Climate Change and Water Resource.

Abstract

The Niger River is the sole permanent surface water used for agriculture and drinking water supply for the area of Niamey, Niger, West Africa. Given that the water distribution network does not cover the entire populated area, and because of recurrent droughts, the River cannot cover the total water demand in the area. Groundwater is pumped through open wells and boreholes to provide water to more than 35% of 1.3 million of people of the city. Groundwater demand for drinking and agriculture purpose is increasing as a result of rapid population growth and urbanization. Simultaneously, episodes of extreme low flows have become more frequent due to increasing demand, sedimentation of the River bed, and increased variability in streamflow upstream of Niamey. The minimum environmental flow for Niamey, set to 55 m^3/s over 10 days, is therefore often not available. In this context, this study investigates ground water surface interactions and the whole hydrological system response under climate change. An equivalent porous medium approach was used to define a hydrogeological conceptual model to understand the hydrodynamic of the fractured aquifer system, and quantify the integrated interaction between this system and surface water resources as well as the climate change impacts. Combined used of hydrochemicals and isotopes have shown that the major source of both groundwater and surface water is provided by silicate weathering. The isotopes signals of water are exempt from strong evaporation influence, implying that groundwater recharge process is strongly dominated by rapid and localized infiltration. A large scale, high resolution fully-integrated hydrologic model was built and calibrated using HydroGeoSphere with a sequential approach of increasing levels of temporal resolution: 1) steady state average conditions; 2) dynamic equilibrium with repeating monthly normal forcing data; and 3) fully transient conditions. Simulations results show that exchange flux between groundwater and surface water are important processes in the basin. The basin average water balance highlights the importance of plant transpiration (58 % of total rainfall) over surface evaporation (8%), with groundwater recharge of up to 5% of total rainfall. Overland flow and infiltration account for 11% and 16 % of the total annual rainfall respectively, and groundwater discharge to the river is 2% of the total rainfall. Historical (1980-2005) and projected (2020-2050) climate scenario derived from the outputs of three regional climate models (RCM), under the RCP 4.5 scenario, were statistically downscaled using the multiscale quantile mapping bias correction method. The durations of the Minimum Environmental Flow (MEF) conditions, required to supply drinking and agriculture water were found to be very sensitive to changes in runoff resulting from climate changes. MEF occurrences and durations are likely to be greater for the first decade (2020-2030) of the mid-century, and then they will be reduced for the last two decades (2030-2050) of the mid-century period. All the three RCMs consistently project a rise in groundwater table of more than 10 meters in topographically high zones where the groundwater table is deep and an increase of 2 meters in the shallow groundwater table.

Keywords: Integrated model, Groundwater, surface water, climate change, impact

Synthèse de la thèse

Resumé

Le fleuve Niger représente l'unique source d'eau de surface permanente utilisée pour l'alimentation en eau des populations, et pour l'agriculture dans la région de Niamey, située à l'ouest du Niger. Cependant, le réseau actuel de distribution de l'eau potable ne couvre pas le besoin en eau de consommation de la population, principalement concentrée dans la ville de Niamey. Ainsi, l'eau souterraine des aquifères sédimentaires et de socle est mobilisée à travers des puits traditionnels et des forages pour couvrir le besoin en eau de plus de 35% de de la population de la vile de Niamey estimée à 1.5 million de personnes. Les eaux souterraines sont donc de plus en plus sollicitées pour couvrir les besoin en eau de consommation et l'irrigation. Les étiages sévères du fleuve sont de plus en plus récurrents du fait de la demande en eau croissante, de l'urbanisation rapide, de la variabilité accrue des écoulements et de l'ensablement du lit du fleuve Niger. Ainsi, le débit sécuritaire du fleuve à Niamey fixé à 55 m3/s pour dix (10) jours consécutifs, n'est souvent pas satisfait. La présente étude s'inscrit dans ce contexte afin de caractériser les interactions entre les eaux de surface et les eaux souterraines, ainsi que d'évaluer la réponse intégrée du système hydrologique global face aux changements et à la variabilité climatiques. Ainsi, l'approche de milieu poreux équivalent a été utilisée pour définir un modèle conceptuel hydrogéologique. Les investigations hydrochimiques et isotopiques ont montré que l'altération des minéraux silicatés représente la source principale de minéralisation des eaux de surface et des eaux souterraines. Aussi, l'évaporation n'a pas une influence significative sur le signal isotopique des eaux mettant en évidence un processus de recharge dominé par l'infiltration rapide et localisée. Le modèle hydrologique intégré HydroGeoSphere, a été calibré à très haute résolution en régime permanent, semi-permanent et transitoire. Les résultats ont montré l'existence d'échanges de flux entre les eaux de surface et les eaux souterraines. Ainsi, le fleuve Niger est principalement drainant sur les aquifères, avec des tronçons perdants, localisés le long des failles. Les cours d'eau temporaires, ou Koris se comportent comme des zones favorables à la recharge localisée des nappes. Les mares quant à elles fonctionnent soit en zone de recharge, soit par évaporation, c'est-à-dire en zone de décharge des nappes. Le bilan hydrologique calculé a montré l'importance de la transpiration des plantes par rapport aux autres composantes du cycle hydrologique. Le bilan hydrologique moyen calculé entre 2013 et 2017 se présente comme suit : Sur une pluie moyenne de 580 mm/an, la transpiration réelle des plantes représente 58%, l'évaporation de surface est de 8%, la recharge des nappes est de 5%. Les écoulements de surface et l'infiltration représentent respectivement 11% et 16%, alors que la décharge des eaux souterraine représente moins de 2%. Les sorties des modèles climatiques sur les périodes historique (1980-2005), et future (2020-2050), ont été extraites à partir des trois (3) modèles climatiques régionaux de résolution spatiale variant entre 50 km et 12 km sous le scenario RCP.4.5. Les simulations ont montré que le débit sécuritaire du fleuve Niger à Niamey, est très sensible aux réductions de ruissèlement dues aux changements climatiques. Ainsi, les stresses hydriques liés au débit sécuritaire du fleuve seront de plus en plus longs, surtout pour la décade 2020-2030. La réponse du niveau de la nappe phréatique face aux changements climatiques, est surtout dictée par la topographie. Ainsi, le niveau de la nappe phréatique connaitra une augmentation allant jusqu'à 10 mètres sur les zones topographiquement élevées, alors que dans les vallées et les zones basses, cette augmentation serait de 2 m.

Mots Clés : Modèle hydrologique intégré, eaux souterraines, eaux de surface, impacts, Changements Climatiques.

Introduction

La région de Niamey tire une importante partie de ses besoins en eau à partir des eaux traitées du fleuve Niger, qui correspond au seul cours d'eau permanent du bassin. Les principaux affluents du fleuve Niger, dans la région de Niamey sont des cours d'eau temporaires, appelés koris. Les nappes du Continental Terminal, et les aquifères fracturés du socle, couvrent une partie importante (plus de 35%) des besoins en eau de la population de Niamey.

La demande en eau souterraine pour répondre aux besoins en eau potable et pour l'irrigation augmente en raison de la croissance démographique et de l'urbanisation rapide. Ceci est encore exacerbé pendant les conditions d'étiage du fleuve Niger où un débit sécuritaire fixé à 55 m3 /s est nécessaire pour assurer les besoins en eau des populations. Pendant ces périodes d'étiage, ce débit sécuritaire n'est souvent pas disponible et les eaux souterraines deviennent la principale source d'eau. Cependant, d'autres contraintes sur l'approvisionnement en eau comprennent une croissance démographique rapide (doublant tous les vingt-cinq ans), la sédimentation du lit du fleuve et une variabilité accrue du débit du fleuve Niger en amont de Niamey.

Par conséquent, le débit sécuritaire du fleuve à Niamey, fixé à 55 m3/s sur une période de dix (10) jours, n'est souvent pas satisfait. Les autorités du Niger craignent que les ressources en eaux souterraines ne deviennent insuffisantes et /ou que les étiages deviennent sévères et fréquents à l'avenir, en raison des changements climatiques et de la demande en eau croissante. Ainsi, une étude qui caractérisera le comportement de l'ensemble du système hydrologique dans la zone en contexte des changements climatiques est importante. La présente étude s'inscrit ainsi dans ce contexte, et son objectif principal est de caractériser les interactions entre les eaux de surface et les eaux souterraines, ainsi que d'évaluer la réponse intégrée du système hydrologique global face aux changements et à la variabilité climatiques.

Zone d'étude

La zone d'étude est un sous-bassin versant du Niger Moyen, avec une superficie de 1 900 km² située au sud-ouest de la République du Niger.

C'est un bassin versant semi-urbain avec une population de 1,3 millions. Les régimes pluviométriques sont caractéristiques du climat semi-aride avec une saison sèche d'octobre à mai, et une saison pluvieuse de juin à septembre. Les précipitations sont dominées par des événements pluvieux intenses à faible fréquence. Les précipitations annuelles moyennes de 1947 à 2007 sont de 560 mm et l'évapotranspiration potentielle annuelle moyenne de Penman Monteith est de 2500 mm avec une température moyenne de 29 ° C. Des cartes récentes d'utilisation et d'occupation des sols (CILSS, 2016) indiquent que les terres agricoles couvrent 11% du bassin versant, la végétation naturelle sous forme de savane sahélienne et de steppe couvre 32%, et le sol nu et sablonneux couvrent 45% du bassin versant. La ville principale et les villages environnants occupent environ 8%, et les plans d'eau couvrent 4%.

Les principales conditions hydrogéologiques de la zone d'étude, sont liées aux conditions géologiques. Ainsi, deux principaux types d'aquifères caractérisent la zone d'étude : il s'agit des aquifères fracturés du socle birrimien du Liptako Gourma, et de l'aquifère sédimentaire du Continental Terminal 3 (CT3). Les aquifères du socle sont constitués principalement des formations birrimiennes des roches vertes, des formations de granitoïdes et de formations des zones altérées.

Matériels et méthodes

Matériels

Les principaux matériels utilisés dans le cadre de cette étude sont :

Le GPS (système de positionnement Global) pour les coordonnées géographiques des affleurements et des points d'eau, les bouteilles en plastique et en verre et les bouteilles ambrées, avec des conteneurs pour la collecte et la manipulation des échantillons d'eau. Les tarières manuelles ont aussi été utilisées pour la réalisation des micropiezometers.

Les principaux logiciels utilisés dans le cadre de cette étude sont :

- Les logiciels de cartographie ARCGIS et QGIS ;
- Rockworks et Daisy pour la modélisation géologique et structurale ;
- Python et R pour l'analyse des données climatiques et hydrologiques ;
- HydroGeoSphere pour la modélisation hydrologique intégrée.

Méthodes

Pour atteindre les objectifs de cette étude, une approche méthodologique multidisciplinaire a été utilisée. Cette approche intègre les investigations de terrain pour caractériser les conditions géologiques et hydrogéologiques, l'approche hydrochimique et isotopique pour la qualité des eaux, ainsi que la modélisation hydrologique intégrée.

Pour la caractérisation des conditions géologiques et hydrogéologiques, 120 coupes de forages ont été interpolées pour créer des cartes de surface 2D à partir desquelles les couches du modèle géologique 3D ont été construites. L'interpolation a été réalisée à l'aide de la méthode de la pondération de la distance inverse (IDW). Les mesures de directions et de pendages des fractures, ont été combinées à la cartographie structurale pour modéliser le système de fractures.

Une analyse statistique séquentielle combinant l'Analyse Hiérarchique Classifiée, l'Analyse en Composante Principale et les rapports ioniques, a été appliquée aux données géochimiques et isotopiques des eaux de surface et souterraines pour déterminer les sources de minéralisations des ions ainsi que les principaux processus de recharge des nappes.

Le modèle hydrologique intégré, utilisé dans le cadre de cette étude, est HydroGeoSphere. C'est un modèle physiquement basé, à éléments finis qui résout de façon simultanée les équations d'écoulements en surface 2D de Saint Venant, et les équations d'écoulements souterrains 3D de Richard. Il intègre le calcul interne de l'évapotranspiration réelle en fonction de types et d'occupation de sols.

Ce modèle intégré, HydroGeoSphere a été appliqué à très haute résolution sur la zone d'étude qui a une superficie de 1900 Km². La résolution horizontale est de 300 mètres en général, et 70 mètres à proximité des cours d'eau.

Ainsi, la zone d'étude a été discrétisée en éléments de maille triangulaire, avec un total de 927,030 éléments triangulaires de maille, et 516,901 nœuds de calculs. Les principales conditions aux limites appliquées au model sont :

- Les conditions de non-écoulements (No flow) aux limites externes du model où les lignes de parte des eaux souterraines sont considérés comme des lignes de limites du bassin modélisé ;
- Les conditions aux limites appliquées à la surface du model sont : La pluie, l'évapotranspiration potentielle, la condition de débit imposé, et la condition de profondeur critique.

La calibration du modèle a été effectuée en trois principales étapes séquentielles avec des résolutions temporelles croissantes : 1) régime permanent, 2) régime semi-transitoire ou d'équilibre dynamique, 3) régime transitoire.

Les sorties des modèles climatiques sur les périodes historique (1980-2005), et future (2020-2050), ont été extraites à partir des trois (3) modèles climatiques régionaux de résolution spatiale variant entre 50 Km et 12 Km sous le scenario RCP.4.5. Ces modèles climatiques régionaux ont ensuite été statistiquement mis à l'échelle, en utilisant une méthode de correction de biais multi temporelle, c'est-à-dire à l'échelle journalière, mensuelle et annuelle. La validation des données climatiques simulées en période historique et future, a été faite à partir des données climatiques et hydrologiques observées, en période historique. Les données hydrologiques utilisées sont : les données journalières du débit du fleuve, et les niveaux piézométriques mesurés. Les données climatiques historiques observées sont : la pluie, les températures minimales et maximales, à la station de Niamey Aéroport.

Résultats et discussions

L'étude structurale conduite à partir des mesures de fractures sur les affleurements des granitoïdes et des roches vertes de la zone d'étude, complétée avec la cartographie de l'intensité de fracturation a permis d'identifier les familles de fractures suivantes en termes des caractéristiques directionnelles :

- Les familles des fractures F1 qui ont des directions comprises entre N140 °et N150° (**NW-SE**) ;
- Les familles des fractures F2 avec des directions comprises entre N100° to N110° ;
- Les familles des fractures F3 correspondant aux directions entre N60° to N70° (**NE-SW**).

La direction caractéristique **NW-SE** correspond à la direction structurale majeure des formations birrimiennes, et est également la direction majeure d'écoulement du fleuve Niger dans la région. La direction NE-SW a été décrite comme la direction majeure des foliations dans les formations birrimiennes.

Aussi, la densité de fracturation modélisée dans ces formations varie de 0 à 163 segments de fractures par kilomètre carrée. La complexité et l'interconnexion des systèmes de fractures, ainsi que le manque de données sur les fractures individuelles, imposent de définir un model conceptuel simplifié.

C'est dans ce sens qu'un model hydrogéologique conceptuel, utilisant l'approche de milieu équivalent poreux a été défini. Ce modèle conceptuel a permis de représenter le système des aquifères fracturés, de caractériser les interactions entre les eaux de surface et les eaux souterraines ainsi que d'évaluer la réponse intégrée du système hydrologique face aux changements et à la variabilité climatiques.

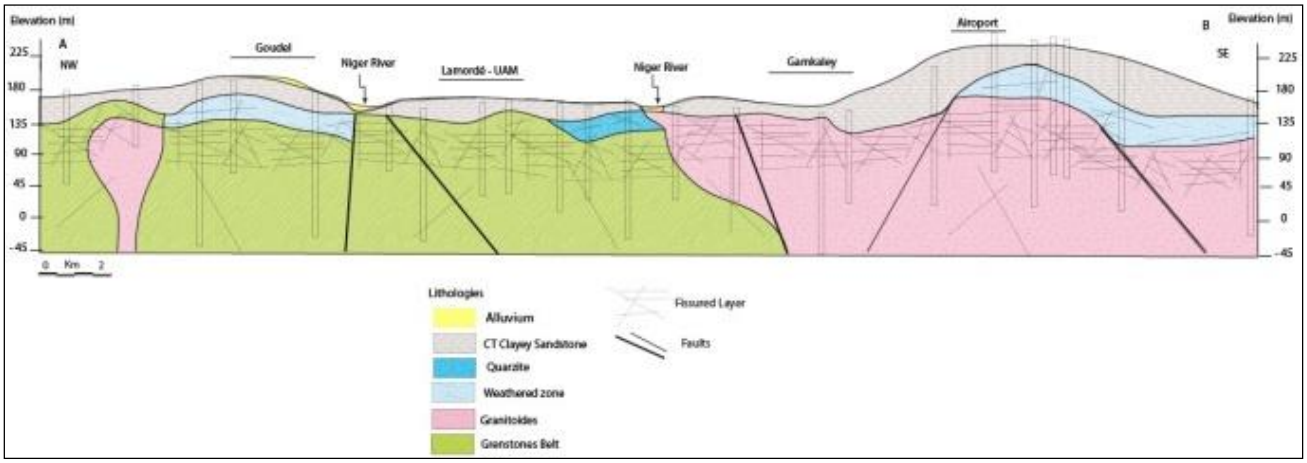

Modèle géologique et hydrogéologique conceptuel

L'investigation hydrochimique et isotopique a montré que le faciès géochimique principal des eaux de surface et des eaux souterraines est de type Na-Ca-HCO3. La source majeure de minéralisation identifiée est l'altération des silicates avec des échanges de cations libérant préférentiellement les ions Na+ lors du processus d'altération. La signature isotopique des eaux n'a pas montré une influence importante du processus d'évaporation. Ce qui a permis de mettre en évidence un processus de recharge par infiltration rapide et localisée.

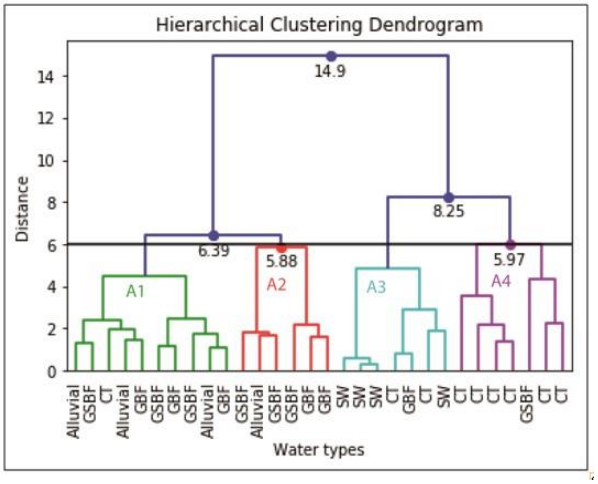

Analyse Hiérarchique Classifiée des données hydrochimiques

La calibration du modèle hydrologique a été effectué en trois étapes séquentielles avec des résolutions temporelles croissantes : 1) régime permanent, 2) régime semi-transitoire ou d'équilibre dynamique, 3) régime transitoire. Ce qui a permis de mettre en évidence une méthode facile et efficace de calibration d'un model hydrologique intégré à grande échelle, et surtout en contexte climatique aride. Les résultats de simulations ont ainsi permis de calculer les échanges de flux entre les eaux de surface et les eaux souterraines, le bilan hydrologique par types d'occupation de sols, et la recharge moyenne à l'échelle de la zone d'étude. Ainsi, le fleuve Niger est principalement drainant sur les aquifères, avec des tronçons perdants, localisés le long des failles. Les cours d'eau temporaires, ou Koris fonctionnent comme des zones favorables à la recharge localisée des nappes. Les mares quant à elles fonctionnent soit en zone de recharge, soit par évaporation, c'est-à-dire en zone de décharge des nappes. Le bilan hydrologique calculé a mis en évidence l'importance de la transpiration des plantes par rapport aux autres composantes du cycle hydrologique. Le bilan hydrologique moyen calculé entre 2013 et 2017 se présente comme suit : Sur une pluie moyenne de 580 mm/an, la transpiration réelle des plantes représente 58%, l'évaporation de surface est de 8%, la recharge des nappes est de 5%. Les écoulements de surface et l'infiltration repensent respectivement 11% et 16%, alors que la décharge des eaux souterraine représente moins de 2%.

Les résultats de mise à l'échelle statistique des modèles climatiques régionaux montrent que la correction des biais au pas de temps journalier et mensuel, est plus optimale que la correction au pas de temps annuel. Aussi, les résolutions spatiales des modèles climatiques régionaux n'ont pas amélioré de façon significative les performances des modèles. Les projections des modèles climatiques régionaux montrent une augmentation pluviométrique moyenne annuelle de 1.6 % d'ici 2050, comparée à la période historique 1980-2005. Les températures moyennes annuelles augmenteront également de 1.58°C d'ici 2050, par rapport à la période historique 1980-2005.

Les simulations des projections climatiques ont montré que le débit sécuritaire du fleuve Niger à Niamey est très sensible aux réductions de ruissèlement dues aux changements climatiques. Ainsi, le stress hydrique lié au débit sécuritaire du fleuve sera de plus en plus long, surtout pour la décade 2020-2030. La durée du stress hydrique va ensuite décroitre durant la période statistique 2030- 2050. La réponse du niveau de la nappe phréatique face aux changements climatiques, est surtout modulée par la topographie. Par conséquent, le niveau de la nappe phréatique pourra connaitre une augmentation allant jusqu'à 10 mètres sur les zones

topographiquement élevées, alors que dans les vallées et les zones basses, cette augmentation serait de 2 mètres.

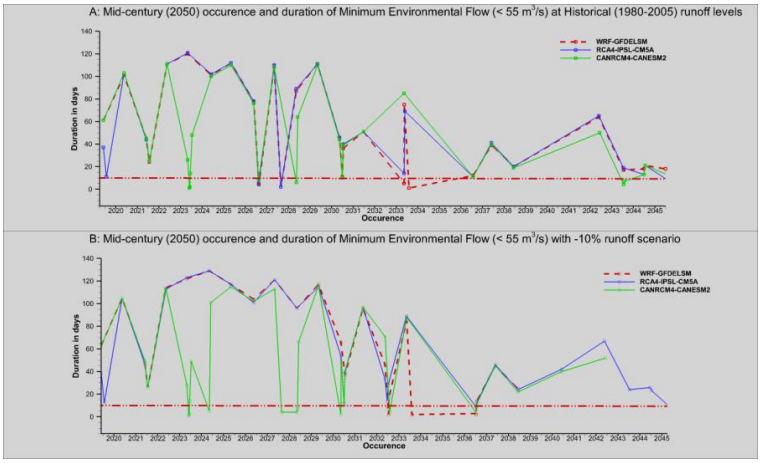

Fréquence et durée d'occurrence du débit environnemental minimum du fleuve Niger entre 2020 et 2050

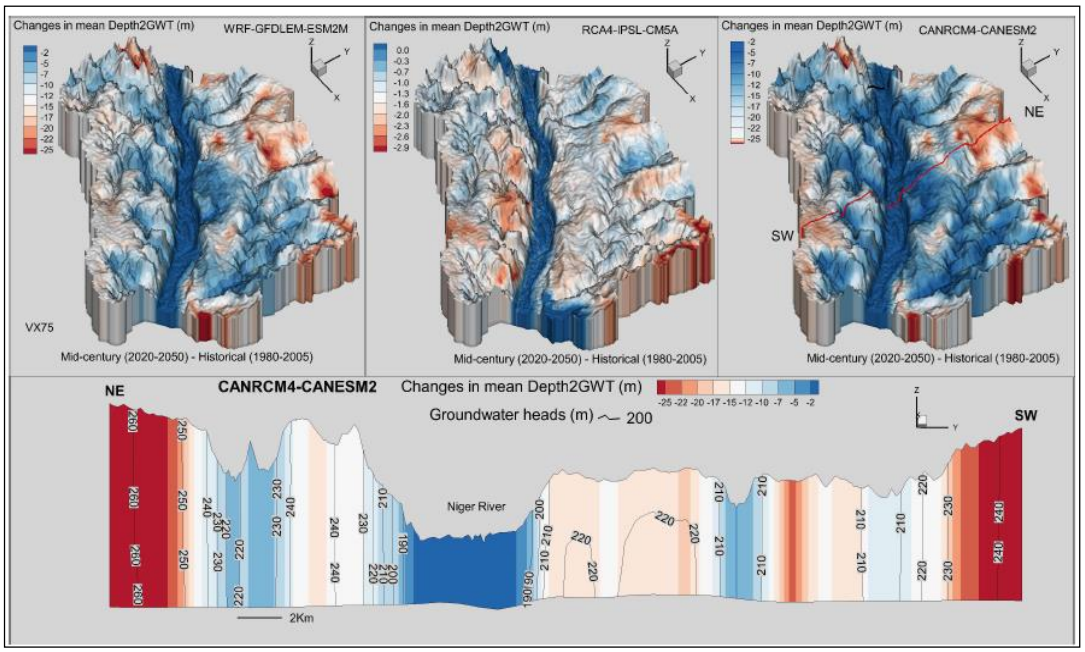

Changements projetés du niveau statique de la nappe entre 2020 et 2050.

Conclusion

A partir des projections climatiques pour l'horizon 2050, faites sur la réponse des eaux de surface aux impacts des changements climatiques, le bassin versant de Niamey en général et la ville en particulier connaîtront des périodes récurrentes et longues où le débit sécuritaire du fleuve ne sera pas satisfait. Le niveau de risque est même plus élevé lorsque le scénario de

réduction du ruissellement de -10% par rapport à la période historique (1980-2005) est envisagé. Cependant, le signal des projections climatiques entre 2020-2050 est plus humide pour les trois modèles climatiques régionaux utilisés, ce qui signifie que la réduction du niveau de ruissellement est moins probable. Mais une augmentation de la demande en eau d'irrigation pendant la période sèche en amont de Niamey créera probablement un risque de stress hydrique élevé si la construction en cours du barrage de Kandadji, censé maintenir le débit sécuritaire n'est pas terminée.

D’autre part, une augmentation du niveau de la nappe phréatique à l'échelle du bassin est prévue, avec une augmentation plus importante à proximité des niveaux statiques profonds et une augmentation relativement plus faible aux niveaux statiques superficiels. Par conséquent, compte tenu de la croissance démographique et du taux d'urbanisation, les eaux souterraines représentent une stratégie d'adaptation durable, pour soutenir le stress hydrique récurrent qui sera induit par la haute sensibilité du débit du fleuve Niger aux impacts des changements climatiques.

Table of Contents

List of Acronyms

AGRHYMET : Centre Régional en AGRiculture, et HYdro METéorologie

CILSS : Comité Permanent Inter Etat de lutte contre la Sécheresse dans le Sahel

DRH/A N : Direction Régionale de l'Hydraulique et de l'Assainissement Niamey

GCM: Global Climate Model

HGS: HydroGeoSphere

IAEA: International Atomic Energy Association

MEF: Minimum Environmental Flow

NBA: Niger Basin Authority

RCM: Regional Climate Model

WASCAL: West African Science Service on Climate Change and Adapted Land Use

List of figures

List of Tables

Chapter 1: General Introduction

This chapter provides the general context and problematic of the study. It also presents the literature review, the objectives of the thesis, research questions and hypothesis as well as the expected results. The originality and scope of this thesis were also discussed in this chapter. Finally, the outline and organization of the thesis document are presented.

1.1.Context and problem statement

Understanding the Climate change impacts on water resources and the hydrological extremes remains a central issue for sustainable water resources management. The impacts are likely to alter the hydrological cycle with negative effects on the availability and quality of water resources (UNFCCC, 2009). Changes in temperature and precipitation, combined with changes in the frequency and intensity of extreme hydro meteorological events, will have important implications for water resources, this will affect the supply, quality and distribution of resources water for billions of people (Kundzewicz and al., 2007).

However, the effects of climate change will not be distributed evenly between sectors, regions, communities, households and individuals. And some are likely to be particularly vulnerable to changes in the global water system.

Even though large uncertainties remain in models capable of simulating the impact of climate change on water resources (Kundzewicz et al 2018; Shen et al., 2017; Clark et al., 2016; Goderniaux et al.,2015; Refsgaard et al., 2016; Moeck et al., 2016; Kurylyk and MacQuarrie, 2013; Stoll et al., 2011; Bastola et al., 2011; van Roosmalen et al., 2009) , the Africa water resources sectors are among the most vulnerable to the effects of climate change (Bates et al., 2008), with particularly large uncertainties regarding climate change impacts on groundwater resources (Taylor et al., 2009).

While most arid region rely on groundwater for agriculture and drinking water supply purpose (MacDonald, et al.,2012), few attention have been given to climate change impacts on groundwater in Africa (Nkhonjera and Dinka, 2017; Touré et al.,2016; Taylor et al.,2009; Nyenje and Batelaan, 2009).

Consequently, semi-arid regions of developing countries, which are already facing serious problems in the management of water resources and food security, and likely to be severely affected by climate change impacts (Nkhonjera and Dinka, 2017; Taylor et al., 2009), need to be provided with scientifically based water resources management policy. Therefore, one of the most prone climate resilience regarding to water resources is toward an integrated water resources management to respond to increasing demand due to demographic growth and climate change and variability pressure on water resources.

The Niger River is the sole permanent surface water used for agriculture and drinking water supply of Niamey city, in the middle Niger River basin (Figure 1). However, due to insufficient water distribution network infrastructure, and recurrent drought, the River could not cover the total demand of water of the city, and groundwater is used through open wells and boreholes to provide water to more 35% (Niger PRSP 2008) of 1.3 million (INS 2012) of people of the city. The importance of the groundwater demand to supply drinking and agriculture purpose is increasing due to rapid population growth and urbanization of the city more intense low flow conditions of the river due partly to increasing demand, and sedimentation of the River bed, leading to low yield, when the minimum environmental flow conditions (55 m^3/s) may not be satisfied for a period of more than ten successive days.

Therefore, for resilient water resources management in the context of increasing demand (irrigation and livestock, demography), along with variability and climate change, characterization of the interactions between the Niger River drainage system, and underlying aquifers is necessary. Furthermore, understanding and quantifying the interactions between the river drainage system and aquifers is very important for alleviating the impact of recurrent extreme events as it can provide valuable guidance for water resources management policies in the region. For instance, determining flux exchange direction and magnitude between the river and underlying aquifers can help support minimum environmental flows of the river or buffer flood events (loosing river). The groundwater table may also act as a flood amplifier in case the river or part of its reach is gaining. Characterization of this type of groundwater surface water interactions is very complex in general, and particularly challenging in data scarce and semi-arid watersheds. Also, with the current level of population growth rate, where the population doubles every twenty-five years, and high climate variability in the region, water resources managers need to be provided with information on potential climate change impacts on groundwater as well as the minimum environmental flow conditions.

1.2. Literature review

In this section, a brief overview of climate change modelling methods will first be provided. In the second section, a more detailed literature review on the integrated hydrological modeling of climate change impacts will be discussed as it represents the focused on this research study.

1.2.1 Climate Change modelling

Global Circulations Models (GCMs) represent the typical tool widely used to simulate and derive climate variables. They are also employed to perform projections of anthropogenic climate change, as described in the 5th Assessment Report issued by the Intergovernmental Panel on Climate Change (IPCC, 2013b). GCMs are complex numerical models that solve atmospheric mass conservation lows, momentum equations for a spherical earth, total energy and water vapors lows to simulate global climate in three dimensional spaces (Waner, 2011). A GCM usually results from a combination between an Atmospheric General Circulation Model (AGCM) and an Oceanic Circulation models. GCMs are therefore used to generate climate change scenarios based on the increase of various range of variables including greenhouse gases emissions and Land Use changes. Also, recent advancements in computational resources have facilitated the coupling of atmospheric and hydrological models in impacts studies (Gilbert et al., 2017; Davison et al, 2018; Kueppers and Snyder, 2012). The GCMs and coupled atmospheric –hydrologic models are computationally expensive.

Also, GCMs generally performed climate simulations at relatively coarse scale, compared to hydrological models, and therefore inadequate in impacts studies (Laprise et al., 2008). In order to overcome these drawbacks in impacts studies, GCMs are typically bias corrected and downscaled.

1.2.1.1 Downscaling techniques

GCMs downscaling is performed either statistically (statistical downscaling) or by using physics-based, dynamical models (Dynamical downscaling).

Dynamical downscaling involves the use of physics-based, Regional Climate Models (RCMs) with relatively higher resolution than the forcing GCM. The boundary conditions of RCMs are derived from GCMs, and therefore RCMs provide more added values, and their simulations are typically performed at 0.5° spatial resolution (Fowler et al, 2007; Giorgi, 2007; Maraun et al., 2010; Teutschbein & Seibert, 2012).

Additionally, to their increased resolution compared to GCMs, RCMs are also able to incorporate specifics regional geographical features such as topography, major water bodies (lake), vegetation covers (Erler et al.,2019; Peltier et al.,2018; Heinzeller et al ,2017; Browne and Sylla 2012). These geographical features are sometimes critical in reproducing the accurate climate seasonality.

Although less expensive than GCMs, the RCMs still have important computational cost and their performance still very dependant to the driving GCMs performance. Statistical downscaling is therefore usually used in hydrological climate change impacts studies.

Statistical downscaling is basically performed using linear or nonlinear statistical/empirical relationships to estimate small-scale local processes based on features of the large-scale climate (Dixon et al., 2016; Waner, 2011). These relationships are mapped into functions that convert the simulated climate outputs into corrected time series which's statistical properties are closer to that of the local observed climate data. The calibration of the mapping function is usually done for the historical or control period, where observed data are available. The calibrated mapping function is then applied on the predictions period to obtain climate change projections. There are various mathematical formulations used for statistical downscaling. These methods range from simple linear approaches based upon regression models to more complex nonlinear approaches that are based on weather typing schemes and weather generators (Fowler, et 2007; Waner, 2011).

While the statistical downscaling methods are relatively easy to use, and computationally less expensive, their major drawback resides in the assumption of temporal stationarity in the empirical relations. Therefore, a mapping function that is trained with current-climate data, at particular temporal resolution may not apply for future climate. The commonly used statistical

bias correction methods in hydrological climate impact studies assume the mapping function to be valid at all temporal resolutions. This it may introduce errors in impacts studies. A recent statistical bias correction method (Hanel et al (2017), involves training iteratively the mapping function at multiple temporal resolutions (daily, monthly, yearly, and 30 years average). The multiscale bias correction methods may provide an alternative solution to the stationarity assumption and reduce errors in hydrological impacts studies that are performed under several greenhouse gas emissions scenarios.

1.2.2 Hydrological modelling

Scientific literature about climate change-related hydrological impacts is considerable, and approaches used ranged from very simplisistc lumped hydrological models to physics-based, fully integrated, surface-subsurface hydrological models. An extensive inventory of the research studies on hydrological impacts of climate change is beyond the following scientific review. Herein we only focused on studies that were performed on climate change impacts on groundwater, as well as on integrated hydrological responses to anthropogenic climate changes impacts.

Because surface water is generally considered more vulnerable to climate change compared to groundwater (Nkhonjera and Dinka, 2017; Armandine Les Landes et al., 2014; Holman et al., 2012: Taylor et al., 2009; Goderniaux et al., 2009; Green et al., 2011) most of the studies have been focused on climate change impacts on surface water, neglecting often groundwater. Moreover, only few (Erler et al., 2019; Goderniaux et al. 2011; Sulis et al., 2012) considered physics-based, fully large scale integrated hydrological modeling when investigating climate change impacts on water resources.

As groundwater recharge represents the most important variable linking directly the surface-subsurface hydrological process to the atmosphere, it represents the most investigated variable in studies on climate change impact on groundwater (Goderniaux et al., 2009). Previous studies on groundwater recharge response to climate change impacts have produced variables results, depending on modelling approaches, climatic conditions, climate change scenarios, and geographic locations (Chen et al., 2019 ; Goderniaux, 2010, Erler et al., 2019; Sulis et al., 2012,

Döll and Feidler., 2008, Touré et al.,2016; Mileham et al., 2009; Colautti, 2010 ; Crosbie et al., 2013 ; Meixner et al.,2016 ; Scibek and Allen, 2006 ; Van Roosmalen et al., 2009 ; Chen et al., 2004).

Chen et al., (2004) employed linear functions-based water balance model to investigate climate change impacts on a carbonate rock aquifer in Manitoba (Canada). In their assumptions, groundwater heads variations could be linearly linked to hydroclimate forcing variables (precipitations, temperatures), and therefore groundwater heads predictions could be performed.

Scibek and Allen, (2006) performed spatially groundwater recharge calculations using HELP model, and then input calculated recharge to the three-dimensional MODFLOW model to investigate climate change impacts on groundwater recharge for the 'Grand Forks' alluvial aquifer located in British Colombia, Canada. Based on four climate change scenarios, they have shown that groundwater response to climate change is more sensitive to spatial variation compared to temporal variations. Using a similar modelling approach, Touré et al., (2016), investigated groundwater recharge response to climate change impacts on Klela Basin, Mali, using a single RCP 4.5 climate scenario. For the mid-century scenario (2010-2050), they have predicted a general groundwater levels decrease of up to 18 meters.

Döll et al., (2008), estimated potential groundwater recharge to decrease by 70% in northeast Brazil, southwest Africa and in the southern rim of the Mediterranean Sea; and to increase by more than 30% in the Sahel, Middle East, northern China, Siberia and the western United States. These predictions are made based on global scale modelling approach, using two climate models, under the A2 and B2 climate change scenario for the mid-century period.

Mileham et al., (2009), used a soil-moisture balance model to project a 53% decrease of groundwater recharge under the A2 emissions scenario. The method used also highlights the importance of the uncertainties source related to the failure of considering daily rainfall distributions changes in downscaling climate models. To overcome this precipitation intensification drawback, Crosbie et al., (2013), estimated episodic groundwater recharge using three global warming scenarios from 15 different global climate models (GCMs) for a 2030 period, with the coefficient of variation at yearly time scale, and the proportion of recharge in the highest 1% of daily recharge, at daily time scale. The two precipitation intensity metrics

have not shown a clear trend in a potential decrease or increase of episodic groundwater recharge.

Meixner et al., (2016), investigated climate change impacts on groundwater recharge using a differential approach in how climate change will affect different type of recharge process and amounts over the Western part of the USA. A synthesis of model-based studies of projected climate change impacts on recharge was combined with a qualitative relationship linking groundwater recharge and hydroclimate forcing data, to show a strong spatial variation of the groundwater recharge response to climate change impacts, with large uncertainties.

A MIKE-SHE based, coupled surface-subsurface model was used by Van Roosmalen et al., (2009) to evaluate climate change and land use change on both groundwater and surface water over a large-scale watershed in Denmark. The model used simulates simultaneously surface and subsurface flow equations, and allow taking into consideration exchange flux between surface and subsurface flow domains.

However, most of previous studies, always employed very simplest saturated groundwater flow models, or loosely coupled surface water –groundwater models to investigate climate change impacts on groundwater. They also often use the traditional approach of statistically bias corrected regional climate projections output as climate forcing data. While these approaches still useful in providing groundwater management decision helping information, they are problematic in arid and semi-arid environments. Because, the most important parameter in the hydrological cycle connecting directly groundwater to the atmosphere, is aquifer recharge, and is provided as model input data. Two main issues can easily be highlighted in using saturated groundwater flow models in climate change impacts studies in arid environments. Groundwater recharge process is dominated in arid environment by localized recharge, through surface water features (Desconnets et al.1997; Leduc et al. 1997; Favreau, 2000; Favreau et al. 2012) and is difficult to be represented adequately in saturated groundwater flow models where groundwater recharge is considered as an input parameter to these models. Then, this creates directly a linear relationship between groundwater recharge, and climate forcing data, with derived evapotranspiration creating large biases from statistically downscaled regional climate projections. It has been shown, that in most climate change impacts studies on water resources, evapotranspiration biases may be important (Milly and Krista, 2017) and often determine the direction of climate change impacts on water resources.

Therefore, to reduce large biases induced by the simplest formulation of groundwater recharge in saturated groundwater models, a recent approach, consist of looking at climate change impacts on groundwater by using integrated model capable of calculating internally actual evapotranspiration and able to integrate different recharge processes (focused recharge, direct recharge, GW-SW), considering land use types (Chen et al., 2019 ; Goderniaux., 2010, Erler et al., 2019; Sulis et al., 2012; Colautti, 2010).

In the fully integrated hydrological models, groundwater recharge is not anymore, an input data, but a part of solution provided by the model. Here, there is no systematic linear relationship between groundwater recharge and climate forcing data, and evapotranspiration is computed internally and spatially, considering different land use, surface water features.

Colautti, (2010), assessed integrated hydrological impacts of climate change over the Grand River Watershed, (Canada), using five different climate change scenarios to force the integrated, physics-based HydroGeoSphere model (HGS). Steady-state simulations were performed, to shown a general decrease in both surface water flow rate and groundwater table. Goderniaux, (2010), employed also the HGS model, to evaluate climate change impacts on a chalky aquifer, within the Geer catchment, of 480 Km^2 surface areas located in Belgium. Quantile mapping bias correction and sophisticated stochastic weather generator were used to derive climate change scenario from six regional climate models under the SRES A2 emission scenario, and then to force daily and monthly transients HGS simulations. Surface water flow rate and groundwater heads were predicted to decrease by the end of the century (2100) period. Also, in this study, advance statistical methods were used to evaluate uncertainties related to climate change impacts on groundwater.

Sulis et al., (2012), evaluated climate change impacts on groundwater –surface water interactions using fully integrated CATHY hydrological model over the 690 km^2 surface area Des Anglais watershed, Quebec, Canada. Transients simulations were performed on the coupled hydrological model under the SREAS A2 scenario, to show a decrease in the summer river discharge. Groundwater table response to climate change was found to be spatially variable, with greater change observed at higher altitudes.

Erler et al., (2019) used dynamically downscaled high-resolution regional climate model (WRF) projections and the fully-integrated 3D hydrologic model (HGS), to investigate climate change impacts on both groundwater and surface water in the Grand River Watershed,

(Canada). The HGS model was run using a representative seasonal cycle with average monthly seasonal cycle, based on climate forcing data from an ensemble of the Weather Research and Forecasting (WRF) dynamically downscaled at different spatial resolutions. Hydrological responses to climate change have been shown not to be very sensitive to the resolution of the climate model, and groundwater table response was also found to be strongly affected by local topography.

1.3 Research Questions

Research questions that guide this study are as follow:

1. Does an Equivalent Porous Medium approach represent an effective representation of the fractured aquifer unit in the integrated model?
2. Does the surface water system constitute alternative or complementary water resources to the aquifer to supply water demand, amplifier or buffer flood issues?
3. Do the water balance components present different characteristics and magnitude for different land use type?
4. How climate change will affect both the groundwater table and minimum environmental flow conditions of the Niger River?

1.4 Thesis objectives

1.4.1 Main objective

The main objective of this study is to evaluate the integrated hydrological response of groundwater and surface water under current and future climate change conditions, in the semi-arid urban watershed of Niamey, Niger.

1.4.2 Specific objective

This study specifically aimed to:

(1) Define a conceptual model for hydrogeological characterization of groundwater surface water interaction, in complex fractured aquifer context;

(2) Determine the magnitude and direction of the exchange of water between the surface water system and complex groundwater aquifer systems;

(3) Provide practical information to water managers on the water balance components considering different land use types, groundwater systems, as well as surface water bodies.

(4) Evaluate the potential climate change impacts on groundwater resources, and the frequency and duration of the minimum environmental conditions.

1.5 Hypothesis

From the above stated research questions, the following hypotheses were drawn;

1. An equivalent porous medium (EPM) approach is considered to represent the fractured aquifer unit in the integrated model;

2. Daily transient simulations are supposed to carry sufficient temporal resolution to quantify and understand the relationship between surface and subsurface exchanges fluxes;

3. Water balance components present different profiles depending on land use types;

4. Groundwater table and Minimum environmental flow conditions of the Niger River are sensitive to future climate change impacts.

1.6 Novelty

To date, in the considered Niamey watershed, studies have focused on rainfall variability, the Niger River flows rainfall characteristics and climate change, groundwater recharge and quality (Anderson et al., 2017; Leduc et al., 2001; Favreau et al., 2009; Girard, 1993; Ibrahim et al., 2014; Hassane et al., 2016; Mascaro et al., 2015). However, presently no studies exist for the Niger River Basin (or sub-basins) which explicitly consider the dynamics of groundwater and surface water interaction in a fully-integrated manner.

Studies carried out in the region have shown that groundwater recharge in the Continental Terminal aquifer is predominantly governed by depression focused recharge (Desconnets et al.,1997; Favreau et al., 2012,) through ponds, with less contribution from diffuse recharge

(Ibrahim et al.,2014) depending on land use types. Girard et al, (1997) has shown that the main recharge process in fractured aquifers is controlled by the fracture system. All of the mentioned existing studies either investigated recharge using traditional water level fluctuation methods combined with hydrochemicals and isotopes approaches, or groundwater models with loosely coupled or simple representation of surface water, and vice versa.

Also, previous groundwater recharge studies in the Sahelian region in general and in Niger in particular have used the classical or modified models of Thornthwaite have been used. This is mainly due to the difficulty of estimating the actual evapotranspiration due the complexity of the unsaturated zone. Therefore, using the integrated hydrological model in which the simultaneous solution of surface and subsurface flow equations as well as the internal calculation of the actual evapotranspiration as a function of the soil moisture at each node of the defined evaporative zone, improve the representation of interdependent processes of groundwater recharge.

Additionally, to the author's knowledge, fully coupled surface-subsurface models have not yet been applied for the whole of the Niger River basin or its sub-basins. Moreover, none of the previous studies quantified directly the relation between Niger River and the underlying aquifer systems.

Also, fully physics-based integrated hydrological models were shown to represent one of the most reliable ways to assess climate change impacts on groundwater (Erler et al., 2019, Barthel and Banzhaf, 2015; Goderniaux et al., 2009; Kollet et al., 2017). However, the application of theses integrated models is computationally expensive, and highly data consuming. That should probably be the reason of few published application of integrated hydrological models at large scale (Barthel and Banzhaf, 2015). Large scales anthropogenic climate change impact using integrated hydrological models is even more rarely investigated in scientific literature. To the author's knowledge, there this currently, only three published climate change impacts studies that employed fully integrated models at watershed scale (Erler et al., 2019; Goderniaux et al. 2011; Sulis et al., 2012).

However, in all these studies, either small scales or relatively coarse meshed resolution were used, (Goderniaux et al. 2011; Sulis et al., 2012), or simulations were performed using representative seasonal cycle to reduce the computational cost (Erler et al., 2019). Also,

previously cited assessments were all performed in wet climate conditions, in more developed countries and where sufficient data are more available.

Therefore, the originality of this study is that simulations with higher resolution (up to 70 m) at large scale (1900 Km^2) were performed, in semi –arid climate environments with spared data. While acknowledging the data challenge for model validations, the use of higher mesh resolution seems to improve simulations quality, and in some extent compensate the spare data issue.

1.7 Scope of the thesis

This study used high resolution fully integrated hydrological model to investigate groundwater –surface water interactions, as well as the integrated hydrological response to climate change impacts.

Because the application of fully integrated hydrological models to large scale watersheds is a growing area of the literature, only a few manuscripts have been published that provide methodologies or guidance on the application of large scale integrated groundwater surface water models (i.e., Erler et al., 2019; Barthel and Banzhaf , 2016, Hwanget al.,2018; Hwang et al.,2015; Chen et al.2019).

One of the scopes of this study is therefore, the development of methodological guidance in the development of watershed scale integrated surface-subsurface models in data scarce and semi-arid environments. While acknowledging the data challenge for model validations, the use of higher mesh resolution is expected to improve simulations quality, and in some extent compensate the spare data issue.

We also acknowledged that evaluating uncertainties related to hydrological climate change impacts should constitute important issue in climate impact studies, but due to high computational demand of fully integrated hydrological models, the evolution of uncertainties, though important, is beyond the scope of the present study.

1.8 Expected results and benefits

Expected results and benefits of this study could be classified at different levels:

- Characterizing groundwater surface water interactions using fully 3D integrated hydrological model in complex aquifer system and spared data semi arid environment, will represent a significant contribution to the rare published scientific research on integrated hydrological model. This will allow providing to scientists a clear methodological framework on calibrating fully integrated hydrological models.
- Quantifying the magnitude of the exchange flux between surface and subsurface flow domains would also be useful for flood forecasting as well as the water resources management issues. For instance, in case surface water system drains the groundwater, the water table can act as a flood amplifier, or if the groundwater drains the river, water table may act as flood buffer. Also, groundwater contamination of either system is likely to impact the other flow system in case of water quality issue.
- Understanding the integrated hydrological response of climate change impacts, will represent important decision-making tool, to help water resources managers to planning integrated adaptation strategies for a resilient water resources management.

1.9 Outline of the thesis

This thesis is composed of eight chapters, with the **chapter 1** describing the general introduction and providing the general context and problematic of the study. It also presents the literature review, the objectives of the thesis, research questions and hypothesis as well as the expected results. The originality and scope of this thesis were also discussed in this chapter. Finally, the outline and organization of the thesis document are presented. In the **Chapter 2**, the general characteristics of the study area are presented and described. In this chapter, the topographical features, hydrography, soil and land use as well as the geological characteristic of the study area are described. The **Chapter 3** provides details on the data, and materials used, as well as the methodological approach that guides the research conducted in this thesis. Geological and structural characterization and the conceptual hydrogeological model definition are discussed in the **Chapter 4.** In the **Chapter 5**, geochemical and isotope analytical groundwater analysis will be used to understand and identify exchange between groundwater

and surface water, as well as mixing between different aquifers. The **chapter 6** provides details information on the development and calibration of the HGS integrated hydrological model used to understand and quantify the exchanges between surface water system and groundwater system. In the **chapter 7,** integrated hydrological response of the groundwater and surface water system are evaluated under future climate change scenario. General conclusion and perspectives of the research work are provided in the **Chapter 8**.

Chapter 2: Study area

2.1 Localization

The study area is a sub watershed of the middle Niger River basin (Figure 1), and is located southwest of Niger, which is centrally positioned in the West Africa. The watershed considered has a total surface area of 1900 Km² and is limited approximately by the longitudes 1.75° and 2.35° East, and the latitudes 13.26° and 13.75° North.

2.2 Relief

The topography of the study area is characterized by two distinct types of physiographic units. The topographically high land corresponds to the CT3 plateau at elevations ranging from 190 m to 250 m (a.m.s.l), while the low land area is occupied by plain containing ephemeral streams and ponds, at altitude between 172 m to 185 m (Figure 1). This alternating succession of plateau and plain corresponds to the typical morphology of the Niamey region (Favreau, 2000), and dictates almost the hydrological characteristic of the region.

2.3 Vegetation

The topographical and hydro pedological characteristics of the study area, present an important control on the vegetation pattern. On the plateau, the vegetation cover is mainly represented by the natural shrub bush, locally referred as tiger bush due to its banded pattern (Goutorbe et al., 1994). The natural vegetation was dominated by the woody savannah, with the dominant species represented mainly by *Acacia sp*. and *Combretum sp*. This natural vegetation has progressively been replaced by fallow with small shrubs dominated by *Guiera senegalensis*, and rain-fed millet fields. In the plain and valley bottoms, the vegetation is dominated by water-demanding crops such as cassava and sorghum. (d'Herbes and Valetin, 1997; Leblanc et al., 2008).

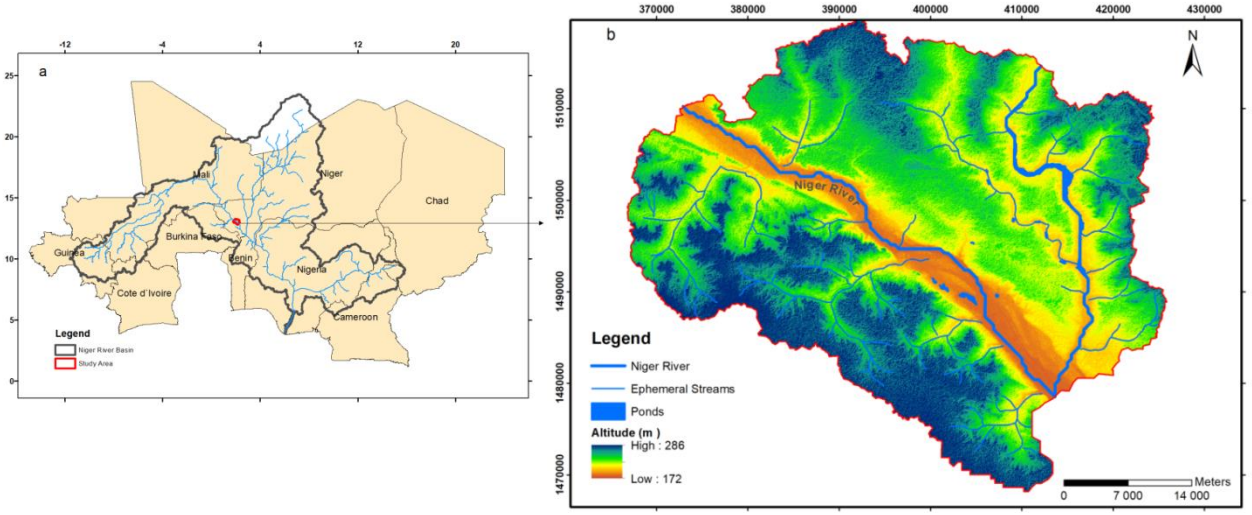

Figure 1: (a) Study area location within the Niger River basin; (b) Local context of the study area with topography and Streams network

2.4 Climate

The climate of the study area is semi-arid, characterized by low frequency intense rainfall events occurring from June to September (rainy season), and alternating with long dry season from October to May (Figure 2). The mean annual rainfall for 1980-2009 period is 514 mm with a standard deviation of 116 mm (Bigi et al.,2018), showing the important spatio temporal inter annual variability of the rainfall. This inter annual variability is directly linked to the variations of the West African monsoon driven by important zonal flows. Theses zonal flows are determined by meridional heating contrasts and their associated direct circulations. The primary factor controlling directly rainfall over the study area is the intertropical convergence zone (ITCZ), resulting from the interaction of two air masses: the hot and dry continental air masses (harmattan) of the Sahara Desert and the moist equatorial air masses (monsoon) originating from the Guinea golf. From a large-scale view, the annual shift of the ITCZ described the WAM, the small-scale structures are, however, pivotal for rainfall generation (Lebel and Ali, 2009).

The mean annual Penman Monteith potential evapotranspiration is 2500 mm that and is four time greater than the mean annual rainfall. The average temperature is of 29°C, and the maximum temperature may exceed 45°C.

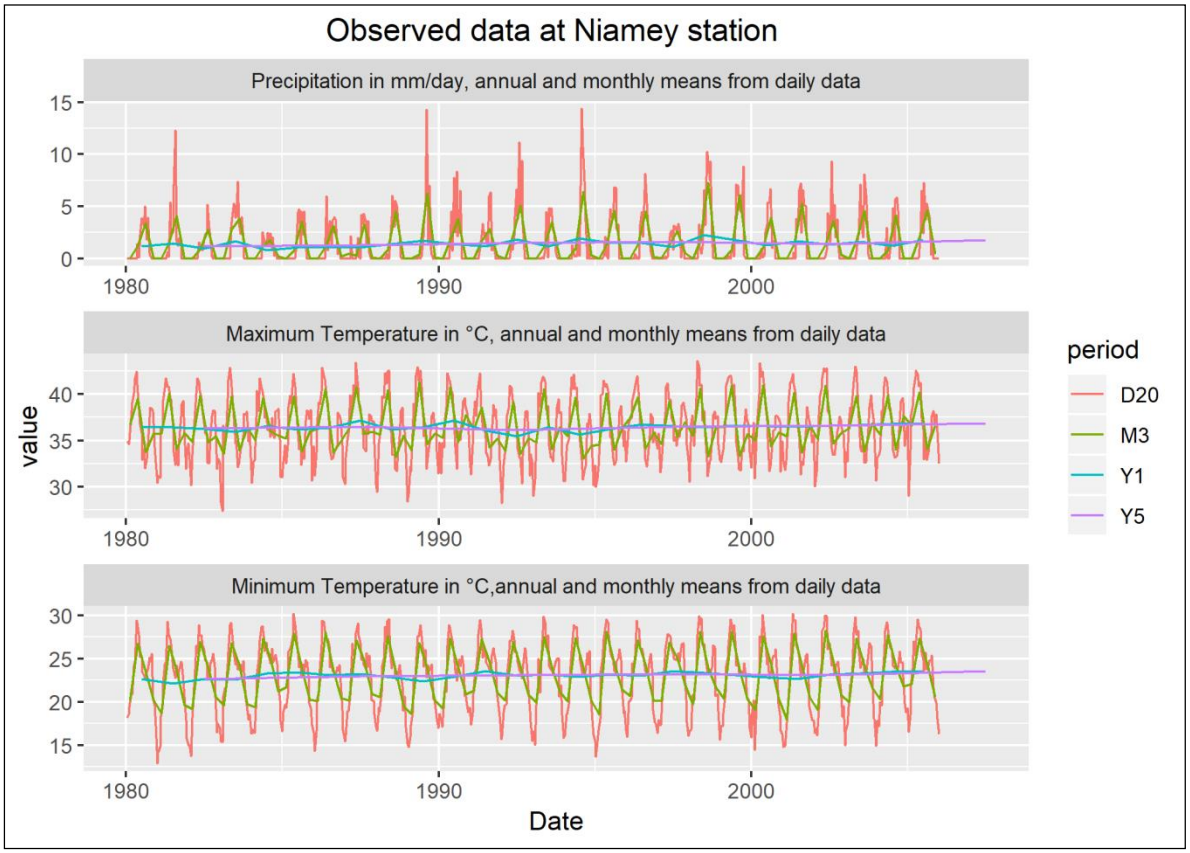

Figure 2: Observed Rainfall, Maximum and Minimum Temperatures for 1980-2005 period at Niamey Airport

2.5 Hydrography

The hydrological conditions of the site are quite complex. The only permanent freshwater source is the Niger River, and its flow is generated from the upper Niger basin in the Fouta Djallon Massif in Guinea. In the study area, the Niger River flow has two peaks, one peak due to the contribution of the local rainy season in September and the other in December due to the inflow from upstream (Andersen et al., 2005). The others hydrological features are ephemeral stream, called koris that are hydrologically active during the rainy season, and some permanent

and semi permanents ponds (Figure 1). Therefore, to summarize the complex hydrological setting, the Niger River flow is driven by the inflow coming from upstream, and the local precipitation that drives ephemeral stream and ponds. Runoff collected by the ephemeral stream, is generally discharged into several temporary and or permanent ponds that are located in the course of the ephemeral streams (Desconnets et al., 1997; Peugeot et al., 1997).

2.6 Soil and land use

The pedological characteristics of the study area were thoroughly defined into typical toposequence of land surface conditions, composed of soil crusts and surfaces units (d'Herbes and Valetin, 1997). In general, the soil types are of ferralic arenosols of sandy formations, and of arenic lixisols, originating from the weathering of clayish sandstone formations. On the lateritic plateau, the soils are dominated with ferralic arenosols composed mainly with clayish sand, locally covered by sands deposits. Downslope, on the glacis, the structure of the soil is dominated by the arenic lixisols types. The valleys bottoms are characterized by sandy soil, with important clayey contents at the vicinity of surface water features, like ponds.

The natural vegetation of the region is composed of woody savannah mainly represented by *Acacia albida*, *Combretum sp*, and *Balanites sp*. This vegetation has been cleared over the last decades to cropping of Rain-fed millet, cultivated in traditional fields (Leblanc et al., 2008). The landscape appears now as a patchwork of fallow and millet fields. Irrigated rice fields and gardens are planted along the Niger River.

The rapid urbanization of Niamey has resulted in progressive settlements infrastructure buildings. Also, for a reforestation purpose, protected 'green belts', of deep *Eucalyptus sp*. trees, and *Azadirachta indica* are planted in the city.

2.7 Demography, environmental, social and economic activities

The main landmark of the study area is the city of Niamey and its environing villages made up with moderns and informal settlements with residential, agricultural and savannah lands. The major socio economics activities of the region are dependent of the Niger River, which is sole permanent surface water used for agriculture and drinking water supply of Niamey city.

However, due to insufficient water distribution network infrastructure, and recurrent drought, the River could not cover the total demand of water of the city, and groundwater is used through open wells and boreholes to provide water to more 35% (Niger PRSP 2008) of 1.3 million (INS 2012) of people of the city. The importance of the groundwater demand to supply drinking and agriculture purpose is increasing due to rapid population growth and urbanization of the city. The annual demographic growth rate of 4.5% is the greatest rate of the country (average of 3.4 % for Niger). The high demographic growth rate is mainly due to birth rates and migration from rural to suburban areas. The density of the population is 2,700 inhabitants per km2 in the center of city. Compared to rural population, the population density at the vicinity of the Niamey city was estimated in 2001 at 30 inhabitants per km2 (INS 2012). This population growth has resulted in important expansion of the urban area and infrastructures building, and decreased agricultural and natural vegetation lands.

2.8 Geological and Hydrogeological Context

2.8.1 General geological context

The major tectono-metamorphic phenomenon related to the orogeny of eburnean (2.4 -1.6 Ga) has modeled Africa to four Craton corresponding of West Africa Craton, Nilotic Craton, Congo Craton and Kalahari Craton (Camil, 1987, Soumaila 2000).

West Africa consists of rocks composed of two Archaean and Proterozoic shields known as Reguibat shield to the north and Baoule Mossi (Man) shield to the south. These shields represent the major Precambrian outcrop of the Craton and are surrounded by the mobile hercynien and Panafrican massifs (Figure 3). The depositional areas are Neo-proterozoic to Paleozoic Taoudeni, Tindouf and Volta basins, and the Meso-Cenozoic to Quaternary Iullemmeden basin (Afaton et al, 2000).

The Baoule Mossi (Man) shield is structurally separated in two geological domains by the Sassandra fault. The eastern part corresponding to Eburnean rocks and the western part constituted mostly with Archean rocks remobilized during the Eburnean orogeny. The present study area is located south west of Niger and lies geologically on the Liptako Gourma region (Figure 4). It corresponds to the north east edge of the Man shield characterized by the Birimien

formations rocks (Precambrian basement), and overlying sedimentary rocks of Iullemeden basin.

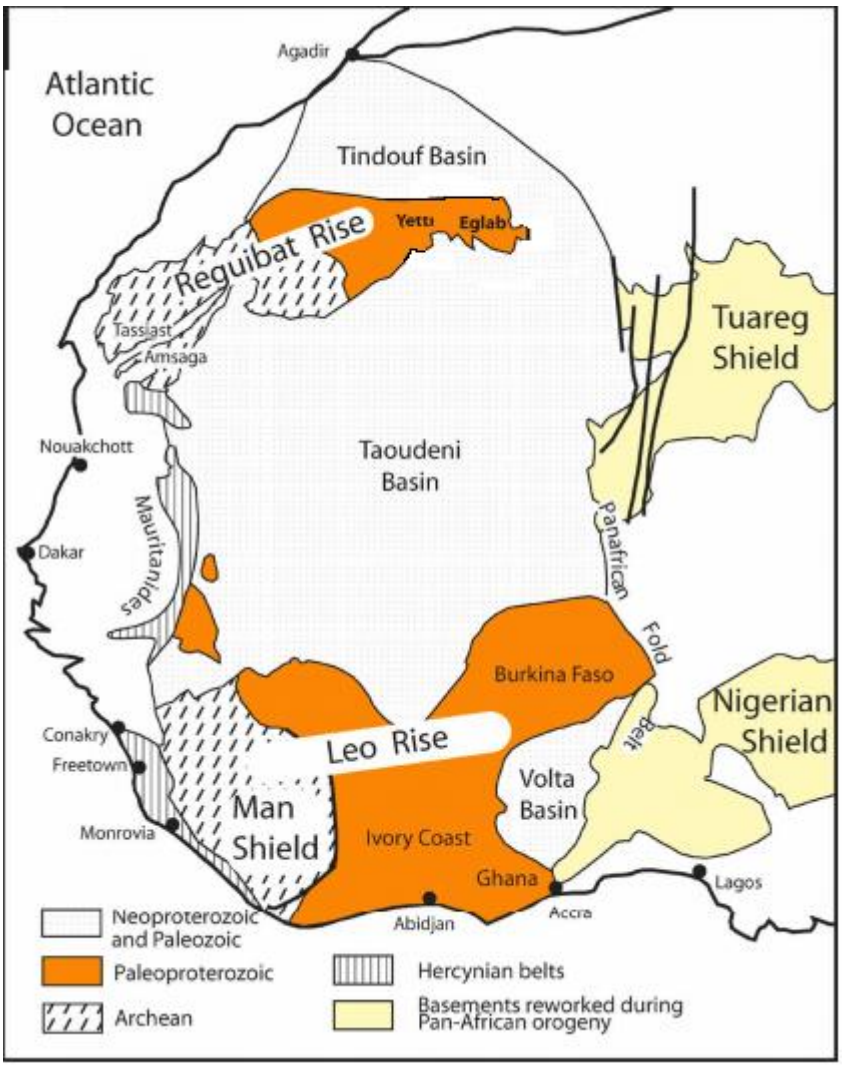

Figure 3: The West African Craton (modified of Peucat et al., 2005)

Precambrian basement formations

The Precambrian basement formations of Liptako, also known as Birimien formations cover 75% of the Liptako area. There are two different geological series described in the Birimien formations: the green rocks belts composed of volcano-sedimentary rocks types of low to medium metamorphic grade and younger granitic intrusions surrounding and cutting the green rocks belts (Figure 4).

The volcano sedimentary formations of the green rocks belts are of grauwakes, micaschists, mafic and ultra mafic rocks consisting of metabasalt, metadiorite and Meta gabbros. The granitic intrusion surrounding and cutting the green belts rocks are oriented north east south west. They exhibit various petrographic rock-types mainly composed of orthogneiss, granites and diorites.

Sedimentary formations

The sedimentary rocks overlying directly in major unconformity the Precambrian basement are of three different series: the Neoproterozoic sandstones, the Continental Terminal formations, and the quaternary alluviums deposits.

Neoproterozoic sandstones formation is mainly constituted with sandstone, quartzite and schistes. These sandstones, when outcropping, lie directly on the Precambrian basement in major unconformity.

Continental Terminal formations of post Eocene represent the upper sedimentary formations of the Iullemeden basin. They are composed of three different petrographic rock types overlying on major unconformity, locally the Neoproterozoic sandstones, or the Precambrian basement. Petrographic rock types are the Ader Doutchi siderolotic formation described as CT1 (Continental Terminal 1), the clayish sand formation known as CT2, and the loosely cemented clay of CT3.

The alluvial deposits are of two types, the fluvial deposits of the Niger River characterized by five terraces formed mainly of fluvial and eolian sand and gravels, and the ephemeral streams alluvial deposits.

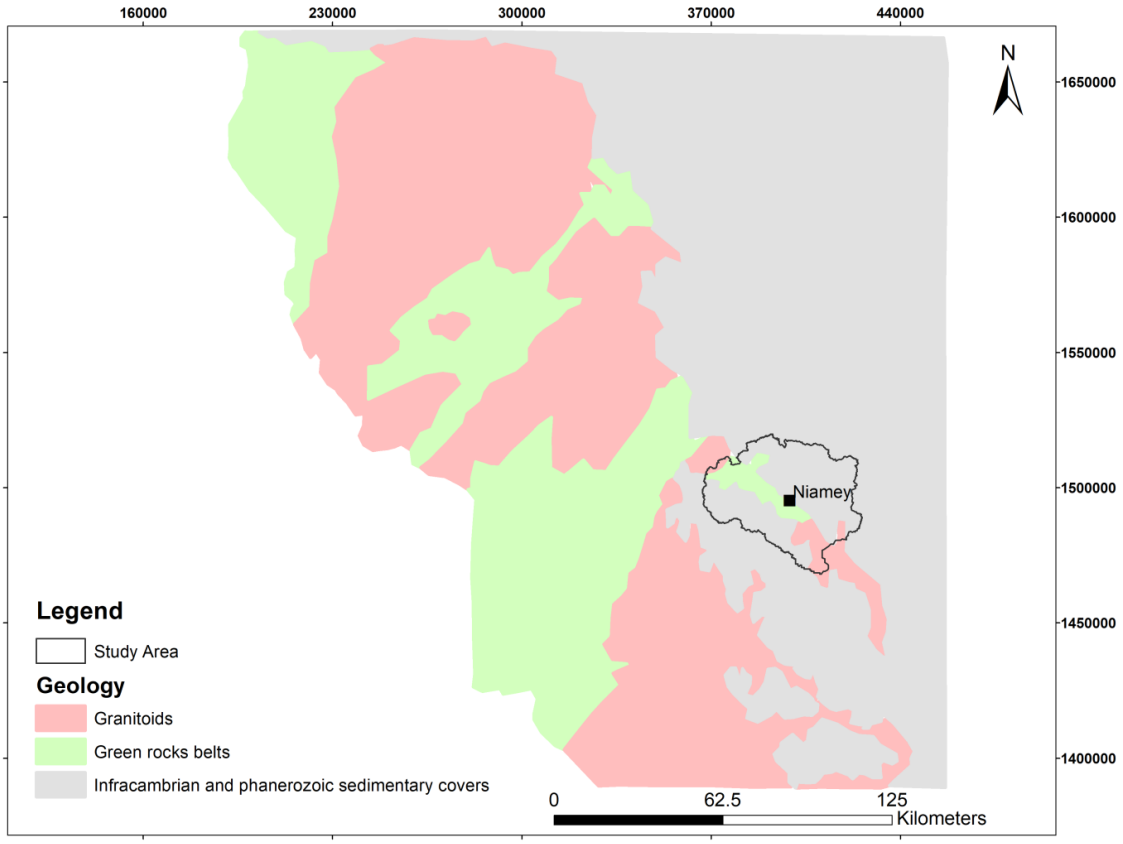

Figure 4: Geological context of Liptako, (modified from Machens, 1973)

2.8.2 Study area geological context

According to its geographical position, the Niamey watershed is located on the western edge of the Paleoproterozoic basement of the Liptako, and on the southeastern part of the Iullemmeden sedimentary basin. The Niamey watershed terrains consist of two main geological units, including:

- The Paleoproterozoic basement (2300-2000 Ma) (Soumaila and Konaté, 2005), which outcrops to the west of the study area at the vicinity of the Niger River. It includes granitoid plutons alternating with Greenstone belts. Granitoids consist of diorite intrusions, quartz diorite to tonalite, monzonite, granodiorite and granite or syenite locally. These intrusive bodies are either syn-tectonic or post-tectonic (Machens, 1973; Soumaila et Konaté, 2005: Perotti et al., 2016). The greenstone belts consist of sandstones-pelitic rocks more or less metamorphosed (shales, sericite schists,

micaceous schists, quartzitic schists) and low to medium metamorphic greenstone (amphibolite, chloritoschists, metabasalts, metagabbros) (Machens, 1973; Soumaila and Konaté, 2005; Perotti et al., 2016).

- The sedimentary deposits overlie unconformably the Paleoproterozoic basement. The lowermost deposits are represented by an older unit essentially consisting of Upper Precambrian sediments (Niamey sandstone) (Machens, 1973) and the uppermost deposits consist of the clayish to silty sandstones of the Oligocene Continental Terminal 3 formation (CT3) (Chardon et al., 2018) and quaternary to recent deposits that infill the ephemeral streams and the Niger River.

The principal direction of schistosity measured in the study area corresponds to N25° to N75° (Soumaila and Konaté, 2005)

There are three different types of faults described in the basement formation: the N00 ° to N10 ° and N70 ° to N80 ° directions corresponding to Eburnean shears; N10 ° to N20 °, N100° to N110° and N130 to N140 ° described as tardi eburnean group of faults and the post eburnean faults of N160 to N175° directions.

2.8.3 Hydrogeological Context

The hydrogeology of the watershed is characterized by the geological conditions, with two types of aquifers. The fractured aquifers of the Liptako basement formations are found in both the granitic and Greenstone belts formations, and the Continental Terminal, CT3 aquifer. Depth to groundwater table varies from 5 m in the fractured aquifers, to 65 m in the CT3 aquifer.

2.8.3.1 Fractured aquifer hydrogeology

The fractured aquifers of the Liptako basement formations mainly composed of granitic Greenstone belts formations represent the main aquifers underlying the city of Niamey. Therefore, fractured aquifers in the study area and in West Africa in general are localized in the permeable fissured/fractured zone located in the first meters or few tens of meters of the unweathered hard rock underlying the unconsolidated weathered layers. The fissured/fractured and altered birrimian basement formations represent multilayers aquifers exploited through boreholes in the city of Niamey (Bernert et al,.1985; Dehays et al,.1986).

These fractured aquifers are underlying both the CT3 sedimentary aquifer as well as the discontinued alluvial aquifer. Also, the alteration product from either the birrimian basement formation or the alluvium associated with ephemeral streams formed the weathered aquifer. The depth of the boreholes in the study area is between 30 meters and 100 meters. The average flow rate in the granitic formation aquifer is between 2 m^3/h to 4 m^3/h, while it is between 3 m^3/h to 8 m^3/h, in the greenstone belts formations aquifers. The hydrodynamic parameters of the fractured aquifers in the study area are characterized by strong spatial variability. This is mainly due to the control of the fracture intensity and or density.

2.8.3.2 CT3 aquifer hydrogeology

The Continental Terminal formation composed of sandstone, clayey and silty rocks represent a multilayers aquifer present as a single aquifer system in the Iullemmeden basin. Therefore, CT represents a relatively continuous aquifer formation in the Iullemmeden basin. In the study area, the reservoir of the CT, is represented by the Clayish sandstone formation referred as CT3 aquifer. At local scale, the lithological heterogeneity of each layer can lead to the formation of aquifer with different characteristics. This is the case for instance in the West where the water table is mainly contained in the oolites reservoir near Niamey while a little further east of Niamey the water table is contained in the clayey sandstones of CT3 (Plote, 1961; Leduc et al., 1997).

This lithological heterogeneity explains the strong spatial variability of the hydrodynamic parameters of the aquifer. Some parts can be totally dry (Boeckh, 1965), while other parts are , conversely, very transmissive . The overall estimated transmissivities are of the order of 10^{-2} to 10^{-5} m^2/s (Greigert, 1968; Greigert et Bernert, 1979).

2.9 Conclusion of the chapter 2

This chapter has provided a general overview of the main hydrological and hydrogeological characteristics of the study area. The Niger River representing the unique permanent surface water source used to provide drinking and agricultural water to the Niamey city, has two flow peaks, one peak due to the contribution of the local rainy season in September and the other in December due to the inflow from upstream. In order, to better represent interaction between surface water and groundwater, it is therefore necessary to define a conceptual model that should take into account, these two peaks patterns of the flow.

Also, the geological conditions presented in this chapter, highlighted the complexity of the sedimentary formations overlying the fractured basements rocks. The representation of the sedimentary formations in any hydrogeological conceptual model is relatively straightforward, compared to discrete fractures network representation. This represents also, a different level of complexity, and it appears very useful to define a conceptual model that should be able to consider both geological conditions.

Finally, the semi-arid climate of the study area implies that groundwater recharge is mainly controlled by temporary or permanent surface water system, and therefore, their representation in the conceptual hydrogeological model is of critical interest.

The challenge that this complex environment needs to be addressed with very sophisticated and state of the art integrated hydrological model, combined with traditional fields and analytical investigations.

Chapter 3: Data, Materials and Methods

In this chapter, data, materials and methods used to perform the research work will be presented. Geological and hydrogeological data collected in situ from fields investigation as well as cartographic (soil, land use, topography) and hydroclimate data obtained at different sources will be described. Materials used for in situ data collection, and those applied to analyze the data are also discussed. It will also be discussed, the methodological approach that guide the research work. The methods used for geological and integrated hydrological modelling, as well as the methods applied to analyze the hydrochemicals and isotopes analytical results will be presented in details.

3.1. Data

3.1. 1 Geological and structural data

The geological map of Machens (1973), combined with 120 borehole logs documented by Bernert et al, (1985) and Dehays et al, (1986) will be used for 3D geological modeling of the study area. The geological map (Machens, 1973), is at a scale of 1/200 000, and the borehole logs documentation includes the lithological descriptions; technical logs of the boreholes (screen depth, fracture presence) as well as the hydrodynamic information (static water level, flow rate). The boreholes were logged by a French Geological Survey (BRGM).

Also, field measurements were performed to determine the fractures directions and number from the Precambrian basement formations outcropping in the study area. The measurements include fracture directions and dips, fractures apertures and spacing, and the outcrop dimensions. These measurements will be used to determine the fracture intensity of the Precambrian basement formations.

3.1. 2 Hydrogeological data

In order to determine the extension and thickness of the alluvial formations, nine micro (9) piezometers were drilled at the vicinity of the ponds and ephemeral streams. In addition to the micro piezometers drilled, a total of 24 observation wells were selected to calibrate the models for hydraulic heads based on the availability and aquifer types screened. 8 observation wells out of the 24 are piezometers equipped with automatic pressure recorder and are installed in the fractured aquifer and groundwater heads were recorded hourly from 2014 to 2017. The rest of observation wells are open wells with large diameter (1m), and/or boreholes pumped mostly to supply water for domestic use, whose pumping rate is as small as $1m^3$/day (Hassane, 2016).

Hydraulic head data for all the observation wells was provided by the Direction Régional de l'Hydraulique et de l'Assainissement de Niamey (DRH/A) and the Niger Basin Authority (NBA). Measured groundwater heads were also reconstituted from historical measurements performed during the 1980's, at the construction of the boreholes.

Hydraulic conductivities and specific storage values for each hydrogeological unit are derived from literature. Initial estimates of hydraulic conductivities for the fractured aquifers are taken from Domenico and Schwartz (1990), while CT3 hydraulic conductivity was from (Favreau 2000).

3.1. 3 Hydrochemicals and isotopes data

In this study, groundwater and surface water samples were collected for analytical hydrochemicals and isotopes analysis. In 2017, thirty-four (34) water samples were collected during three separate sampling campaigns, corresponding to the rainy season (July-September), the cold dry season (October-January), and the hot dry season (March-June). These periods are considered to represent the respectively the high flow conditions of the surface water system, the groundwater table rise period, and the base flow conditions for both groundwater and surface water. Out of the 34 water samples, 4 are for the alluvial aquifer, 5 for surface water, 14 for the fractured aquifer and 11 for the Continental Terminal 3 aquifer (CT3). The collected groundwater samples were completed with water samples measured by the Direction Régional de l'Hydraulique et de l'Assainissement de Niamey (DRH/AN) in collaboration with the Niger Basin Authority from 2012-2014. A total of 140 water samples were collected and analyzed.

3.1. 4 Soil, land use and topographic data

Soil data used in this study are derived from Graef et al., (1998), who used soil types, geomorphologic and hydrological criteria to extensively map the soil and terrain in south west Niger, and provide a complete Soil and Terrain Digital Database (SOTER). Land use maps of 2013, obtained from CILSS, (2016) at 2km resolution was used as source data to derive land use map of 30 m resolution. Digital Elevation Model (DEM) of the study area, of 30 m x 30 m resolution was obtained at Agriculture Hydrologie et Meteorologie (AGRHYMET) Regional Center, and will be used to assign elevations to the top most 2D layer of the integrated hydrological model.

3.1. 5 Hydro Climate Data

Hourly climate data for rainfall, maximum and minimum temperatures (Tmax, Tmin), wind speed, relative humidity and solar radiation from 2011 to 2017 were obtained from an automatic weather station installed at the Agriculture Hydrologie et Meteorologie (AGRHYMET) Regional Center. Daily Penman-Monteith potential evapotranspiration was computed using aggregated hourly data from the above weather station. Also, for long term hydrological modeling, 1980-2005, observed precipitation, maximum and minimum temperatures (Tmax, Tmin) data of Niamey Airport station provided by the Direction de la Meteorologie Nationale (DMN) will be used.

Daily stream flow time series for Niamey and Kandadji gauging stations were obtained from the Niger Basin Authority (NBA) database, for 1980 -2017 periods.

For climate change impacts assessment, historical (1980-2005) and projected (2020-2050) rainfall, maximum and minimum temperatures (Tmax, Tmin) were derived from three regional climate models (RCMs) data. These data were provided by the WASCAL competence Center. Table 1 provides the RCMs, the forcing global circulations models GCMs as well as the RCM resolutions used.

Table 1: RCMs and the forcing GCMs used in this study

Institution	RCM	GCM	Resolution
Canadian Centre for Climate Modelling and Analysis	CanRCM4	CanESM2	50 km
Institut Pierre-Simon Laplace, France	RCA4	IPSL -CM5A	50 km
West African Science Service Center on Climate Change and Adapted Land Use (WASCAL)	WRFV3.5.1	GFDL-ESM2M	12 km

The diagram of Figure 5 provides a general overview of the complete set of data used in this study.

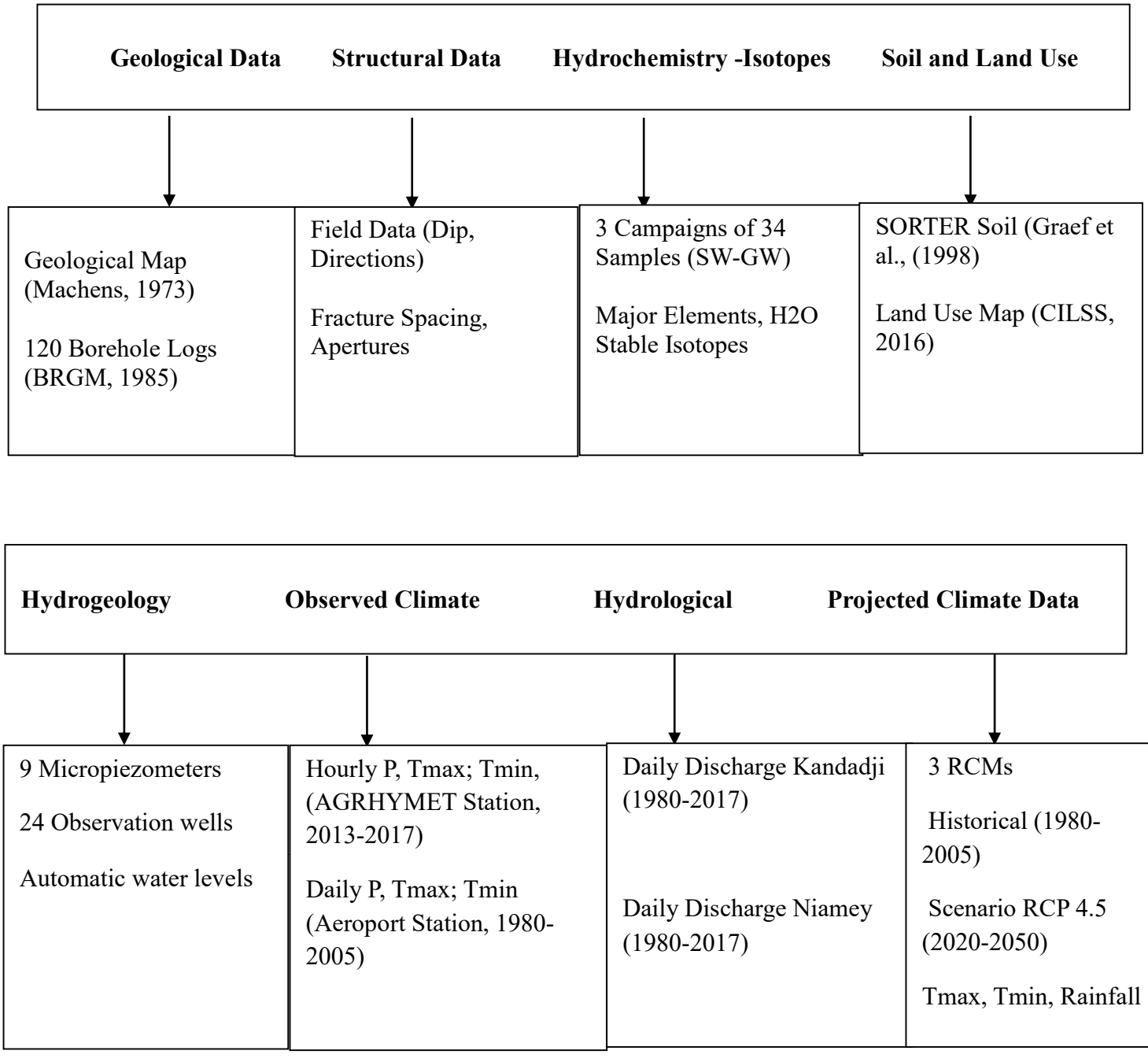

Figure 5: General overview of the complete set of data used in this study.

3.2 Materials

The materials used in this study consist of hard and soft materials. The hard materials are composed of:

- Global positioning system (GPS) for fields coordinates recording, and a magnetometer for fracture directions and dip measurements;
- Portable hand auger for micro-piezometers drilling, water level indicator, Ph-Meter, and conductivity meter for in situ measurement of groundwater heads, Ph and conductivity;
- Plastic and glass bottles and amber bottles, with containers for water samples collections and handling.

The soft materials consist of:

- ArcGis and Quantum GIS for cartography;
- Rockworks software for geological modelling;
- Daisy for structural geologic data processing
- Python and R for hydroclimate data processing and analysis;
- HydroGeoSphere (HGS) for the Integrated hydrological modelling

3.3. Methods

The following sections describe the different methodological approaches employed to perform the research work. First, geological and structural modeling will be presented for conceptual model definition, then hydrochemicals and isotopes methods to understand groundwater surface water interaction will be described. Finally, methods for integrated hydrological modeling for groundwater surface water exchange flux quantification, as well as future climate change impacts assessment will be presented.

3.3.1 Soil and Land Use mapping

The study area is discretized in 41 soil zones derived from the SOTER database. Unsaturated soil zone hydraulic conductivity values K values, porosity and Van Genuchten (1980) soil

hydraulics parameters for the 41 SORTER based soil zones are estimated by grain-size derived estimates using the ROSETTA neural network prediction method (Schaap et al. 2001).

Validated Land use map of 2013 (CILSS, 2016) at 2km resolution was reclassified at 30m resolution based on 2013 Landsat 8 image of the study area, using supervised maximum Likelihood classification method.

3.3.2 3. Geological modeling and structural modeling

3.3.2 .1 3D geological modeling

The construction of the 3D geological model of the study area involves the lithological interpretation of the individual 120 borehole logs to create 2D surface maps of model layers. The interpolation was performed using the Inverse Distance Weighted method. Based on different lithological elevations of the boreholes, a grid model and contour map of geological layers are built. Then, from the grid model and contour map of the different geological layers, a 3D geological model is built in the HGS grok command file.

The Inverse-Distance method represents one of the more common gridding methods. In this method, the value assigned to a grid node (cell value) is a weighted average of either all of the data points or a number of directionally distributed neighbors. The cell value represents herein the absolute elevation of the lithological formations derived from the boreholes. The value of each of the data points is weighted accordingly to the inverse of its distance from the grid node, taken to a user-defined power. The greater the value of the exponent specified, the more localized the gridding, as father away points will have relatively less influence on the value assigned to each grid node (Philip and Watson 1982). The advantage of this method is that it produces smooth and continuous grid, and it honors the data since extrapolation are not allowed beyond the points data provided (Davis, 2002).

Also, from the micro-piezometers and borehole logs, cross sections were realized to represent the conceptual model, using the traditional log to log geological correlations.

3.3.2.2 Structural characterization

In order to characterize the fractured aquifer system, fields orientation and dip measurements were performed on the geological outcrops in the study area. In addition to the orientation and dip measurements, fracture numbers, spacing, length, as well as the outcrops lengths were recorded. The **appendix 1** provides the field data used to perform the in-situ fractures fracture

characterization. While orientation and dip measurements are common structural methods, fracture spacing is performed according to the following method.

To determine fracture spacing on outcrops, a perpendicular line of some given length is drawn along the fracture set of interest, and then, number of individual fractures encountered along this line is counted and divided by the total number of fractures. Figure 6 provides a representation of the fields method used for fracture spacing measurements.

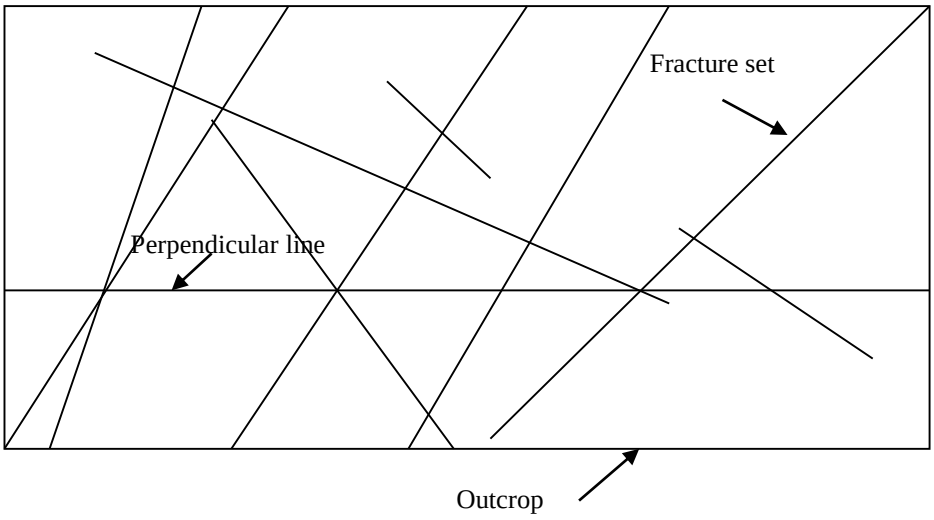

Figure 6: In situ Fracture spacing measurement methods

Fracture spacing measurement provides fields-based methods of charactering fracture intensity of naturally fractured reservoirs (Nelson, 1985; Manda et al., 2013; Boro et al., 2014; Bisdom et al., 2016).

3.3.4 Hydrochemicals and isotopes characterization

A sequential statistical multivariate analysis is performed to understand the hydrochemicals process in the watershed (Figure 7). The first step in the methodological approach consists of verifying the quality of the data using the charge balance equation as described below:

The accuracy of a geochemical analysis can be verified by comparing the total of the negative charges in solution with the total of positive charges. The laboratory analytical results are converted to equivalents or milliequivalence units (meq/L = ppm × valence/ gfw) for the major and minor species. The difference between the sum of all major cations (Σcat) and anions (Σan) is then compared with the sum of all major ions to give the charge balance error:

$$\%CBE = [\Sigma cations - \Sigma anions] / [\Sigma cations + \Sigma anions] \text{ X } 100 \quad (1)$$

Where %CBE is the Charge Balance Errors in percentage, Σcations is the Somme of the cations, and Σanions is the Somme of anions. Generally, CBE value equals or less than 5% are indication of good analytical results (Fetter, 1994).

The second step involves exploring the variance of the data through the correlation matrix and testing their normality, as most of the multivariate statistical analysis that will further be performed assume that data are normally distributed (Everitt and Hothorn, 2011). Then, if required, adequate data transformation will be applied to satisfy the multivariate normal distribution assumption of the data.

From the explanatory analysis, a sequential multivariate statistical analysis on the hydrochemicals and isotopic water analysis is performed. Sequential analysis involves first, the application of the Hierarchical clustering Analysis (HCA) on the major ions and Physico-chemical parameters. The major ions are composed of Na, K, Ca, Mg, HCO3, Cl and SO4, and the Physico-chemical parameters include Ph, Conductivity, and Temperatures.

The HCA is a multivariate data reduction technique which allows partitioning a set of observations into a distinct number of groups (clusters) based on the statistical similarity of a set of parameters (Kumar et al., 2009; Guggenmos et al., 2011; Everitt and Hothorn, 2011). Herein, HCA will be combined with facies identification from piper diagram, to identify potential water types origin or mixing based on the clusters hydrochemistry.

Principal Component Analysis (PCA) is applied on the HCA identified groups in order to determine the main hydrochemicals factors that account for the numerical variation of the clusters. This step is useful in providing insight into the hydrochemicals processes and probable sources of solutes forming the water facies.

Sequential multivariate statistical analysis has already been successfully applied to investigate groundwater surface water interaction (Guggenmos et al., 2011; King et al. 2014; Oyarzún et al. 2014; Martinez et al., 2015).

Furthermore, the above multivariate statistical analysis will be combined with stable isotopes including Deuterium H^2, and Oxygen 18 O^{18} of water to investigate groundwater surface water interaction. Stables isotopes of water represent a useful tool in tracing the water cycle, including groundwater recharge and surface water groundwater interactions (Clark, 2015). Stable isotope concentrations are used for such purposes. They are measured as a ratio (R) of the rare to the abundant isotope and expressed as the difference in this ratio between the sample and a known reference (equations 2 and 3).

$$\boldsymbol{R = \frac{\text{atomic number of rare element}}{\text{atomic number of abundant element}}} \qquad \textbf{(2)}$$

$$\boldsymbol{\delta = \frac{R_{sample}}{R_{SMOW}} - 1 \times 1000\ ‰\ VS\ SMOW} \qquad \textbf{(3)}$$

Where $\boldsymbol{\delta}$, represents the difference in ratio from the Standard Vienna Standard Mean Ocean Water (VSMOW).

The strong correlation between δO^{18} and δD provides the characteristic meteoric water lines (MWLs) for different regions, and is used to understand different hydrological purposes (evaporation, groundwater recharge). The Global Meteoric Water Line (GMWL) is defined (Craig, 1961) in equation (4) and is used as reference to compare the isotopic composition of surface and groundwater water.

$$\delta D = 8\,\delta^{18}O + 10\ ‰ \qquad \textbf{(4)}$$

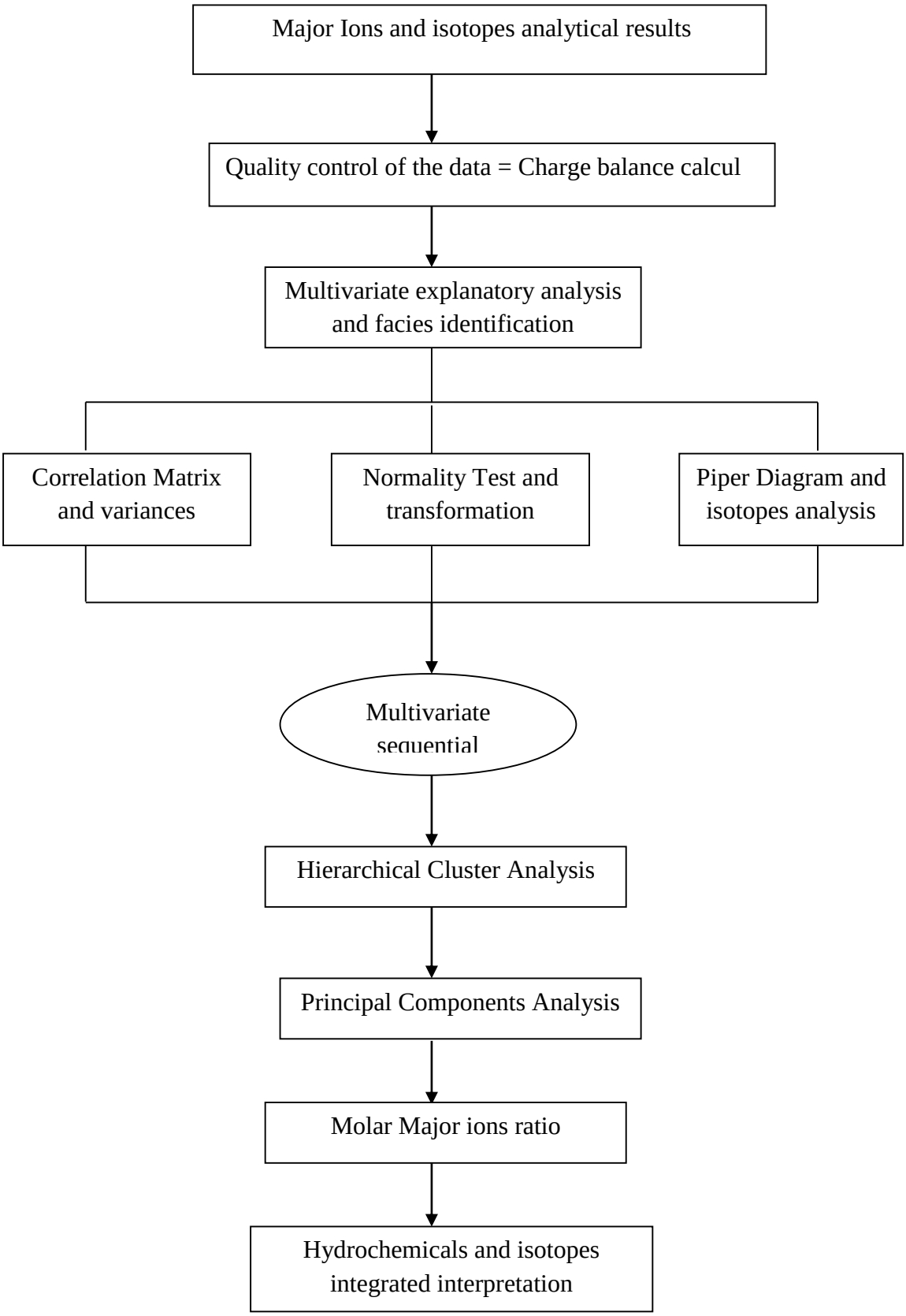

Figure 7: Methodological flow chart of sequential Multivariate statistical analysis of hydrochemicals and isotopes analysis

3.3.3.5 Integrated modeling of groundwater surface water interaction

3.3.3.5.1 Hydrological Model

A 3D fully-integrated surface and subsurface hydrologic model, HydroGeoSphere (HGS) (Figure 8) was used to calculate overland flow, variably saturated groundwater flow, flux exchange between the Niger river, ephemeral stream, ponds and the aquifer system (i.e., CT3 and the fractured aquifer), as well as water balance components such as groundwater recharge and evapotranspiration for various land use types. HGS is a fully-integrated surface and variably-saturated subsurface flow and evapotranspiration simulator (Aquanty Inc, 2018).

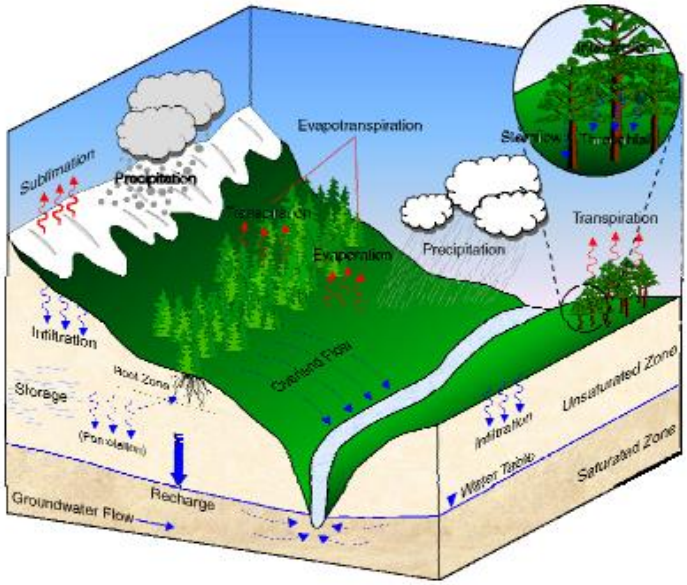

Figure 8: Integrated fully coupled 3D surface –subsurface HydroGeoSphere Model (Aquanty, 2018)

HGS uses a three-dimensional control-volume finite element method that implicitly solves a modified form of Richards' equation for variably-saturated subsurface flow and a depth-integrated Saint Venant diffusion wave equation for surface water flow in a parallelized manner (Hwang et al., 2014) as described in Equation (5).

$$\nabla \cdot \mathbf{k_r K} \cdot \nabla \mathbf{h} \pm \mathbf{Q} + \mathbf{\Gamma} = \frac{\partial}{\partial \mathbf{t}} (\boldsymbol{\theta}_\mathbf{s} \mathbf{S_w}) \qquad \textbf{(5)}$$

where k_r is the relative permeability, which is a function of the water saturation S_w or the pressure head ψ, K is the hydraulic conductivity tensor, h is the total head given by ψ+z where z is the elevation, θ_s is the saturated water content, Q is the volumetric flow rate per unit volume representing a source or sink, and the fluid exchange between the surface-subsurface is represented by Γ.

The depth-integrated surface flow equation adopted in HGS involves the 2D diffusion-wave approximation:

$$\nabla \cdot d_o K_o \cdot \nabla h_o \pm Q_o + \Gamma_o = \frac{\partial h_o}{\partial t} \qquad (6)$$

Where d_o is the depth of flow, h_o is the water surface elevation ($= d_0 + z$), and K_o is the surface conductances that depends on the friction slope of the surface and isapproximated by the Manning's equation in the x- and y- directions as

$$K_{ox} = \frac{d_o^{2/3}}{n_x} \frac{1}{[\partial h_o/\partial s]^{1/2}};\ K_{oy} = \frac{d_o^{2/3}}{n_y} \frac{1}{[\partial h_o/\partial s]^{1/2}} \qquad (7)$$

Where n_x and n_y are the Manning's roughness coefficients and **s** is the direction of maximum surface-water slope. The surface conductances K_{ox} and K_{oy} are complex functions of the dependent variables d_0 or h_0 ($= d_0 + z$), and the relationships make Equation (6) nonlinear.

The surface and subsurface flow equations are coupled with a third type flux equation as follows:

3.3.3.5.2 Flux exchange equations

The individual surface and subsurface flow equations can be coupled by assuming that the two flow regimes are separated by a thin boundary layer. Thus, Γ_o represents a first-order exchange between the subsurface and surface domains as follows:

$$\Gamma_o = (k_r)_{exch} K_{exch} (h - h_o)/l_{exch} \qquad (7)$$

where $(k_r)_{exch}$ is the relative permeability for fluid exchange, K_{exch} is the surface/subsurface conductance, and l_{exch} is the thickness of the interface layer between surface and subsurface domains. In Equation (7), a positive Γ_0 indicates movement from the subsurface to the surface domain through the interface (A_{interf}). HGS is referred as a fully-integrated globally-implicit

model because the surface-subsurface governing Equations (5) and (6) are solved simultaneously with the coupling provided by Equation (7).

3.3.3.5.3 Actual evapotranspiration equations

In this study, the actual evapotranspiration (AET) is computed following the approach suggested by Kristensen and Jensen (1975).

The evapotranspiration model used in HGS is a rigorous mechanistic process forced by the potential evapotranspiration as a function of transpiration parameters represented by soil moisture, land-use type, and leaf area index (LAI) and rooting depth (Kristensen and Jensen (1975). It is therefore possible to reduce evapotranspiration biases by using mechanistic evapotranspiration model analogue to climate models while being able to apply bias correction to deal with coarse resolution of climate models.

The evapotranspiration model used in this study assumes that evaporation and transpiration affect both the surface and subsurface domain and occurs the same time, when evaporation is a result of the energy penetrating the vegetation cover. The transpiration rate (T_p) is estimated as a function of a set of parameters (Equations 8 - 13) that describe the net capacity of transpiration (Aquanty, 2018).

Equation (8) describes the evapotranspiration rate where f_1 (LAI) is a function of leaf area index [-], f_2 (θ) is a function of nodal water content [-] and RDF is the time-varying root distribution function. Equation 9 express the vegetation term as a linear function of LAI, with C_1 and C_2 representing the transpiration fitting parameters.

The root zone term is expressed by the equation 10, where Lr is the effective root length [L], z' is the depth coordinate from the soil surface and TF represents the root extraction function [$L^3 T^{-1}$] that is linked logarithmically with depth.

The moisture content relationship is provided in the equation 11, were the function f2 is correlating the transpiration rate with the moisture state of the roots and allows taking into consideration the root process in the transpiration rate (Aquanty Inc, 2018). θ is the moisture content, $\theta_{fc}$is the moisture content at field capacity, θ_{wp} is the moisture content at the wilting point, θ_o is the moisture content at the oxic limit, and θ_{an} is moisture content at the anoxic

limit. The transpiration rate is equal to zero below the wilting point moisture content, and increases to its maximum at the field capacity moisture content. The maximum transpiration rate is maintained until the oxic moisture content is reached, and beyond which transpiration rate decreases to zero at the anoxic moisture content.

The evaporation model is defined in the equation 12, where α^* represents the wetness factor and is defined in the equation 8. θ_{e1} Is the moisture content at the end of the energy-limiting stage and θ_{e2} is the limiting moisture content below which evaporation is zero (Allen et al., 1998).

EDF represents the evaporation distribution function that includes the overland and subsurface ow domains. Equation 13, gives the moisture availability term for the subsurface domain. For the overland flow domain, α^* is calculated as varying between unity when the elevation of flow is at or above depression storage zo + HD and zero for a flow elevation at the land surface (zo), therefore representing the reduced evaporative area of available water in the overland flow domain within the depressions.

$$\boldsymbol{T_p = f_1\ (LAI)\ f_2\ (\theta)\ RDF\ (E_p - E_{can}\ )} \quad \textbf{(8)}$$

$$\boldsymbol{f_1\ (LAI) = \max\{0,\ \min[1, (C_2 + C_1\ LAI)]\}} \quad \textbf{(9)}$$

$$\boldsymbol{RDF = \frac{\int_{z'\ 1}^{z'\ 2} TF\ (z')\ dz'}{\int_0^{Lr} TF\ (z')\ dz}} \quad \textbf{(10)}$$

$$f2\ (\boldsymbol{\theta}) = \begin{cases} \boldsymbol{0\ for\ \ 0 \le \theta \le \theta_{wp}} \\ \boldsymbol{f_3\ \ for\ \ \theta_{wp} \le \theta \le \theta_{fc}} \\ \boldsymbol{1\ for\ \theta_{fc} \le \theta \le \theta_o} \\ \boldsymbol{f_4\ for\ \theta_{\theta_o} \le \theta \le \theta_{an}} \\ \boldsymbol{0\ for\ \theta_{an} \le \ \ \theta} \end{cases} \quad \textbf{(11)}$$

$$f3 = 1 - \left[\frac{\theta_{fc} - \theta}{\theta_{fc} - \theta_{wp}}\right]^{C3} \quad (12)$$

$$f4 = 1 - \left[\frac{\theta_{an} - \theta}{\theta_{an} - \theta_o}\right]^{C3} \quad (13)$$

$$E_s = \alpha^*\left(E_p - E_{can}\right)[1 - f_1(LAI)]EDF \quad (14)$$

$$\alpha = \begin{cases} \frac{\theta - \theta_{e2}}{\theta_{e1} - \theta_{e2}} \\ 1 \ for \ \theta > \theta_{e1} \\ 0 \ for \ \theta_{e1} < \theta_{e2} \end{cases} \quad (15)$$

3.3.3.5.4 Groundwater recharge

The definition of groundwater recharge considered is the same approach followed by Erler et al, (2019); wherein groundwater recharge is derived from the HGS output of exchange flux between surface and subsurface domains as described in equations 16 and 17.

Equation 5 describes the groundwater recharge for a terrestrial landscape where there is no standing surface water (i.e., ponds, river, and spring).

$$R = \Gamma_o - (Ss_e + Ss_t) \quad (16)$$

Where R is the groundwater recharge, Γ_o corresponds to the HGS exchange flux between surface and subsurface, and Ss_e and Ss_t are respectively the subsurface evaporation and subsurface transpiration.

With standing surface water such as river or ponds, groundwater recharge corresponds to the HGS exchange flux term (Equation 17).

$$\boldsymbol{R = \Gamma_o} \qquad \textbf{(17)}$$

Since the exchange flux term is calculated after surface evaporation, and when standing water is present, no subsurface evapotranspiration occurs, groundwater recharge equals exchange flux where standing water (i.e., ponds) are present.

3.3.3.5.5 Model conceptualization

The modelled study area covers both the sandstone CT3 aquifer, and the fractured Precambrian basement aquifers. An equivalent porous medium (EPM) approach is considered to represent the fractured aquifer unit in the integrated model. The first motivation in applying an EPM approach is the complexity of the fractured distribution in the study area. The data required to simulate flow in the fractured aquifer (vertical fracture distribution, spacing, and aperture) are not available, and even with these data; the spatial heterogeneity is variable and may not be well represented at the watershed scale. Since this study only focuses on water quantity, we believe that an effective representation of the fracture aquifer unit with the EPM approach is appropriate.

The second reason for applying an EPM approach is that, while HGS is able to simulate flow in discrete fractures, it solves the Brooks-Corey (1964) equation for both porous medium and discrete fractures in the unsaturated flow domain.

3.3.3.5.6 Boundary conditions

The modeled area corresponds to Niamey watershed as delineated by the hydrological watershed of the city and its surrounding villages. No flow boundary conditions were assigned to all outer subsurface model domain boundaries, and groundwater flow divides are assumed to correspond to the hydrological watershed limits. Four additional boundary conditions types were applied to the top surface of the model domain: precipitation, potential evapotranspiration (PET), critical depth and surface water flux. Precipitation and PET were assigned to the top of the model as hydroclimate forcing variables. A critical depth boundary condition was applied at the outer edge boundary of the model at Niamey gauging station to let surface water flow out of the model domain. A critical-depth boundary condition forces the water depth at the boundary to be equal to the ‘critical depth’. The ‘critical depth’ is the water elevation for where

the energy of the flowing water relative to the stream bottom is minimum (Hornberger et al., 1998; Therrien et al., 2005, Hwang et al., 2018). A surface water flux boundary condition was assigned at the most northern point to represent the Niger River inflow coming from upstream which was not generated in the modeled hydrological watershed.

3.3.3.5.7 Model Discretization

The surface domain of the model was discretized into triangular mesh elements with a resolution ranging from 300 m on average to 70 m near surface flow features. The subsurface model consists of triangular prism-shaped elements which are each defined by 6 nodes. The model has eleven layers with a total of 516,901 nodes, and 927,030 elements. In order to represent the surface water-groundwater exchange and evapotranspiration processes more accurately near the top surface, the first three meters were discretized vertically into five layers at 0.1, 0.15, 0.25, 0.5- and 1.5-meters resolution. The interpolated geological materials from the boreholes were used for the remaining six lowest bedrock layers. The digital elevation model (DEM) of 30 m x 30 m was used to assign elevations to the top most 2D layer. The DEM was hydrologically corrected to avoid artificial lakes along stream channels by modifying nodal elevations to decrease from upstream to downstream.

3.3.3.5.8 Calibration Approach

The calibration procedure adopted in this study is done in three steps (Figure 9).

<u>Step 1: Steady State Calibration</u>

The steady state calibration involved forcing the model with a 30 year (1980-2005) long-term average net precipitation and potential evapotranspiration. The net precipitation was calculated based on the increase in average stream flow across the study area (Equation 18):

$$Pnet = (Qin - Qout)/A \quad \textbf{(18)}$$

Where P_{net} is the net precipitation, Q_{in} corresponds to the river inflow, and Q_{out} is the surface water outflow, at the outer edge of the basin. This approach enables us to take into consideration the inflow part of the river hydrograph that is not generated due to local precipitation, and also to better represent the river aquifer interaction at the early stage of the model calibration.

Step 2: Dynamic Equilibrium

The second model calibration step is intermediate between steady state and daily transient simulations referred here as dynamic equilibrium. It consists of forcing the model with monthly normal precipitation and PET and while using steady state results as initial conditions. Essentially, the long-term hydro climate forcing data (1980-2005) used to force the model are aggregated into one synthetic year of twelve months, representing the average seasonal cycle. The monthly normal forcing data are considered to represent the long-term average seasonal cycle. This forcing data is repeatedly applied to the model until dynamic equilibrium is achieved. Dynamic equilibrium is determined to have been reached when no significant variations of the river and groundwater hydrographs are observed from year to year. This approach has the advantage of training the model from theoretical steady state to a more naturally occurring transient conditions represented by the monthly normal forcing. It is particularly important for the dry climate conditions, where monsoonal intermittent precipitations are driving the hydrological cycle and will allow for providing reasonable initial conditions to the daily transient simulations. The dynamic equilibrium is considered here to be a transitional state much closer to natural equilibrium than a traditional steady state condition (Erler et al., 2019).

The model state at the end of the dynamic equilibrium is then used as an initial condition for the daily transient simulations. The daily transient is run for the period of 2011-2017 where continuous groundwater observation data are available. Manual calibration was performed by trial and error until a satisfactory match was achieved between simulated and observed groundwater heads and surface water flow rates.

Step 3: Daily Transient Calibration

The initial conditions at the end of the dynamic equilibrium are then used to force the model for the daily transient simulations. The daily transient is run for the period of 2011-2017 where continuous groundwater observation data are available. Manual calibration was performed until a satisfactory match was found between simulated and observed groundwater head, and surface water flow rate.

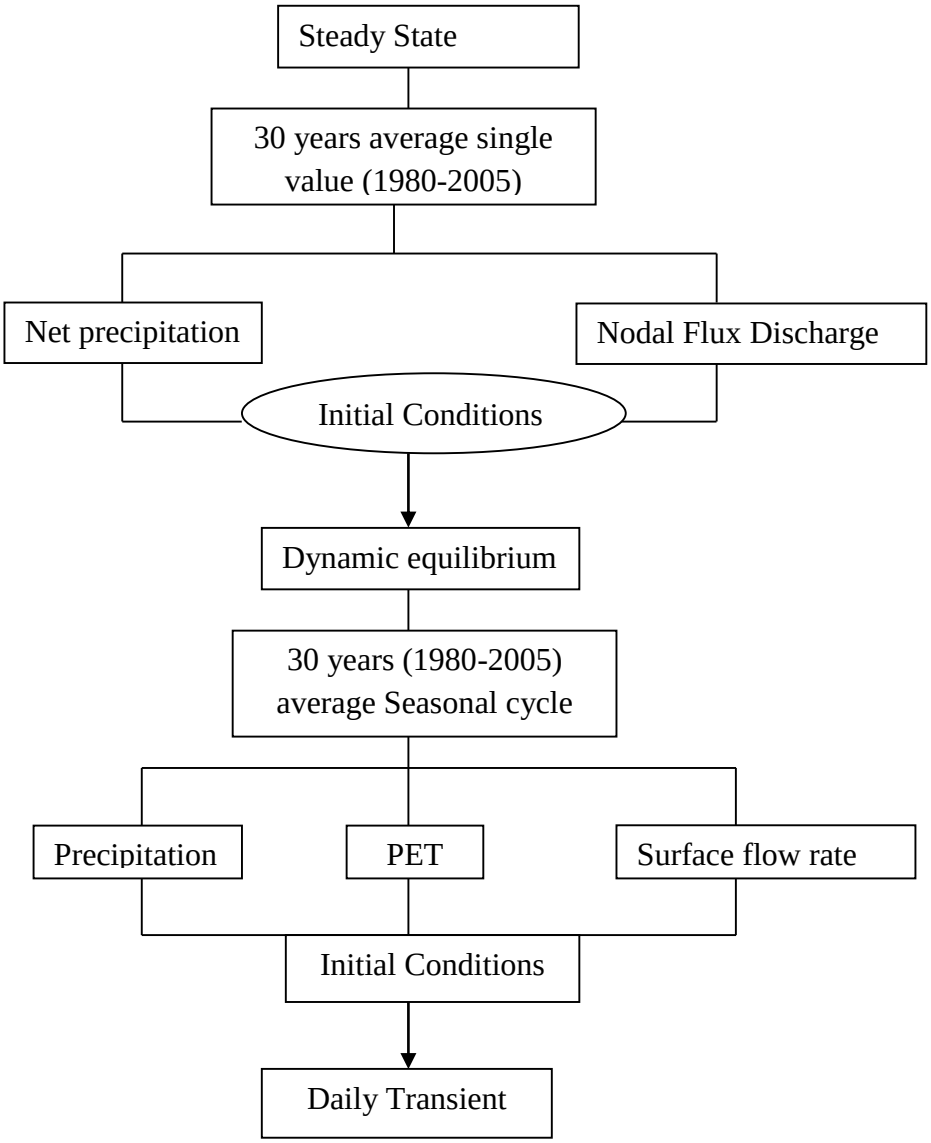

Figure 8: Calibration method flow chart

3.3.3.6 Integrated Hydrological modeling of climate change impacts

3.3.3.6.1 Observed historical hydro climate forcing

The model was forced in daily transient simulations using a 30 years (1980-2005) observed precipitation, maximum and minimum temperatures (Tmax, Tmin) data of Niamey Airport station provided by the Direction de la Meteorologie Nationale (DMN). Potential evapotranspiration was calculated using the Hargreaves method, described in Equation 19.

$$\boldsymbol{ET_{o=}\ 0.0023\ \times\ 0.408\,RA\ \times\left(T_{avg}\ +\ 17.8\right)\times TD^{0.5}} \qquad \textbf{(19)}$$

Where ET_o is the reference evapotranspiration, RA is extraterrestrial radiation expressed in (MJ m−2 d−1), T_{avg} is the average daily temperature (°C) defined as the average of the mean daily maximum and mean daily minimum temperatures, is the temperature range, estimated as the difference between mean daily maximum and mean daily minimum temperatures, and 0.408 corresponds to the constant used to convert the radiation to evaporation equivalents in mm. Hargreaves reference evapotranspiration method is recommended in area where there is no sufficient data to compute Penman montheith reference evapotranspiration (Droogers and Allen, 2002).

The Niamey gauging station was used to calibrate the model for surface water flow using 30 years (1980-2005) daily stream flow data provided by the Niger Basin Authority (NBA).

A total of 25 groundwater observations wells were previously used for steady state groundwater heads calibration for the 1980-2005 period. No continuous transients groundwater heads observations data are available for the 1980-2005 simulation period, and the model was previously calibrated for 2012-2017 period. However, groundwater punctual heads measurements were reconstituted from historical measurements performed during the 1980's, at the construction of the boreholes. While uncertainly related to groundwater models may be important between calibration and predictions periods, these uncertainties are considerably reduced for physically- based models even with different climatic conditions between calibration and prediction periods (Moeck et al., 2018). Therefore, the physically based HGS's simulated groundwater heads for the 1980-2005 periods could be used to predict climate change impacts on groundwater based on HGS calibrated simulation of 2012-2017, in absence of observations, with relatively less uncertainties.

3.3.3.6.2 Climate projections and Bias Corrections

Two regional climates models of CORDEX experiments, and one high resolution regional climate model (RCM) of West African Science Service Center on Climate Change and adapted land use (WASCAL) experiment were selected to predict climate change impacts on groundwater resources in the study area under the RCP 4.5 (Representative Concentration Pathway) scenario. The use of the RCP 4.5 was motivated by the limited computational resources available and also considering the fact that the differences between RCP 4.5 and 8.5 become important only beyond 2040 period (Heinzeller et al., 2018). The regional climate models of CORDEX were selected from a set of 18 GCM- RCM combinations accounting for 10 forcing GCMs and 5 RCMs with a resolution of 50 km. CANRCM4-CANESM2 and RCA4-IPSL-CM5A are the two RCMs selected from the CORDEX based and on their ability to reproduce the hydrological cycle in the Niger River basin. The metrics used to evaluate the models are well described in Mascaro et al. (2016).

The WASCAL WRF-GFDELM-ESM2M at 12 km resolution was selected in order to compare the added value of the high resolution WRF-GFDELM-ESM2M to the coarse resolution CORDEX models (CANRCM4-CANESM2, RCA4-IPSL-CM5A. For the three RCMs, basin average simulated rainfall; maximum and minimum temperatures were calculated from the grid points intersecting the basin as a weighted mean, proportionally to the area of the intersection.

Hydrological impacts of climate change are typically evaluated using dynamical or statistical bias corrected climate output to force the hydrological models (Erler et al., 2019; Goderniaux, 2015; Barthel and Banzhaf, 2015).

Dynamical downscaling involves use of physics-based, regional climate models with relatively high resolution than the forcing GCM and where the relevant climate local features are directly resolved. High resolution dynamically downscaled RCMs are computationally expensive, which limit their use in large scale hydrological impact studies (Goderniaux et al., 2011; Erler et al., 2019).

Statistical bias correction is performed based on predictor fields derived from observed local climate that transform the simulated climate outputs data in order to match statistical properties of local climate data. The calibration between statistical properties of local climate data and the RCMs is usually done for the historical or control period, where observed data are available,

and then calibrated fields predictors are applied to the predictions period derived from the climate projections.

However, the widely used statistical bias correction method in hydrological climate impact studies assumes a stationary bias between the RCM and local climate. This constitutes the major drawback of applying stationary assumed statistical bias correction method due to potential errors it may introduce in impacts studies (Hanel et al., 2017; Chen et al., 2015).

In order to reduce potential errors associated with the stationary assumption, historical and projected climate output from the 3 RCMs were bias corrected to observed climate station of Niamey Airport using two different methods : standard quantile mapping calibrated at daily time scale and multiscale bias correction calibrated at daily (D1), monthly (M1), seasonal (M3) and annual (Y1) time scale. The multiscale bias correction method is a new statistical downscaling method developed by Hanel et al., (2017) to reduce the stationary bias introduced by the majority of the statistical bias correction methods. The method uses standard quantile mapping method iteratively at multiple combined timescales (daily, monthly, and annual) as described in the equations 20 and 21 respectively for precipitation and temperatures variables (Hanel et al., 2017).

$$\boldsymbol{X^{M}_{s[0]}t(0) = X^{C}_{s[0]} \prod_{i>0} \frac{X^{C}_{s[i]}\ t(i)}{X^{A}_{s[i]}\ t(i)}} \qquad \textbf{(20)}$$

$$\boldsymbol{X^{M}_{s[0]}t(0) = X^{C}_{s[0]} \sum_{i>0} \frac{X^{C}_{s[i]}\ t(i)}{X^{A}_{s[i]}\ t(i)}} \qquad \textbf{(21)}$$

Where $X^{M}_{s[0]}$ represents the variable to be corrected iteratively at different time scales $S = S[0], [S1], S[2]$ ... with $S[0]$ representing the original time scale. The $X_{s[i]}$ correspond to the time series in which X is aggregated into $S[i]$ scales, and is independently corrected for every time scale using the standard quantile mapping bias correction method. Therefore, $X^{C}_{s[i]}$ representing the resulting precipitation time series corrected at multiple time scales.

Values at different time scales $S[i]$ can be found by aggregating the corrected variables from the closest smaller time scale such as $X^{A}_{s[i]} = A\left(X^{C}_{s[i-1]}\right)$ with A equals to the Somme

from $S[i-1]$ to $S[i]$ and the elements of the time series at the original are specified by temporal index corresponding to $t_{s[O]}, t_{s[1]}, t_{s[2]} \ldots\ldots$

Therefore, comparison between the standard quantile mapping (Gudmundsson et al., 2012) and multiscale bias correction (Hanel et al., 2017) methods was then performed to choose the best bias correction method.
Statistical downscaling was applied to historical (1980-2005), and Mid-century (2020-2050) periods for each climate model, resulting in a total of six (25 and 30 years) daily transients simulations.

3.3.3.6.3 Validation of historical and projected climate change simulations

To validate the historical hydrological simulations, depth to groundwater table and groundwater heads will be used as metrics for the validation of the subsurface component of the HydroGeoSphere.

While groundwater recharge is a useful variable for hydrologist and scientist, in climate studies, herein depth to groundwater table is used as metric. This is because this variable is of great interest for water resources managers in the study area where information of depth to groundwater table is crucial for drilling and managing water supply wells for both drinking and agriculture purposes. The elevation of the depth to groundwater table is calculated in HGS as a linear interpolation of the pressure head at a null pressure level. Depth to groundwater table is then derived from subtraction between the elevation of the groundwater table and surface elevations calculated from the Digital Elevation Model (DEM).

Bias in mean depth to groundwater table is used to validate historical simulations and is calculated herein as the difference between simulated observed historical and simulated historical climate scenario for the three RCMs considered.

Considering the validation of historical HGS simulations for surface water component of the integrated hydrological models, surface water flow rates at Niamey gauging station are used. But, for projected climate change impacts on surface water flow rate, the Minimum Environmental flow of Niger River at Niamey is used as metric. As previously stated, the Niger River is the sole surface water source from which water is continuously pumped in order to

provide drinking and irrigation water for population of Niamey city. Therefore, even though directions and guidance on projected climate change impacts on river discharge still useful information, in this study, a minimum environmental flow is used as a variable to assess climate changes impact on surface water. The Minimum Environmental Flow (MEF) is defined as the minimum flow rate of the River at Niamey, required to satisfy the drinking and agriculture water demand. Herein, the required minimum low flow value considered for Niamey is $55 m^3/s$ for 10 days average period, as defined in the 2005 reference period (Grijsen et al., 2013). To assess occurrence and duration of the MEF by the end of the mid-century period (2020-2050), we develop a python command line tool that takes as input an HGS hydrograph file, resample it to daily average values, and count the occurrence and duration of low/high flow. The python command line tool is freely available on GitHub: https://github.com/aerler and the source code of the command line tool are provided also.

MEF duration and occurrences are assessed under historical runoff (1980-2005), where the mid-century runoff is kept to the historical levels, and under 10 % runoff reduction scenarios where runoff conditions are considered to be reduced by 10 % compared to historical levels.

3.4. Conclusion of Chapter 3

The first Chapter of this thesis has shown that both surface water and groundwater represent together, not only important resources, but vital for the socio-economic activity of the study area. In the second chapter, the complexity of geological and hydrogeological conditions highlighted the need of using integrated methodological approach to provide a scientifically based water management decision making tool. While the multidisciplinary approach employed herein and presented in the third chapter may provide useful information and an added value on the results reliability, it also shows the challenge of sparse data and modest computing resources.

Chapter 4: Geological and Hydrogeological Characterization

In this chapter, geologic and hydrogeological field's investigation results will be presented. This includes the geological mapping, 2D hydrogeological cross sections realized, 3D geological model results as well as fractures directions and intensity. A conceptual model will be defined based on the above results, and this conceptual model will be used in the next chapters for the integrated hydrological modelling.

4.1 Geological and hydrogeological setting

The 2D cross-sections drawn over the study area from the borehole logs and geological map (Figure 9) provides a general geological setting within the study area. The NW-SE (A-B) and N-S (C-D) oriented cross sections show four main hydrogeological units, in accordance with the geological maps (Figure 9). The formations are composed of the granitic Precambrian basement formations, the greenstones rocks belts Precambrian basement formations, the undifferenced weathered layer of granitoids and greenstones, and the CT3 formation. Locally, there are also thin alluvial formations, and quartzite formations (Figures 10, 11).

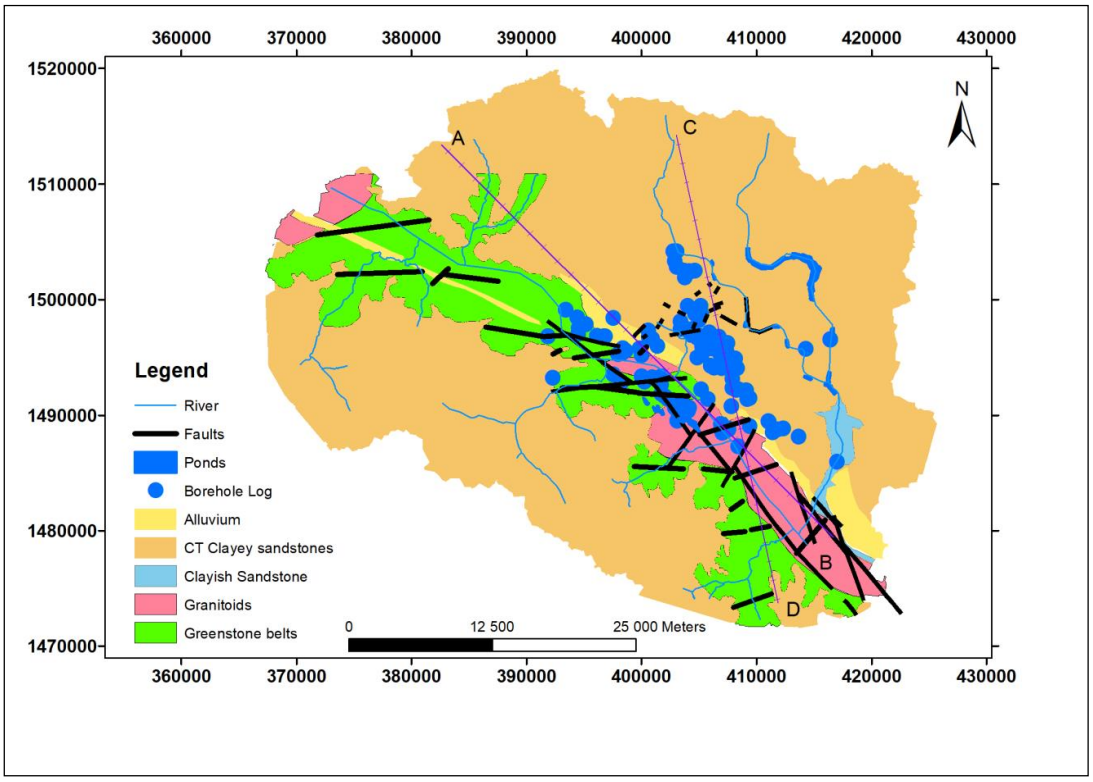

Figure 9: Boreholes log and local geological context of the study area

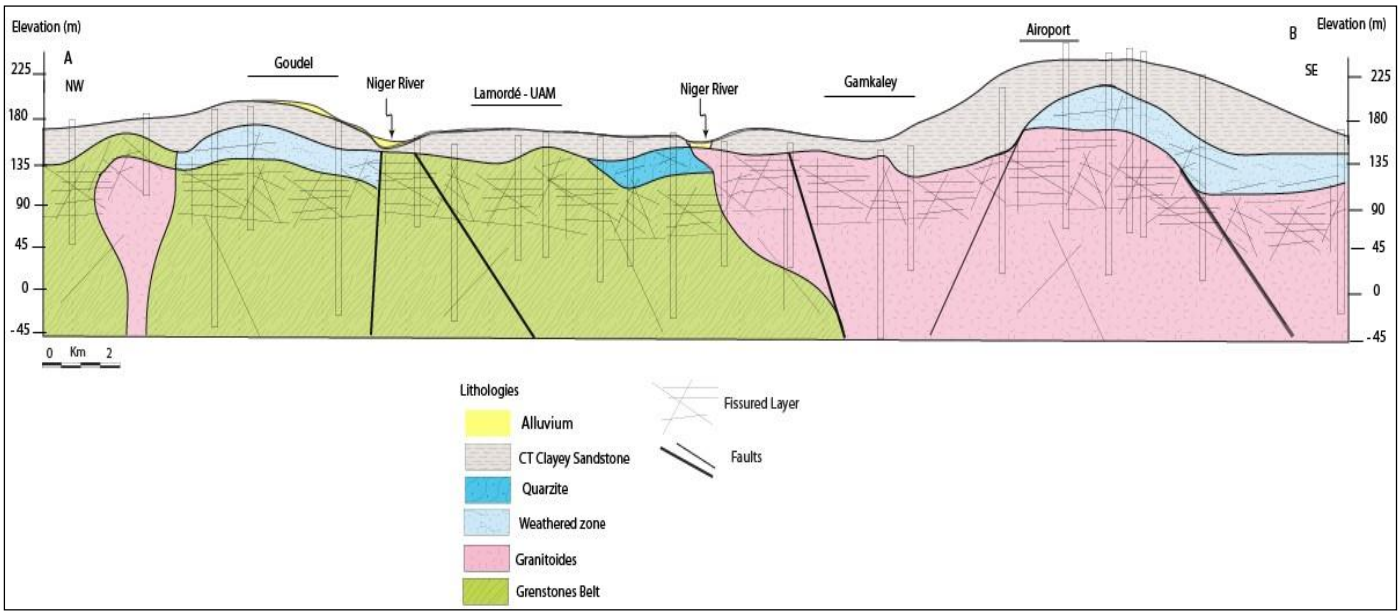

Figure 10: NW-SE geologic cross section

The NW-SE oriented cross section (Figure 10) shows that the basement is mainly composed of granitoids Precambrian formations in the SE part of the study area, while in the NW, the predominant formations are of the greenstone's belts. Theses greenstones belts are mainly composed of metabasit and metasediments locally cut by intrusive gabbros and granites. Both granitoids and greenstones belts represent important water bearing formations in the study area. The Figure 10 also shows schematically an important weathered zone in the SE part, under the granitoids as well as in the NW, beneath the schist formations of the greenstones belts. The CT3 clayey sandstone formation thickness is greater in the SE than in the NW part of the study area (Figure 10).

The N-S oriented cross section (Figure 11) displays the same geological pattern of the Precambrian basement formations as the NW-SE cross section. However, the CT3 clayey sandstone formation thickness is shown to decrease from the south toward the northern part of the study area.

Both NW-SE and N-S cross sections (Figures 10 and 11) show that the alluvial formation is not continuous over the study area, and when the formation is present, its thickness seems be small.

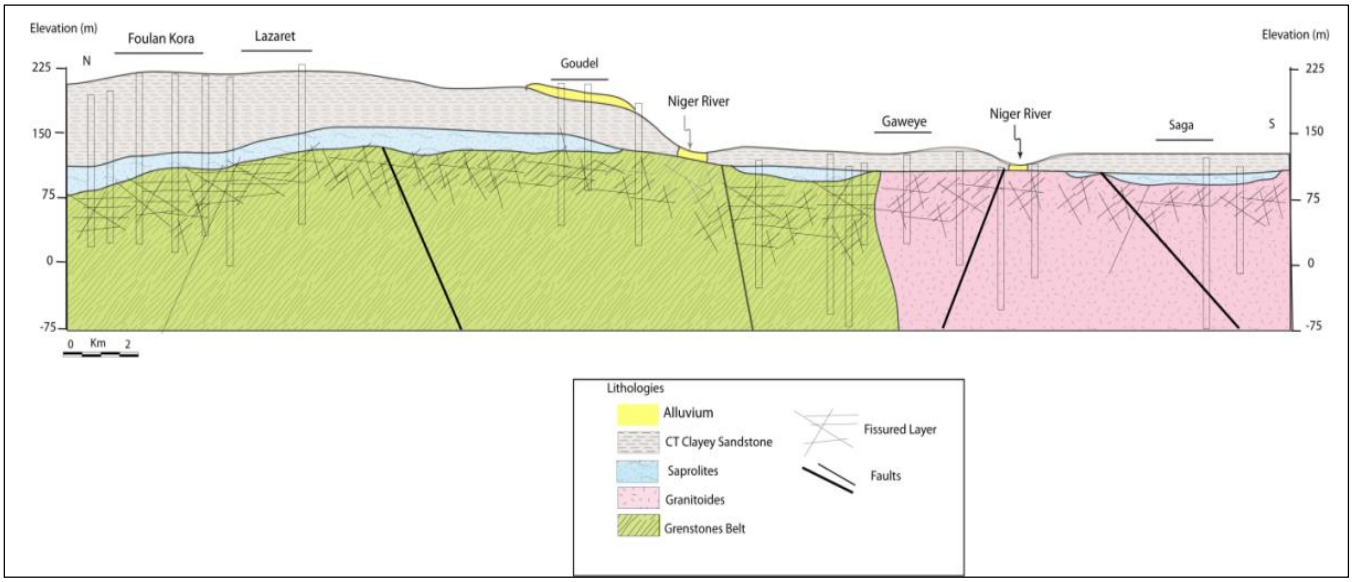

Figure 11: N-S geologic cross section

4.2 Structural characterization and fractures intensity

Outcrops from the greenstones belts and granitoids formations were investigated in the study area. Considering the greenstones belts formations, two main types of deformations were observed, opened and quartz filled fractures and schistosity more or less folded affecting both the schists (of greenstones belts) and their weathered horizon (Figure 12). The majority of fractures measured in the schists outcrops were opened fractures (Figure 12). Few of the fractures were observed to be filled with quartz mineralization (Figure 12) that may occur during the alteration process. This quartz mineralization suggests fluid circulation process that has taking place during the different tectonic deformations phases involving an increase in the induced permeability of the greenstone belt formations.

A- Opened fractures in an altered schist formation

B- Opened fractures in schist formation

C. Refolded schists

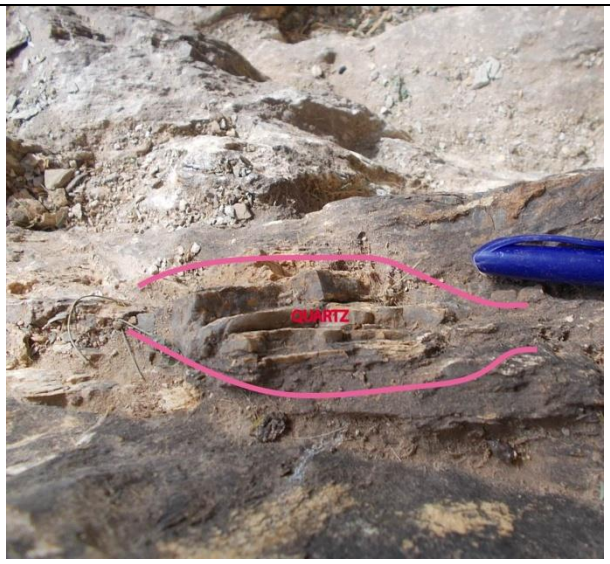

D. Schistosity plan on altered and folded schists

Figure 12: Different fractures shapes on schist outcrops

The outcrops of the schists formations are intensely fractured (Figure 12) and geometrical characteristics of fractures (directions and dips) were measured. The fractures networks of the schists formations measured from the entire outcrops accessible in the study area present quite complex patterns with different fractures sets (Figure 13). The measured fractures were projected altogether onto the equal area stereonets. The contoured equal area nets of fractures in the schists (Figure 13 a) used to identify the fractures sets and their mean orientation represented as great circles (Figure 13 b) show four major fractures set networks. The fracture set F1 has a mean direction of 64 °N with a steep dip angle of 77°. The F2 fracture set has a mean direction of 63°N with the steepest dip angle of 84°. These two fractures sets have very close strikes values and steep dip angles. The fractures set F3 and F4 have nearly identical shallow dip of 47° and 38° with different strikes values of 44°N to 140°N respectively.

The four fracture sets of the schists outcrops could be grouped in one global and main pattern represented by the Pi-Plane great circle. This Pi-plane has a mean strike of 150°N and a moderate dip of 63°, corresponding to the NW-SE direction. The NW-SE direction corresponds to the major direction of the first ductile to semi-ductile deformation event associated to the diachronous crustal block collage in the birrimian greenstone belts of the Liptako (Soumaila and Konaté, 2005). This direction corresponds also to the main flow direction of the Niger River (Soumaila, 2000, Bonnot et al., 1998).

.

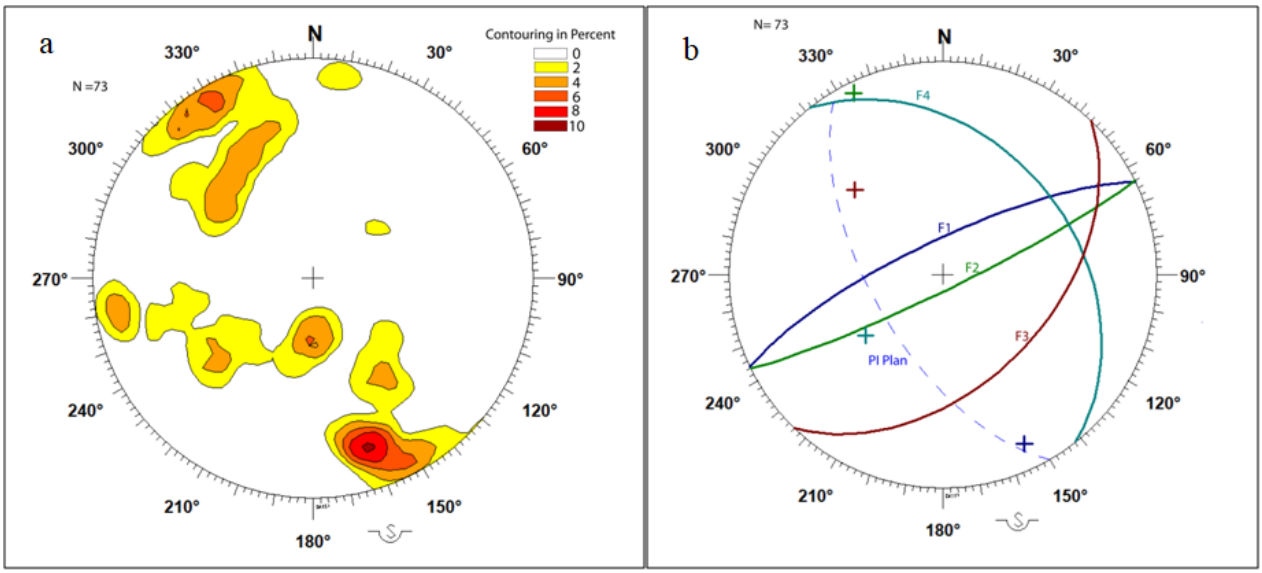

Figure 13: Contoured equal stereonets of fractures data on greenstones belts rocks outcrops (a), and great circles showing the main orientation of the fractures sets (b)

The complex and intense fracture system of the greenstone belt associated with the alteration level constitute major elements inducing important secondary permeability of the schists formation, and therefore allowing them to be a transmitive water bearing formations in the basement context.

Considering the granitoids basement formations, outcrops observations reveal an important weathered zone horizon of up to 25 m tackiness (Figure 14). The importance of basement alteration process provides thickened alteration horizon that constitutes a potential aquifer formation. Outcrops investigation also reveals that the main types of structural deformations elements affecting the granitoids basement formation are opened fractures, micro faults, as well as quartz filled fractures (Figure 14). The fractal deformations on micro faults mirror as well as the quartz crystallization of the fractures show not only the intense deformation process of granitoids formations, but also important fluids circulation process through the fractures.

Fractures data collected on the granitoids formations show various geometrical characteristics. The great circle of the fractures network (Figure 15 a) derived from the countered equal area stereonets (Figure 15 b) show four main fracture sets (Figure 15). The fractures set F1 and F2 have nearly identical strikes of N109° and N106° respectively. They also have the steepest dips angle of the fractures networks corresponding to 84° and 90° for F1 and F2 fractures set, respectively. The fractures set F3 and F4 present nearly identical dip angle values of 34° for F3 and 39° for F4. These fractures set show the shallowest dip angle values, while their strike values range from N46° for F3, to N49° for F4 (Figure 15). Similarly, to schistes formations, granitoids formations fractures set were also grouped in one main directional and dip angle pattern provided by the Pi-Plane, which has the strike value of N26° and a dip angle of 76°. The strike value of the Pi-Plane corresponds globally to the NE-SW direction, that has been described as the trending stretchening event associated to the brittle deformation event that has resulted in the emplacement of the dolerite dykes (Soumaila and Konaté,2005).

This intense and interconnected fractures network induced a secondary porosity to the granitoids formations, and makes them an exploitable water bearing formations.

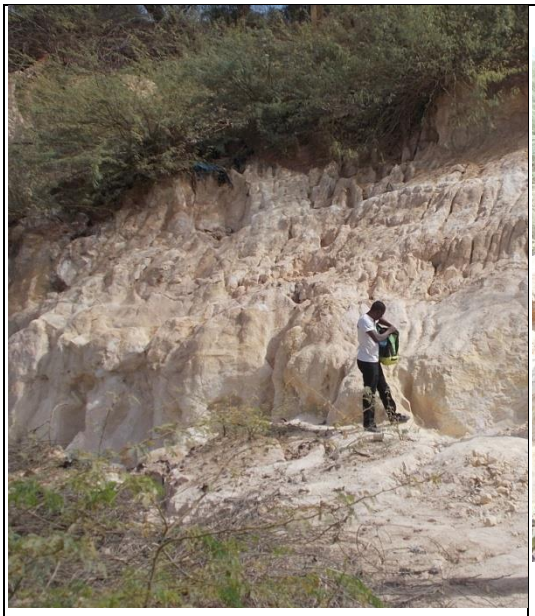

A- Thickened Granitic Weathered zone

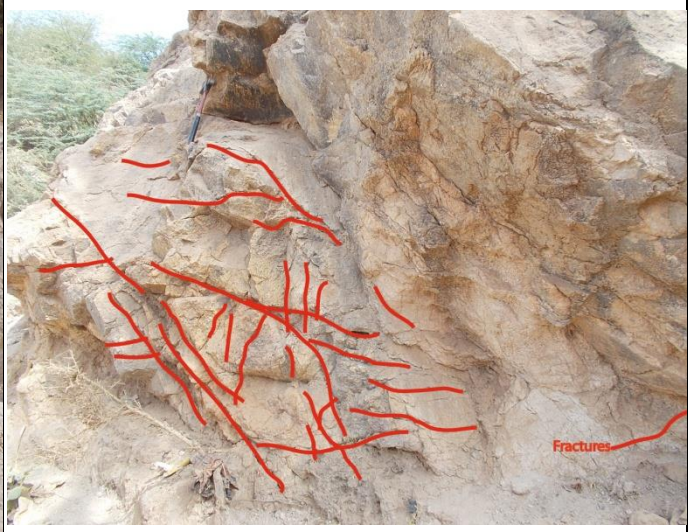

B- Opened fractures in granitic formation

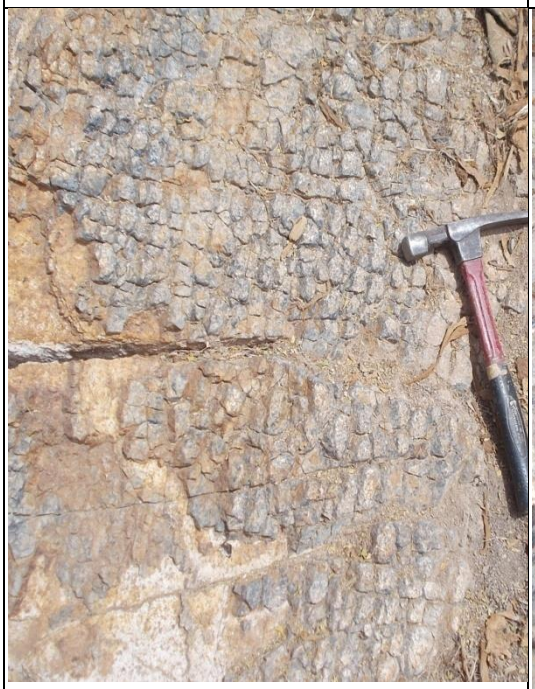

C. Fractal deformation on granitic fault mirror with quartz crystallization

D. Fracture filled with quartz in granitic formation

Figure 14: Fractures characteristics on granitoids outcrops

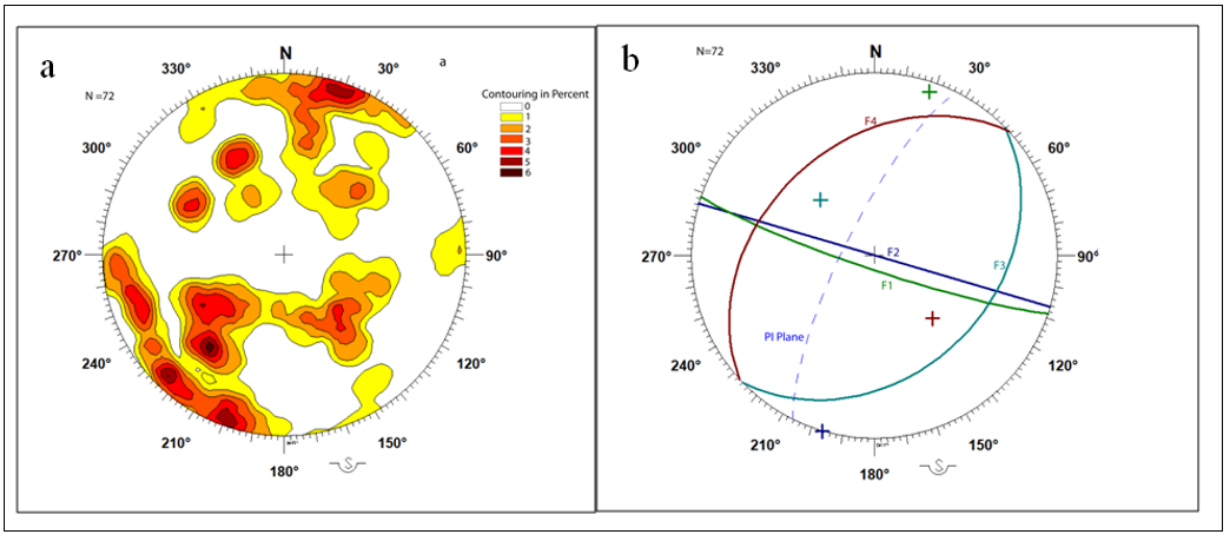

Figure 15: Contoured equal stereonets of fractures data on granitoids outcrops (a), and great circles showing the main orientation of the fractures sets (b)

In terms of structural directions, the fractures sets could be summarized in three majors fractures families for greenstones belts and granitoids formations:

- ✓ ***Fractures System S1= N140° to N150° (NW-SE)***
- ✓ ***Fractures System S2= N100° to N110°***
- ✓ ***Fractures System S3= N60° to N70° (NE-SW)***

The ***NW-SE*** direction corresponds to the major structural direction and is also the global direction of the Niger River *(*Soumaila and Konaté, 2005*).* The NE-SW direction, has been described as the major foliation direction.

Fields measurements of fractures spacing and opening, combined with structural and geological maps (Bonnot, 1998; Machens, 1973) were used to calculate the fracture intensity of both greenstones belts and granitoids Precambrian basement formations. Fracture density ranges from 0 to 163 fractures segments per square kilometers (Figure 16). The high fracture density values highlight the intense deformation process of the Precambrian basement formation.

Therefore, considering the important weathered zone profile of the greenstones belts and granitoids formations, the weathered zone is considered to be a distinct and individual water bearing formation. Also, the eight different fractures set characterized on the outcrops of greenstones belts and granitic formations, as well as the intense and dense fracturation network

lead to consider both greenstone belts and granitic formations as individual and distinct aquifers. Furthermore, the various types of fracture sets, and their interconnection show the complexity of the fractures distribution system, and a more simplified hydrogeological conceptual model is need to understand the different aquifer hydrodynamic.

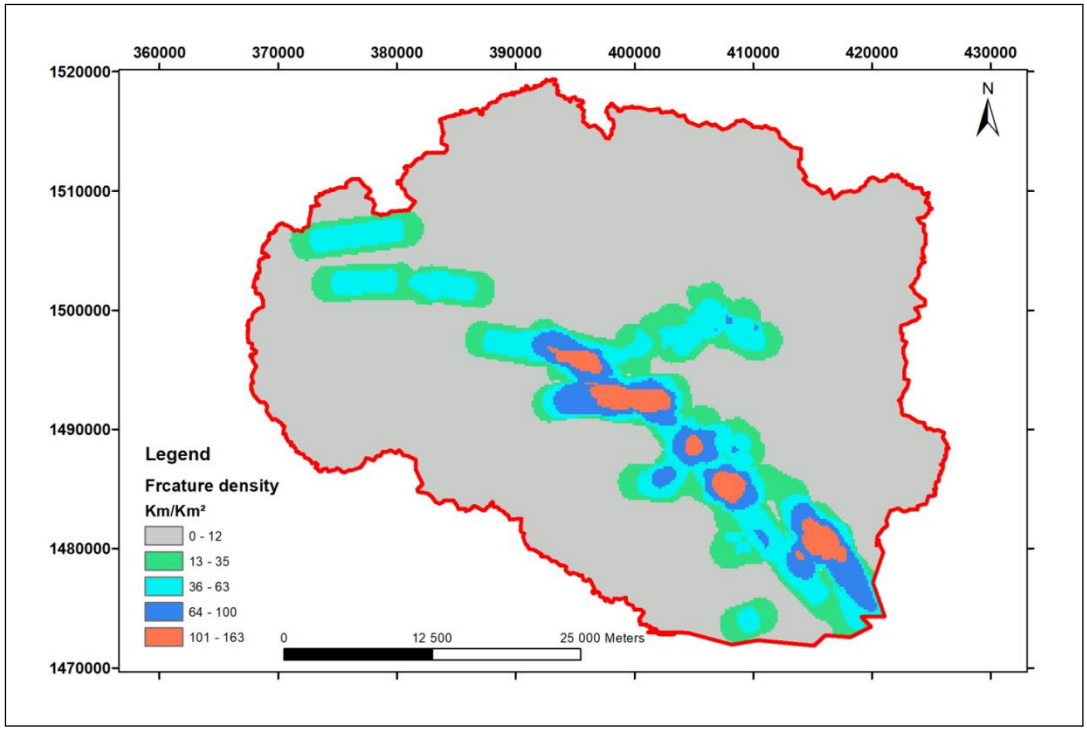

Figure 16: Fracture density map

4.3. 3D Hydrogeological conceptual model

The conceptual geological model (Figure 17) is composed of four hydrogeological units. The CT3 unit is represented at the top of the conceptual model and considered to be in hydraulic connection with the alluvial aquifer. The CT3 is conceptually represented by three different geological facies of clay, clayish sandstones, and silty sand. The fractured aquifer is characterized by three different units: The granitic formations are intrusive into the birrimian greenstones belts formation. However, this geological configuration is simplified in the conceptual model (Figure 17) by considering the granitic aquifer at the bottom of the model and the greenstones belts formations aquifer at the top of the granitic layer. The third aquifer is

composed of the weathered formation, consisting to the undifferentiated weathering horizons of both granites and schist formations.

Also, another approach for defining the conceptual model would have been to consider the CT3 geological layer and the weathered zone has single aquifer. However, the main drawback of this simplification resides in the hydraulic conductivities' differences between the two geological units.

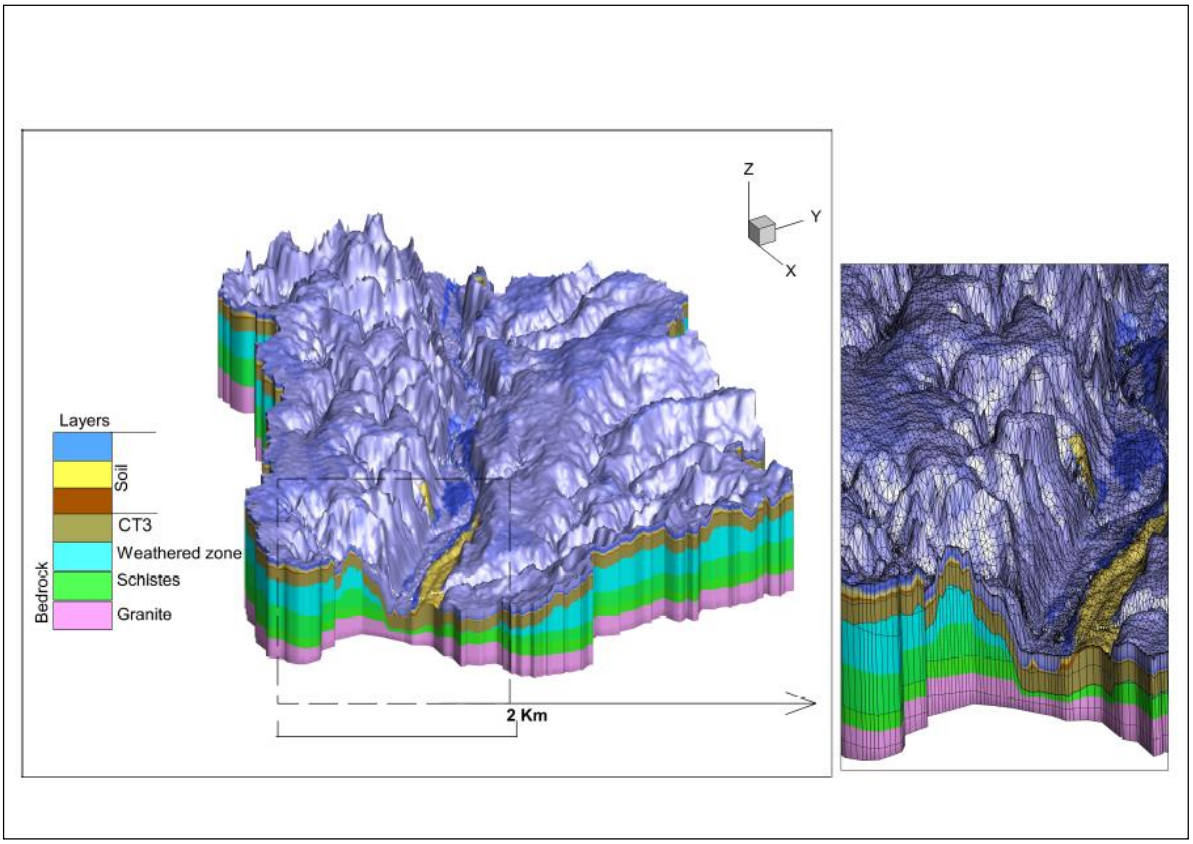

Figure 17: 3D surface-subsurface hydrogeological conceptual model of the study area

4.4 Conclusion of Chapter 4

The geological characteristics of the sedimentary and fractured aquifers formation presented in this chapter highlighted the complexity and heterogeneity of the aquifer system in the study area. Therefore, a more simplified conceptual hydrogeological model was developed in order to represent the complex hydrogeological system and quantify the integrated interaction between this system and surface water resources as well as the climate change impacts.

Chapter 5: Hydrochemicals and isotopes characterization

In this chapter hydrochemicals and isotopes analytical results will be used to determine the origin of water source of the different aquifers, the major hydrochemicals process controlling the hydrochemicals facies as well as groundwater surface water interactions. The isotopes and major elements hydrochemicals characteristics will be analyzed, and an integrated conceptual model of groundwater surface water interaction will be presented.

5.1 Quality control and Physico-chemical characteristics

The spatial distribution of the analytical water samples is shown in the Figure 18 and they are composed of alluvial aquifer, the Continental Terminal aquifer (CT), the GreenStones Belts Formations aquifer (GSBF), the Granitoids Basement Formation aquifer (GBF) and Surface Water (SW) water.

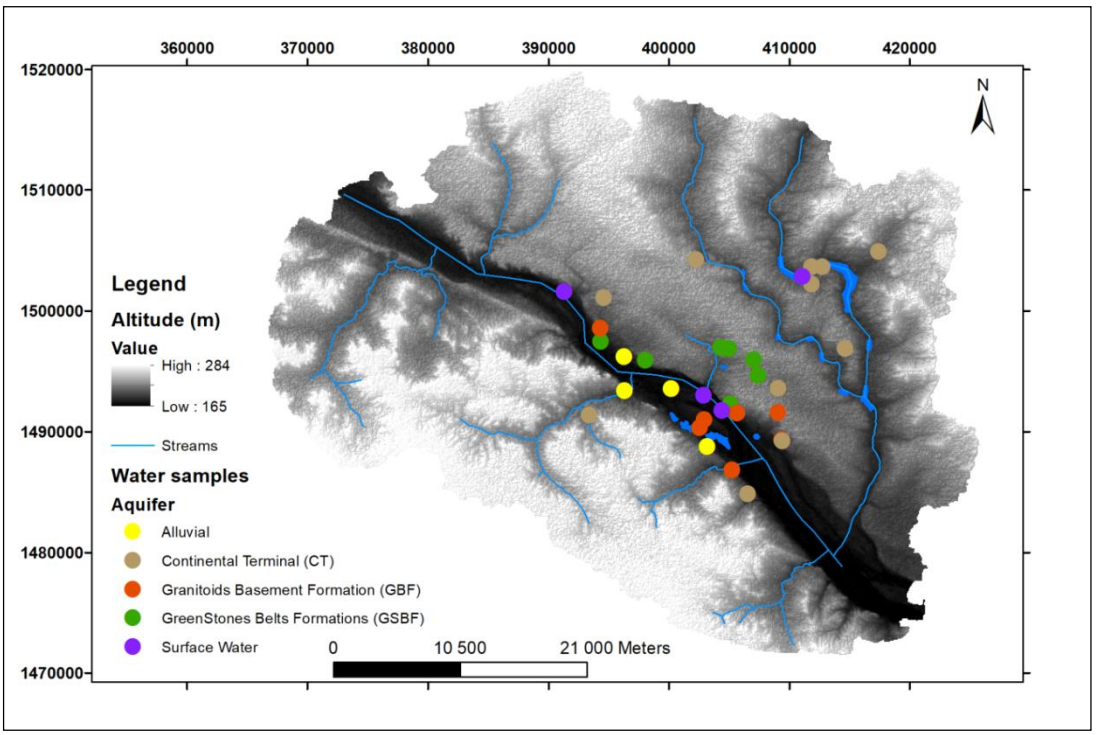

Figure 18: Spatial distribution of analytical water samples

The dataset was qualitatively assessed based on charge balance error (CBE). The CBE errors calculated for all the samples are less than 5% with only one groundwater sample that recorded a CBE value of 7%. The range of CBE values calculated (less than 10%), are considered herein to be acceptable, as only high CBE values greater than 10% are considered to be indicative of sampling, analytical or data entry errors (Gûller et al.,2002; Guggenmos et al .,2011).

For all the three (3) sampling campaigns composed of 140 water samples, there was not significant differences between the campaigns, and therefore average values are considered in the analysis. For all the sampling campaigns, the average pH values range from 6.5 to 7.3 with less variability between the different aquifers and surface water sources. The mean temperature values measured are 27°C for surface water, 30°C for both the CT and alluvial aquifers, and 32°C for the GSBF and GBF aquifers. The temperature differences between the different water sources are related to their respective depth, with the surface water and shallow aquifers (alluvial and CT) being the most influenced by the air temperatures than the basement aquifers (GSBF, GBF) that are more or less confined.

Throughout the year, the mean Electrical Conductivity (EC) values range from 52 µs/cm to 616 µs/cm for the different water sources. The EC values are of 52 µs/cm, 550 µs/cm, 225 µs/cm, 494 µs/cm, and 494 µs/cm for the SW, Alluvial, CT, GSBF and GBF surface water sources respectively.

5.2 Exploratory chemical data analysis

For most of the multivariate statistical methods that will be used in the next sections, it is interesting to test the normality assumption of the chemical data distributions (Guggenmos et al.,2011), and also identity potential outliers within the data. Therefore, the normal probability plot for the EC, Na, K, Ca, Mg, HCO3, Cl and SO4 and NO3 variables are shown in Figure 19. The variables values represented in the y axis are plotted against the quantile of a normal distribution (Figure 19). Most of the variables seem to deviate from the linearity, suggesting that their respective distributions do not satisfy the assumption of the normal distribution as expected in most geochemical data behavior (Reimann and Filzmoser, 2000). Moreover, only EC, Ca and Mg show only one potential outlier in the data, and the entire remaining variable have more than 2 potential outliers. Also, the presence of slope changes and breaks in the individual plots suggest that different types of process are involved in the current values of the variables, and multiple source origin could be used to explain the behavior of the data.

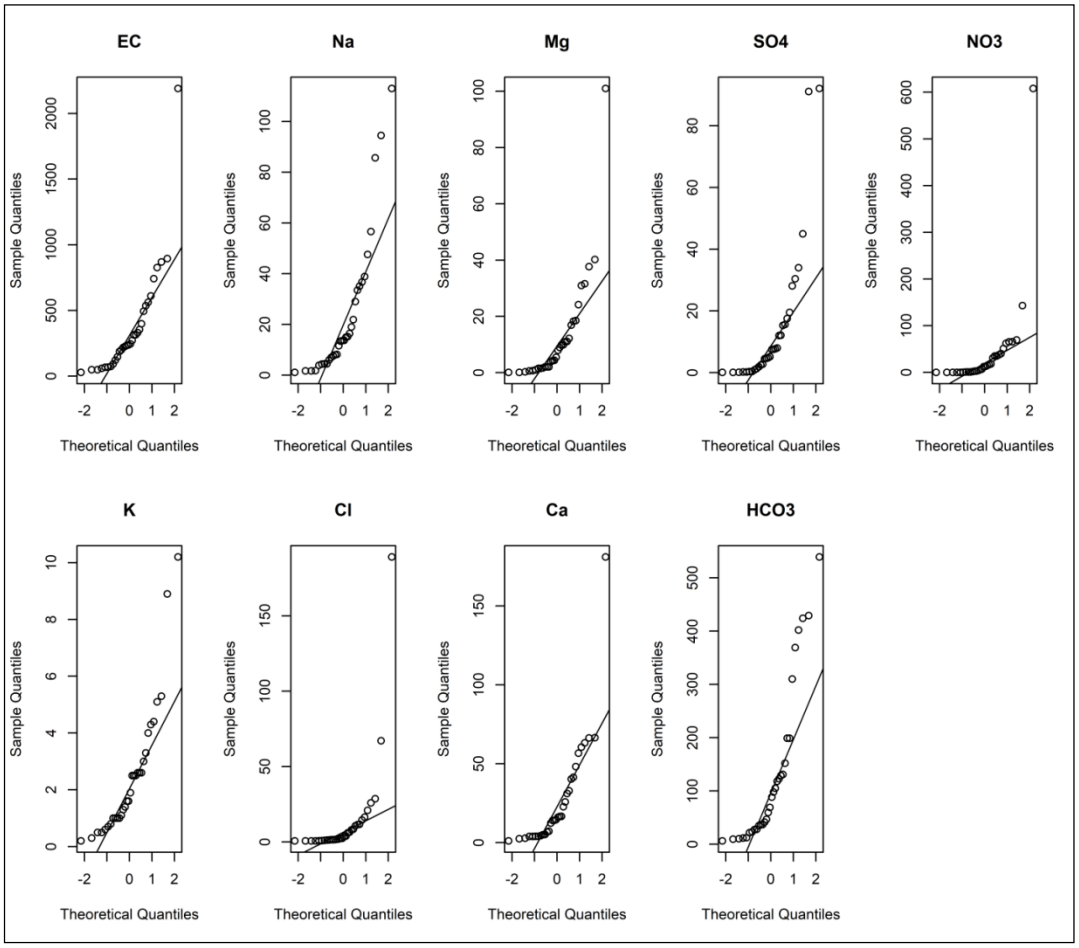

Figure 19: Normal probability plot of the EC and major ions

However, the univariate analysis of the separate variables does not necessarily mean the data do or do not follow a multivariate normal distribution (Everitt and Hothorn, 2011).

Therefore, the ordered distances against the corresponding quantiles of the 9 variable chi-squares are plotted (Figure 20 a) before and after the log transformation (Figure 20 b). The Figure 20a shows that the data do not satisfy the normal distribution assumption, as they clearly deviate from the straight line through the origin, but rather approach more likely a lognormal distribution (Figure 20 b) as stated in many geochemical data behavior (Reimann and Filzmoser, 2000).

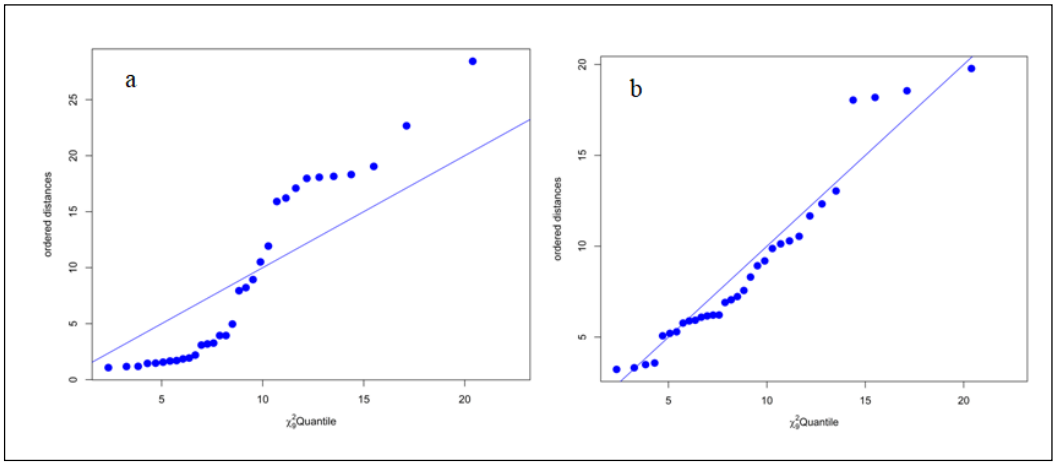

Figure 20: Chi square plot of the generalized distances of hydrochemicals data: a) before the log transformation, b) after the log transformation

The exploratory analysis has highlighted that the data obviously present outliers, and are their chemical characteristics probably originate from more than one source and therefore further multivariate statistical analysis is required to determine sources and explain the origin of the sources. Figure 21 shows the identified outlier's locations highlighted in red circles. These outliers correspond to the Bassora and CSI Gaweye samples, and are respectively from the CT and GBF aquifers. These samples recorded abnormally high concentrations values of EC of 613 µs/cm and 2190 µs/cm respectively. Their respective chloride values of 67 mg/l and 188 mg/l are also high compared to the average values of others samples. Field observations performed during the sampling campaigns showed that the Bassora sample was collected from opened and abandoned well, and thus vulnerable to point sources pollution. This well happened to have bad sanitation conditions. For the CSI Gaweye water sample, though it was collected from closed borehole, conditions around the borehole were characterized by human and animal fecal discharge. Therefore, theses outliers will be removed before further multivariate statistical analysis is performed as there are impacted by anthropogenic pollution, and will likely affect the clustering and principal component analysis.

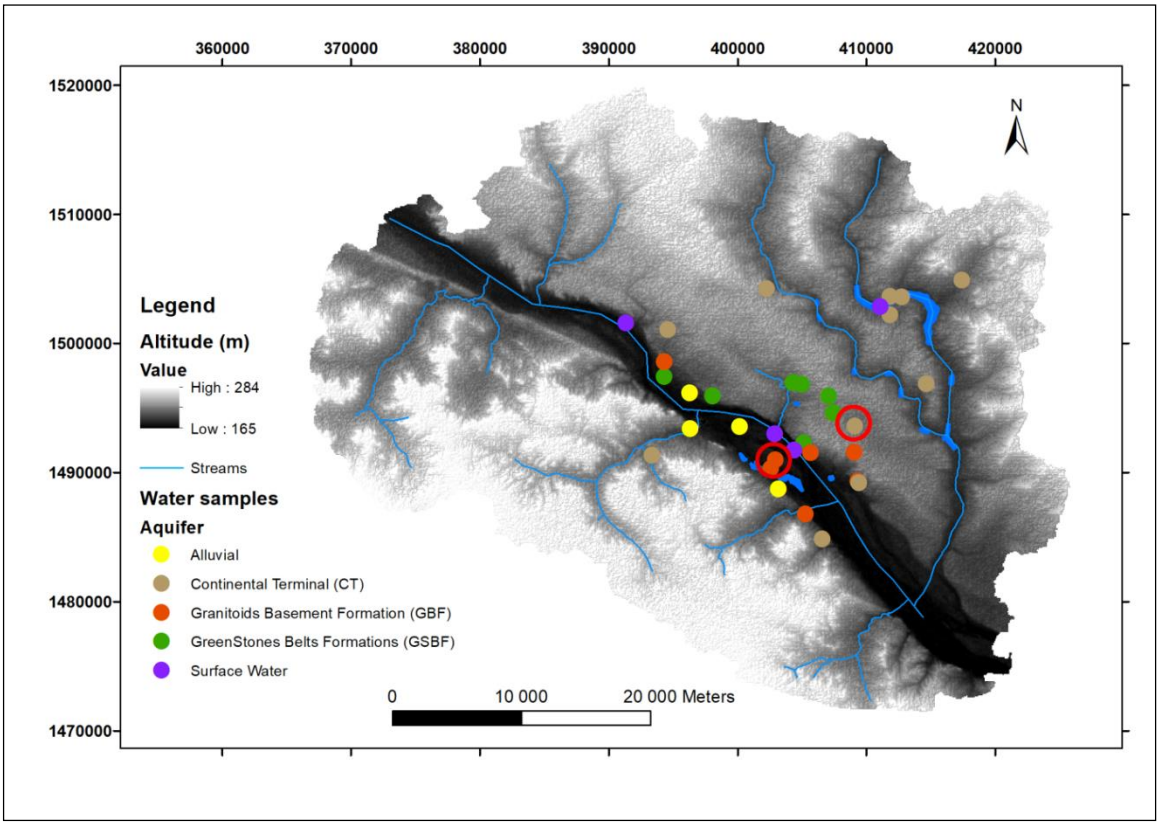

Figure 21: Location of hydrochemicals data outliers within the study area

Also, prior to cluster analysis, statistical variances of the hydrochemicals data are calculated (Table 2). The data range on very different variances, and a scaling of their variances is performed using to allow data have zero mean and unit variance. The scaling was required because EC, HCO3 and NO3 have variances that are orders of magnitude larger than others variables, and performing cluster analysis on raw data will not provide meaningful results.

Table 2: Variances of raw and scaled hydrochemicals data

Parameters	EC	K	Na	Cl	Mg	Ca	SO4	HCO3	NO3
Variances (Original)	65083	6	556	61	140	419	535	21484	1045
Variances (Scaled)	1.03	1.03	1.03	1.03	1.03	1.03	1.03	1.03	1.03

5.3 Cluster analysis

The Hierarchical Cluster Analysis (HCA) was performed on the log transformed and standardized data using the Ward's linkage method that uses the analysis of variances to evaluate the distance between clusters. It has the advantage of producing smaller and more distinct clusters than others HCA linkage methods (Guggenmos et al.,2011, Cloutier et al., 2008).

The resulting dendrogram of the cluster analysis (Figure 22) suggests an initial identification of four major clusters or hydrochemicals facies herein annotated as A1, A2, A3, A4. The threshold of six (6) used to identify the clusters is based on the inter clusters distances and is shown as straight black line on Figure 22. However, in order to deeply examine the first four clusters solution provided by the visual inspection of the dendrogram, a neighborhood plot of clusters is presented in Figure 23. The neighborhood plot uses the distance of each observation from its own cluster centroid distance to determine similarity between different cluster groups.

The examination of the neighborhood plot (Figure 23) confirms the four clusters solution. However, that thicker black lines joining the centroids of clusters 3 and 4 strongly suggest that both clusters overlap to a considerable extent and should likely be considered as sub-cluster or sub-group of a single cluster. Nevertheless, A3 and A4 clusters are respectively under strong dominance of SW and CT water samples, which are different water sources. Therefore, the four clusters (groups) solution will be considered keeping in mind the strong relationship of A3 and A4 clusters.

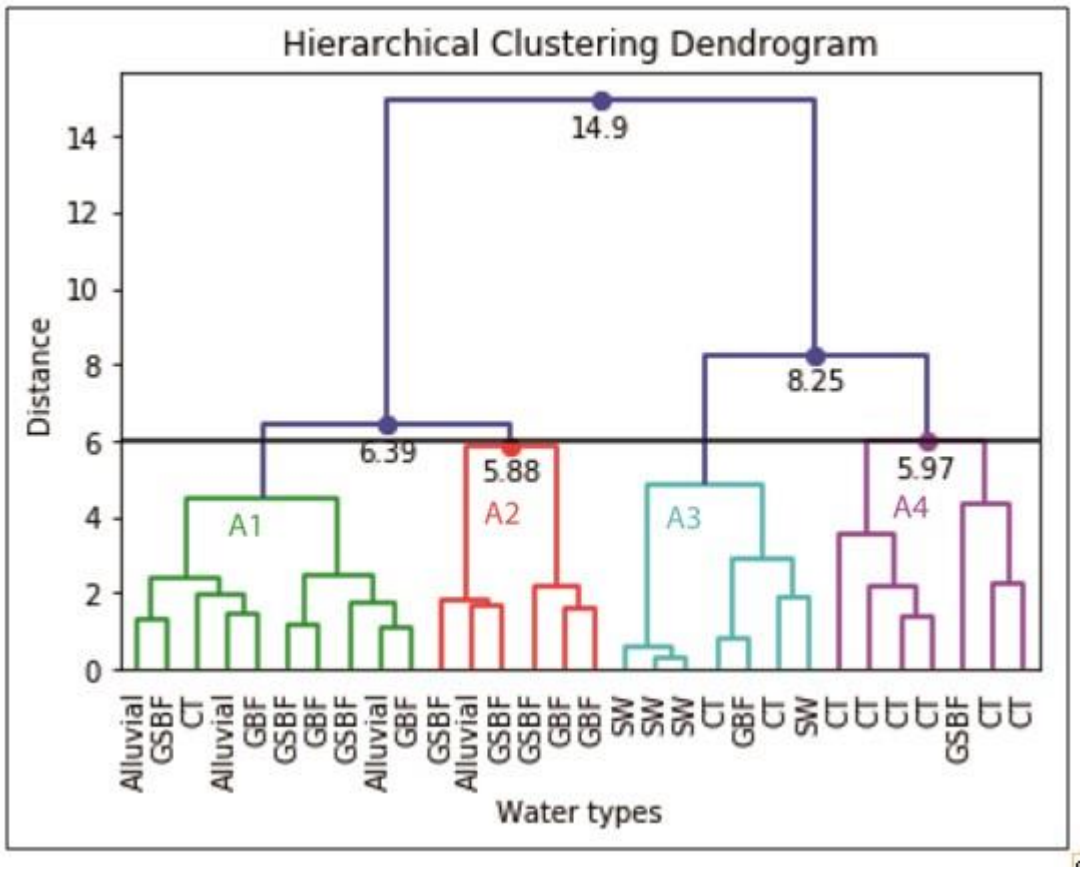

Figure 22: Dendrogram of the water samples classified into four (4) clusters (A1-A4)

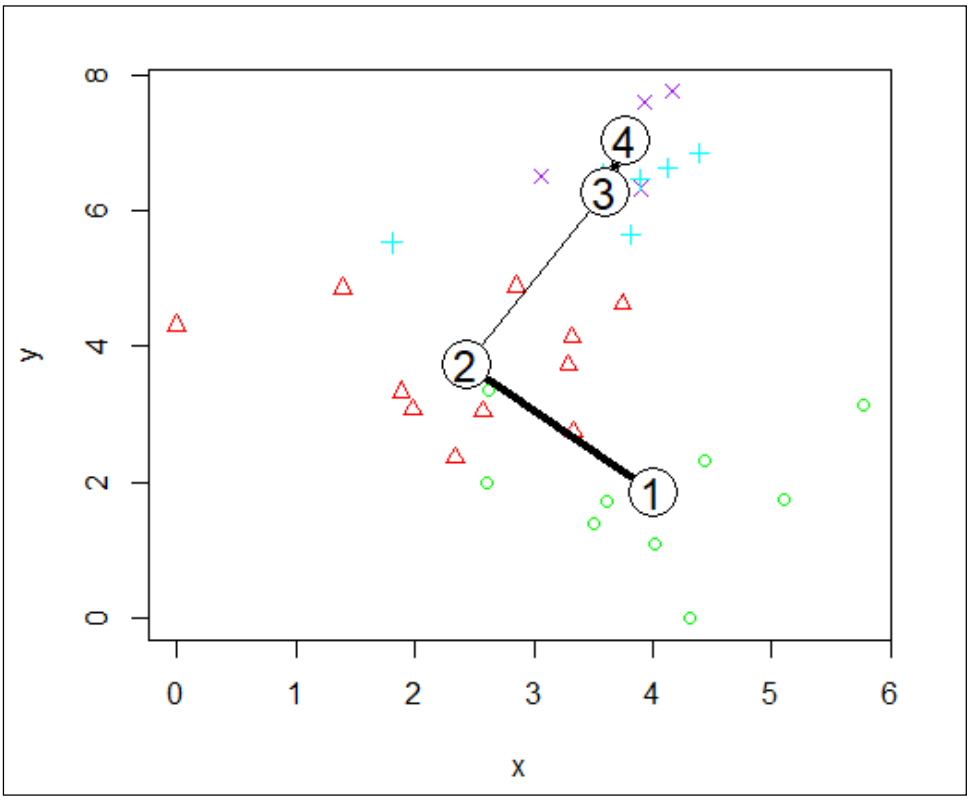

Figure 23: Neighborhood plot of water sampling displaying the four clusters solution

The hydrochemicals medians values of the variables, as well as the predominant hydrogeological formations of each cluster are presented in Table 3. Median EC values of clusters increase in the following order of A3-A4-A1-A2. This EC concentration difference is suggesting that water samples from clusters A3 and A4 (Low EC) are generally diluted with rapid low EC recharge water rates and shorter residence time (Hassane, 2016; Martinez; et al.,2015; Guggenmos et al.,2011) . The clusters A3 and A4 samples are mainly associated to all surface SW, and the CT waters. Only few GSBF and GBF samples are associated with these clusters (Table 3). This low EC recharge water associated with clusters A3 and A4 suggest that the dominant recharge process involved is direct recharge inferred from rainfall water. This direct recharge includes in increasing order of importance the CT and few GBF and GSBF aquifers water samples respectively. The relatively high EC concentration of clusters A1 and A2 is likely indicating more intense rock-water interaction process suggesting and delayed recharge process. The water samples involved are mainly composed of GSBF, Alluvial and GBF aquifers.

Table 3: Median values of variables and predominant hydrogeological formations for each cluster

Clusters	K (mg/l)	Na (mg/l)	Cl (mg/l)	Mg (mg/l)	Ca (mg/l)	SO4 (mg/l)	HCO3 (mg/l)	NO3 (mg/l)	EC (µs/cm)	Predominant source
A4	0.70	7.60	2.42	1.55	6.70	4.62	27.60	16.70	188.30	93 % CT; 7% GSBF
A3	2.50	1.80	0.85	1.53	3.94	0.19	23.30	0.89	59.00	57% SW; 29% CT; 14% GBF
A2	3.85	25.45	6.16	18.40	31.50	29.25	220.50	0.61	439.00	50% GSBF; 33% GBF; 17% Alluvial
A1	1.15	15.70	8.25	11.60	31.95	7.74	120.50	38.90	343.50	30% GBF;30% GSBF;30% Alluvial

5.3 Hydrochemicals facies of Cluster

In the previous section, the individual water samples have been grouped into clusters based on their respective hydrochemicals similarities. The hydrochemicals characteristics of each cluster will be examined using rectangular piper diagrams and Principal Components Analysis (PCA). The interpretation of hydrochemicals facies using ordinary triangular piper diagram (Piper, 1944), and rectangular coordinates piper diagrams used herein is essentially identical (Ray and Mukherjee, 2008). The aim of using the rectangular coordinates is to only simplify the view and interpretation. Nitrate are excluded in the representation of the rectangular piper diagram to only display major ions exempt from strong anthropogenic influence.

5.3.1 Hydrochemicals difference between clusters

The Figures 24 and 25 respectively present major ion geochemistry in a rectangular Piper plot with all samples relative to cluster membership, and median values of each clusters. The major ions are characterized by high variability in cations compositions within clusters and all the samples tend to be dominated by HCO3 anion (Figure 24). Only few samples of cluster A2 are dominated by SO4 anion. The high variability of the cations composition within clusters samples is interesting as it may indicate different processes that infer the cations characteristics, and therefore different cations sources origins.

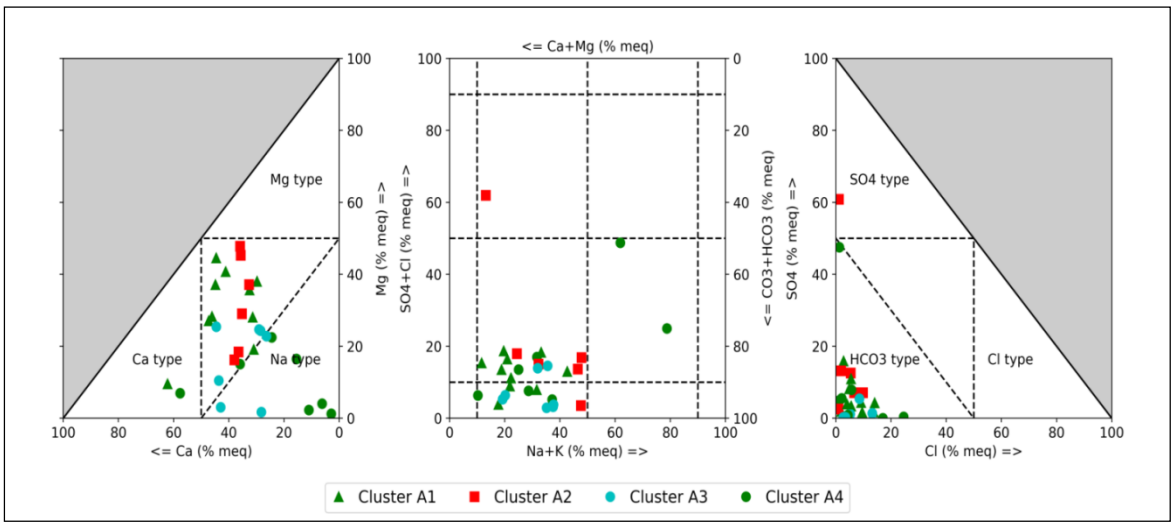

Figure 24: Rectangular Piper diagram plot of the A1-A4 clusters

Considering the inter cluster hydrochemicals median values (Figure 25 and Table 2), It is obvious from Figure 25 that there is no dominant cation for most clusters, and that bicarbonate represent the most important anion for all clusters. For each cluster the following facies are described based on Table 2 and Figure 25.

Cluster A1 is dominated by Ca-HCO3 water type with Calcium representing the major cation, and bicarbonate the dominant anion. This cluster is associated with relatively high EC concentration (343 µs/cm) and is mainly associated with water samples proportionally belonging to Alluvial, GBF and GSBF aquifers.

The Cluster A2 is also characterized by Ca-HCO3 water type with however, more HCO3 concentration and higher EC (439 µs/cm) than cluster A1. The Cluster A2 is more associated with GSBF and GBF aquifers water, with relatively few samples from alluvial aquifer.

This third cluster A3 is typified as Ca-HCO3 water with however, very low HCO3 and EC concentrations (59 µs/cm), compared to the first two clusters A1 and A2. This cluster is largely dominated by surface water samples and CT waters, with marginal GBF water samples proportions.

The Cluster A4 is characterized by Na-HCO3 water type and medium to low EC (188 µs/cm) concentration, relatively to the three clusters. This cluster is largely composed of CT aquifer water samples, and very few GSBF aquifer water samples.

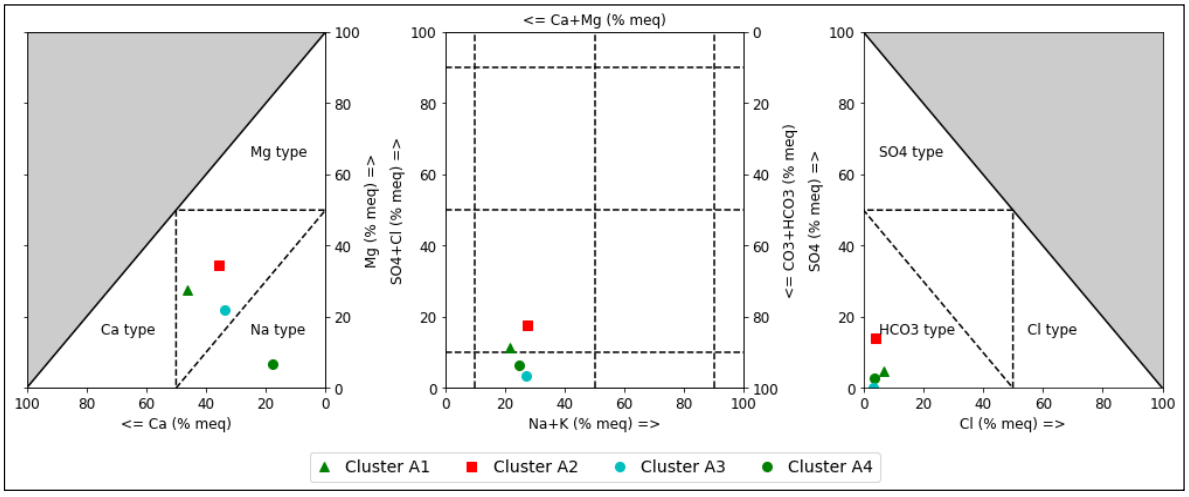

Figure 25: Rectangular Piper diagram plot of clusters based on their median values

The cluster analysis has revealed a mixing of different water sources type into the same cluster, as well as water source from the aquifer may belong to different clusters. Therefore, in order to determine the information on the specific water quality parameters that distinguish and differentiate the clusters, Principal Components Analysis is performed on the scaled data.

5.3.2 Principal Components Analysis

The results of the PCA analysis using the nine (9) scaled variables, and including eigenvalues, proportion of variance, cumulative proportion of variance, and the factor loading are shown in Table 4. Blanks values in the Table 4 indicate a near zero loadings. The PCA analysis indicates that 84% of the variation between samples can be explained by the first three components that recorded and eigenvalues greater than one (1). The three first components loading are also presented in Figure 26. The PC1 accounts for 56.20% of the total variance and is dominated by strong positive loading of EC, Ca, HCO3 as well as Mg, Cl and Na to a later extent (Figure 26). The PC2 explains 15.87% of the total variance and has high negative loading of NO3, and medium negative loading of Cl. SO4 and K have medium positive loading in this PC2 component. The PC3 is responsible of 12.11% of the total variance and is dominated by negative loading of K, low negative loading of Cl, and medium positive loading of SO4.

Table 4: PCA loading of Eigenvalues and variances of the scaled hydrochemicals variables

Scaled Variables	PC1	PC2	PC3
EC	0.44		
K		0.32	-0.82
Na	0.37	0.19	
Cl	0.35	-0.30	-0.27
Mg	0.40		0.22
Ca	0.42		
SO4	0.15	0.47	0.44
HCO3	0.42	0.14	
NO3	0.11	-0.73	
Eigenvalues	2.25	1.19	1.04
Proportion of Variance	56.20%	15.87%	12.11%
Cumulative Proportion	56.20%	72.06%	84.17%

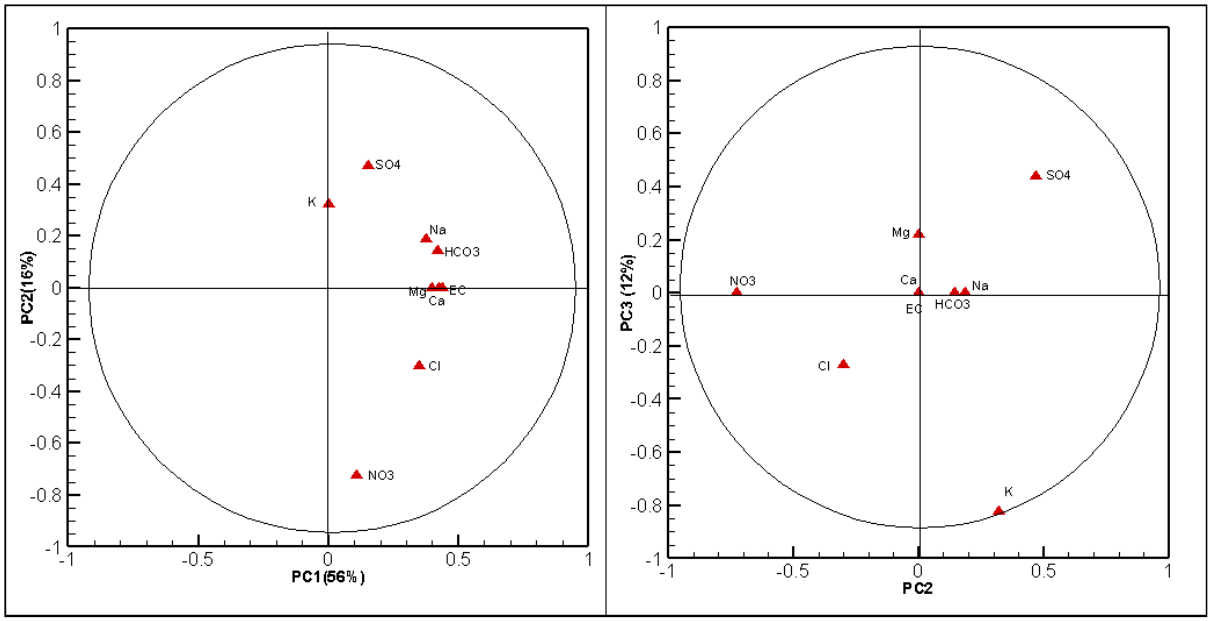

Figure 26: Projection of the first three components axis of the PCA

The high bicarbonate positive loading of the PC1 component could be generated due to the weathering of the silicate bedrock formations with carbonic acid incorporated from the soil. This is consistent with the strong correlation between EC, and HCO3 (Figure 27) indicating the intense water -rock interaction process. The high positive loading of Ca, Mg, and Na likely resulted as the most soluble base cations from the weathering of the calcic aluminosilicate feldspars and ferromagnesian minerals which are shown to be important in the Liptako bedrocks formations (Soumaila, 2000). However, the presence of Cl with relatively medium positive loading can also indicate either a rainfall input, and/ or the evaporation process. This is obviously shown in the correlation matrix (Figure 27) with a correlation coefficient of 0.87 between EC and Cl. The correlation between the two elements is relevant as Cl is a conservative element and is expected to increase when evaporation increases, which leads also to high EC. Therefore, the main process that is likely controlling the source of the PC1 is the rock-water interaction, specifically the silicate weathering process, and in later extent, the rainfall input (direct recharge) and evaporation (indirect recharge).

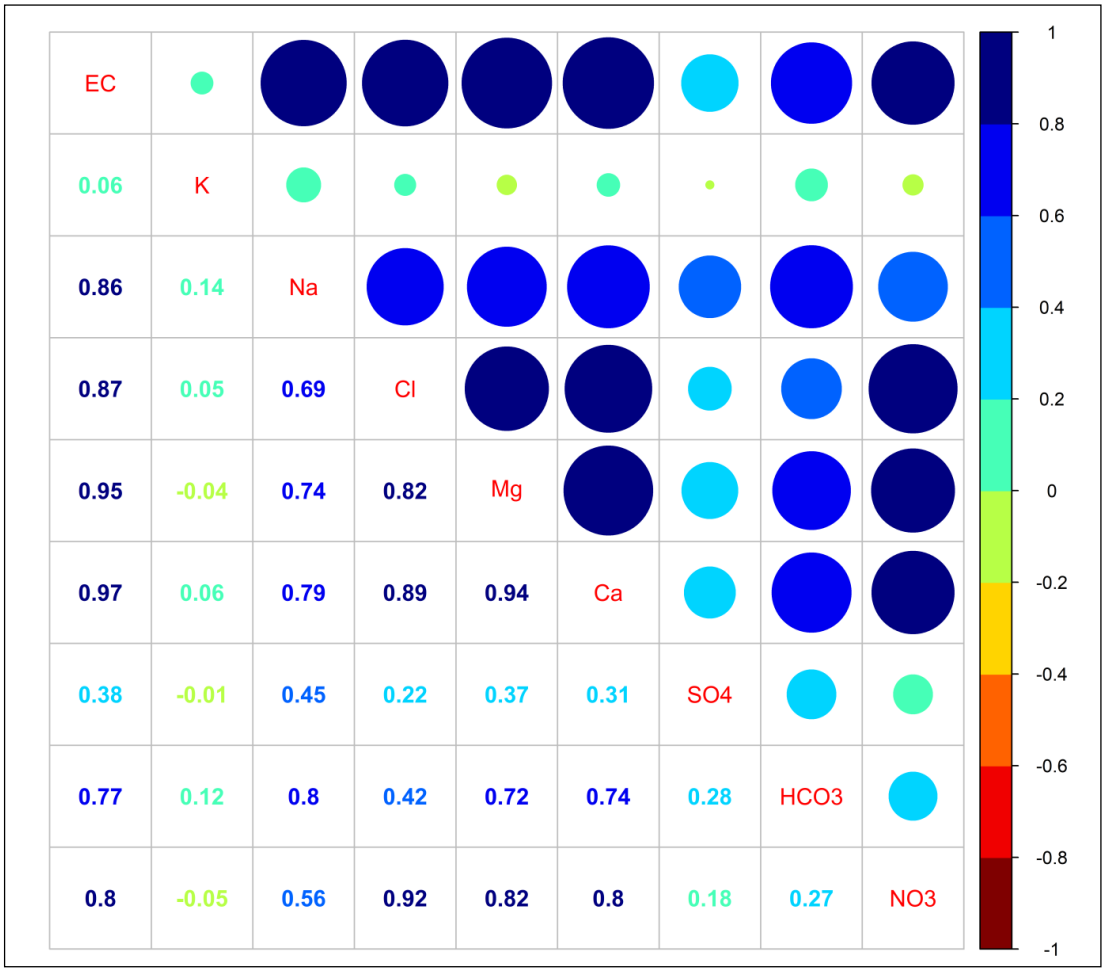

Figure 27: Correlation matrix of the major ions variables: the greater the circle is, the high is the correlation coefficient. Positive correlation is shown green to blue colors, while negative correlation is shown in light green to red colors.

The negative loading of NO3 and Cl indicates that theses anions are originating from different source from the positive loading of SO4 and K, in the PC2 component. The NO3 of this component (PC2) is likely related to anthropogenic activity which may indicate nitrate pollution into the water sources as previously reported in the study area (Hassane,2016, Babayé,2012). This anthropogenic activity resulting in groundwater quality deterioration is sustained by the high load of sulphate, that may originate from agricultural related activities.

The Cl of this PC2 may have been generated from several sources including weathering of the host rocks, and evaporation and or even rainfall inputs. The SO4 and K positive loading signify

identical source of these ions, and may both originate from weathering. While K may come from orthoclase feldspar weathering, SO4 is also expected to be dissolved from additional weathering material dominated by oxidation process.

In order to explain and constraint the origin of the several possible sources of cations and anions described in the PCA analysis, majors' ions ratios, binary plot ions as well as isotopes tracers will be used in the next sections.

The first major process described by the PCA analysis is related to weathering process and cations dissolution and exchange. Discriminating between evaporates, silicates, and carbonates weathering process is usually achieved using normalized molar ratio (Matiatos et al., 2018; Clark, 2015) that are more conservative than absolute concentrations which are dependent on dilution and evaporation processes. Figure 28 presents the Na normalized molar ratio of Ca/Na and HCO3/SiO2 of surface water (pond and Niger River) as well as groundwater (Alluvial, CT, GSBF, GBF). All the samples are obviously dominated by silicate weathering, and have therefore Na /Ca normalized ratio between 0.1 and 10. This is consistent with the dominance of the alkali earth elements especially Na+ that are indicative of feldspar weathering in silicate terrains. The normalized Na ratio was corrected by subtracting the Na that are supported by Cl ions from others sources (halite). The silica SiO2 and bicarbonate HCO3 provide additional information of the silicate weathering. Compared to the mafic, the granitic weathering tends to have higher influence on water sample chemistry (Figure 28).

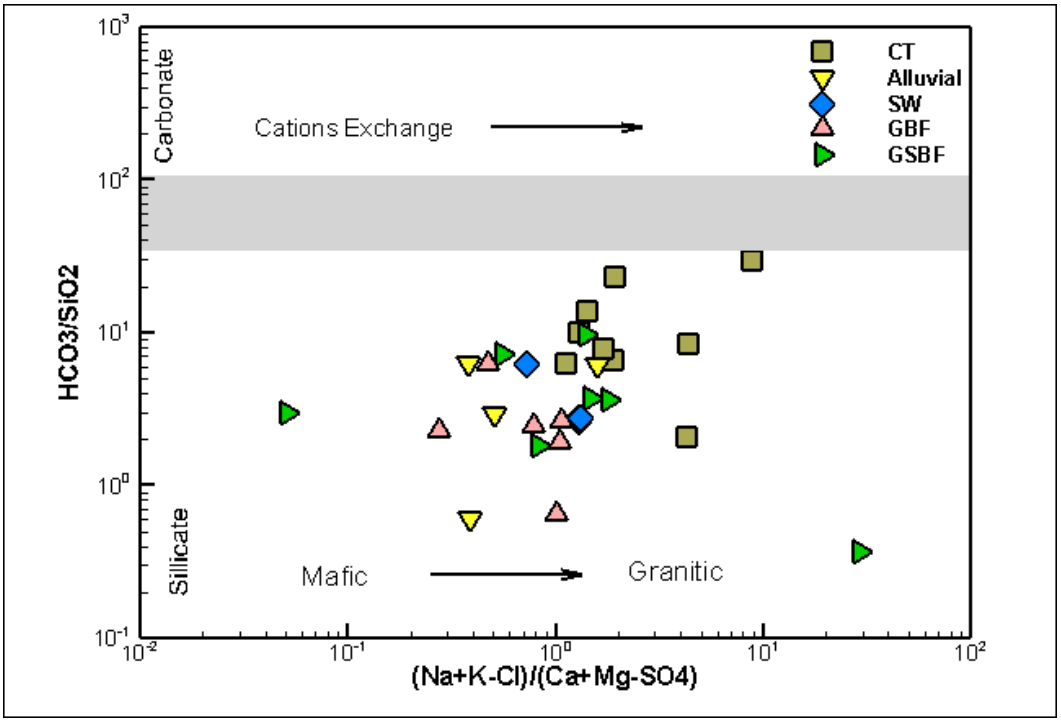

Figure 28: Molar ration of groundwater and surface water as indicators of silicate versus carbonate weathering.

Most of the previous studies in the Liptako basement formations have shown the strong dominance of the silicate weathering process in the groundwater chemistry (Babayé, 2012, Hassane, 2010, Ousmane, 1988). The Figure 28 also highlights that both groundwater and surface water major cations are sourced from silicate weathering and strong cation exchange is also having influence on the water chemistry.

In order to determine the silicate weathering and rainfall end members influence as well as mixing between different water sources, Mg/Na and K/Na molar ratio are plotted against Ca/Na ratios (Figure 29). The rainfall end member is clearly shown to have influence on pond water, CT 3 aquifer water samples, and 2 alluvial aquifer water samples, one GSBF and one GBF water samples (Figure 29). Most of the aquifer water samples and Niger River are shown to be under the influence of the silicate weathering and cation exchange process. The difference between pond water and river water ions sources may be explained by the weathering materials of the River being more draining the Precambrian basement, while the pond is likely to be draining on more clayey materials.

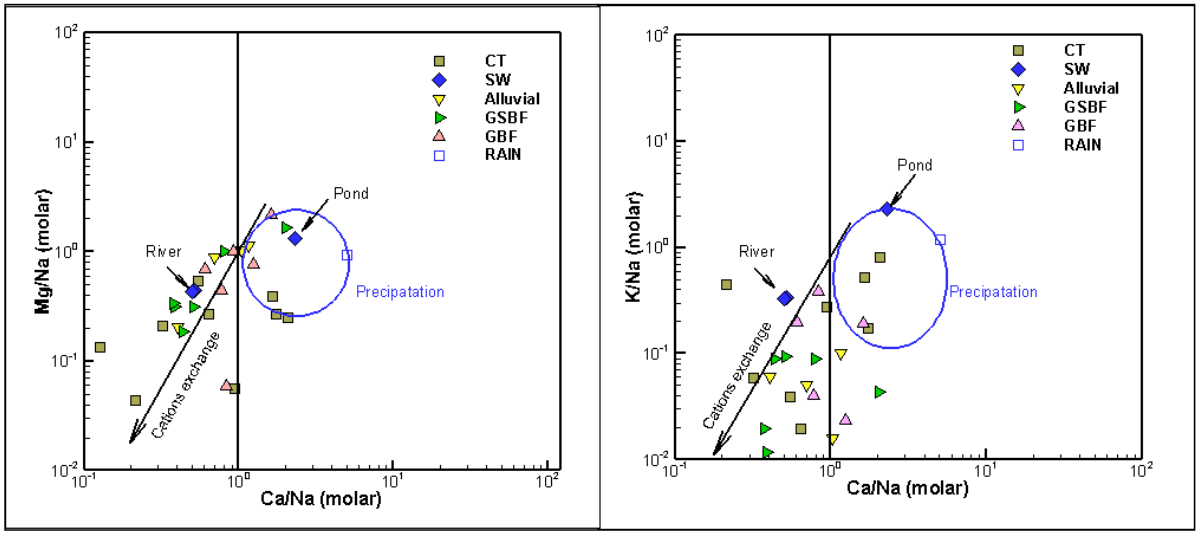

Figure 29: Major ions ratio comparison between surface water and groundwater

Compared to the rainfall and pond water end member, most of the groundwater samples and Niger River water tend to show a lower molar ratio of Mg/Na and Ca/ Na, as a result of interaction with silicate materials, releasing preferentially Na cation during the cation exchange process. This is further sustained by the strong correlation coefficient of 0.8 between Na and HCO3 (Figure 27).

Therefore, the PCA identified end members of rainfall and silicate wreathing are obviously the major source of control on the water chemistry, and therefore clusters identified group of water could reasonably be used to explain the similarity of hydrochemicals facies between rainfall, surface water and groundwater as being the result of interaction between them.

Although this hydrochemicals similarity approach has been previously used for delineating groundwater surface water interaction (Zhang et al., 2018; Guggenmos et al., 2011, Kumar et al., 2009), it appears important to provide further constraint based on isotopes ratio in supporting this assumption.

5.3.3 Isotopes Compositions of Rainfall in Niamey

Groundwater origin can successfully be traced using stables isotopes (groundwater18O and Deuterium 2H) composition of precipitation and surface water. Generally, it is assumed that the long-term average or weighted mean annual value of δ18O and D in precipitation represent the isotopic signature of groundwater (Clark,2015). Therefore, a most accurate determination of groundwater surface water interaction, as well as groundwater recharge requires a deep understanding of the stable isotopic composition of precipitation as it constitutes the main hydrological inputs (Harvey and Welker, 2000).

The International Atomic Energy Association (IAEA) recorded δ18O and δ D in precipitation at Niamey from 1992 to 2016, and these data were used in this study. Table 5 presents the weighted mean annual isotopes composition of rainfall in Niamey. The weighted mean annual rainfall values of δ18O Vs SMOW range from -5.8 ‰ to 2.14 ‰, while the values of δ D Vs SMOW range from -37 ‰ to -6.1

These weighted mean annual values of $\delta^{18}O$ and δ D do not show strong correlation (less than 0.35) with the rainfall amount, and confirm the high variability associated with stable isotopes of water in the Sahel, in line with the strong spatio temporal rainfall variability of the region (Taupin et al.,2002, Leduc et al.,2000, Dakouré, 2003).

The weighted interannual mean values of δ18O Vs SMOW and δ D Vs SMOW are respectively of -3.8 ‰ and -21.8 ‰, and are consistent of average values for the Sahel region (Ousmane, 1988, Babayé, 2012). The Deuterium excess d, averaged over 1992-2016 is of 8.3 and 8.39 (Table 5), and is less than the deuterium excess of the Global Meteoric Water Line of 10

.

Table 5: weighted mean annual isotopes composition of rainfall in Niamey (data are from www.iaea.org)

Dates	1992	1993	1994	1995	1996	1997	1998	1999	2009	2010	2011	2012	2013	2014	2016	Mean
Rainfall	471.00	452.00	677.00	533.00	429.00	406.80	956.50	537.50	473.00	526.00	415.45	610.10	453.52	650.00	538.00	**541.92**
$\delta^{18}O$ (‰) Vs SMOW	-3.50	-2.40	-4.60	-5.00	-4.70	-3.20	-4.40	-5.80	-4.00	-4.02	-2.14	-4.02	-3.68	-3.05	-3.11	**-3.84**
δ D (‰) Vs SMOW	-22.00	-17.00	-29.00	-33.00		-19.00	-26.00	-37.00	-20.53	-22.94	-6.13	-23.37	-19.46	-15.37	-15.00	**-21.84**
d (deuterium excess)	6.00	2.20	7.80	7.00		6.60	9.20	9.40	11.44	9.22	11.02	8.80	9.96	9.05	9.86	**8.40**

In order to determine the Local Meteoric Water Line (LMWL) of Niamey, that is most representative of the precipitation stable isotope slope and intercept that contributes to recharge, monthly weighed and un-weighted LMWLs lines are shown in Figure 30.

The un-weighted LMWL has a regression line with a slope of 6.9 while the precipitation weighted LMWL has a slope of 7.48 (Figure 30). The slope value of 6.9 in the un-weighted LMWL is indicating an early precipitation evaporation process, in contrast of the slope value of 7.5 in the weighted LMWL. This early evaporation in the precipitation isotopes is known as the amount effect, and is resulting from a selective enrichment in ^{18}O of residual rainfall. This process is due to a kinetic fractionation by partial evaporation on the drop of rainfall through a dry air column below the cloud base and is well described in arid regions (Clark, 2015, Hughes and Crawford 2012, Taupin et al., 2003). The increase in the slope of the weighted LMWL is due to the exclusion of the light rainfall events, which do not generally contribute to significant groundwater recharge. The evaporated rain samples characterized by ^{18}O enrichment correspond herein to rainfall amount in the range of 5-10 mm (Figure 30).

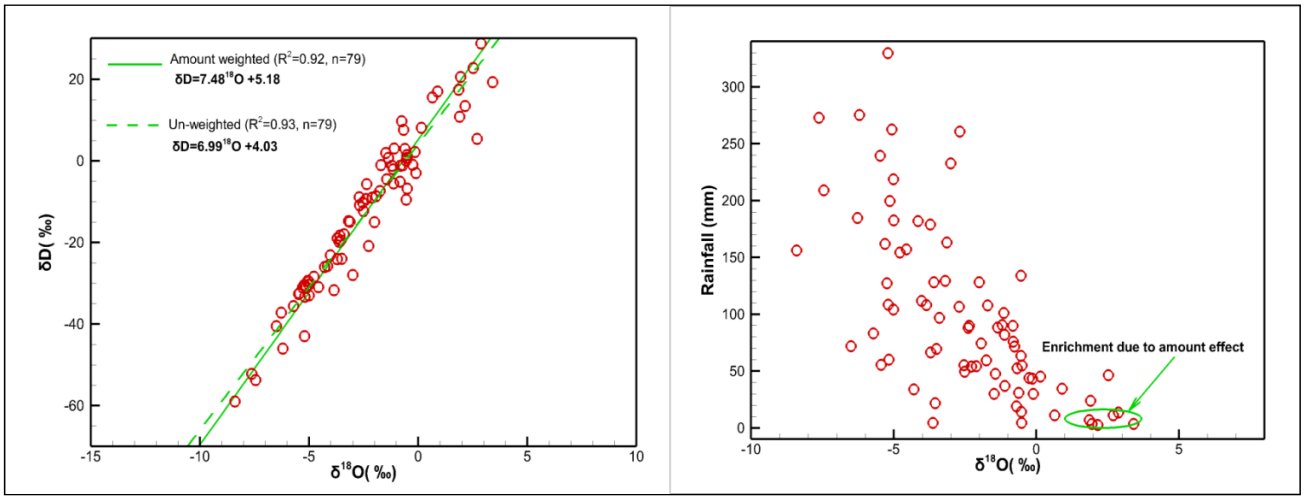

Figure 30: Monthly precipitation weighted and un-weighted isotope composition of precipitation at Niamey showing the amount effect induced evaporation.

Therefore, the precipitation weighted LMWL described in the equation 22, reflects more the isotopes composition of precipitation, and provides a better reference against which

groundwater and surface water can be assessed to determine if they experienced a secondary evaporation.

$$\delta D = 7.48\ ^{18}O + 5.18 \qquad (22)$$

The slope and intercept of this LMWL is consistent with those found previously in the study area (Taupin et al, 1997; Favreau, 2000). The LMWL found herein has however, slightly greater slope value, and smaller intercept compared to the LMWL found by Ousmane, (1988).

5.3.4 Origin of surface and Groundwater water

In order to characterize the origin of water and major groundwater recharge process in the study area, long term average precipitation weighted isotopes compositions are first compared to pond and Niger River water (Figure 31). The signal of $\delta\ ^{18}O$- δ D in precipitation is expected to be modified during overland flow by evaporation enrichment that will result in an isotopic enrichment of residual ponds and Niger River water. The Figure 31 shows two different evaporation patterns for Niger River and pond water. The isotopic signature of the pond water lies in between the LMWL and the GMWL, with no significant evaporation induced enrichment. The pond water isotopes signature is only slightly more enriched than the long-term precipitation weighted isotope composition (Figure 31). The $\delta\ ^{18}O$ and δD of the pond water is of -3.48 ‰ and -17.8 and ‰ respectively. These values are slightly greater than the δ 18O and δD precipitation mean weighted value of -3.87‰, and -21.84 ‰ and correspond to a typical isotope composition of pond in the study area (Favreau, 2000). The Niger River samples median values of δ 18O and δD are respectively of 2.78 -3.87‰, and 7.7 ‰ and higly greater than precipitation and pond water isotope composition. (Figure 31). The slope value of 4.4 of the evaporation line is characteristic of evaporated surface water in low humidity of 0.2-0.3 % (Clark, 2015) and suggests that Niger River water is more enriched due to evaporation than pond water (Figure 31).

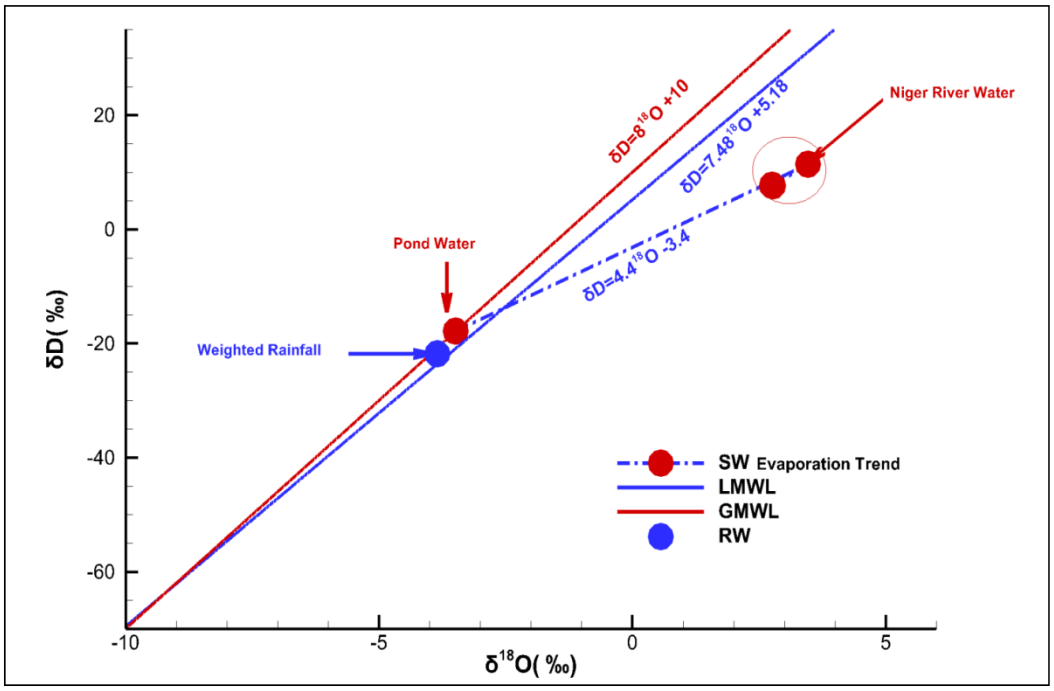

Figure 31: Evaporation line drawn from pond and Niger River water at the end of the dry season (April, 2017).

The groundwater stable isotope signature is presented in Figure 32 and 33, respectively for sedimentary aquifers of CT and alluvial (Figure 32) as well as the Precambrian bedrock aquifers of GBF and GSBF (Figure 33).

The CT aquifer has an isotope composition that fall within the range of precipitation isotope signature with median value of δ ^{18}O and δD corresponding to -3.98 ‰ and -23.8 ‰ respectively (Figure 32). The isotope signature of CT3 also plots near to the pond water. Similarly, to CT3, most of the alluvial samples present the isotope signature of precipitation and plot closely in between the GMWL and LMWL. However, there is one alluvial sample that has an enriched isotope signature with ^{18}O value -1.51‰ and δD value of -11.1‰. This enriched alluvial sample is typical of evaporation of surface water, and likely results to be under influence of infiltration of evaporated Niger River water. This sample is 250 m distance of the main Niger River channel (Figure 32).

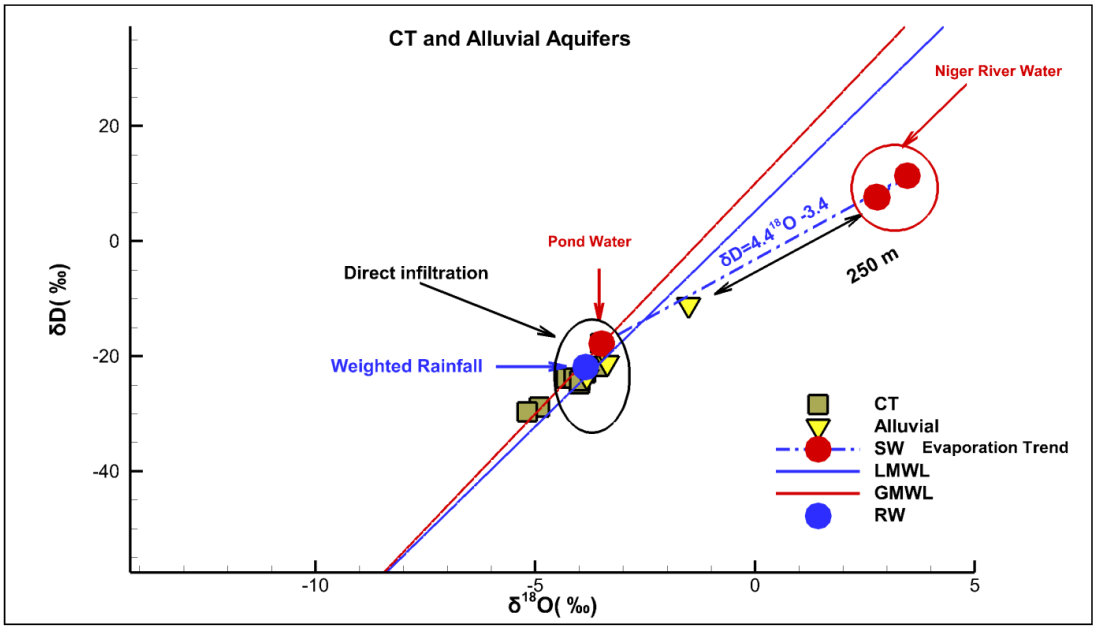

Figure 32: ^{18}O and δD diagram of CT3 and Alluvial showing the sedimentary groundwater isotope composition compared to precipitation and surface water isotope signatures.

Considering the Precambrian bedrock of GBF and GSBF aquifers, the isotope signature ranges within the same order of precipitation isotope signature in exception of two samples of GSBF aquifer (Figure 33). These samples are located within a distance of 750 meters to 1 Km from the Niger River channel, and present an enriched isotope signal that is typical of evaporated surface water.

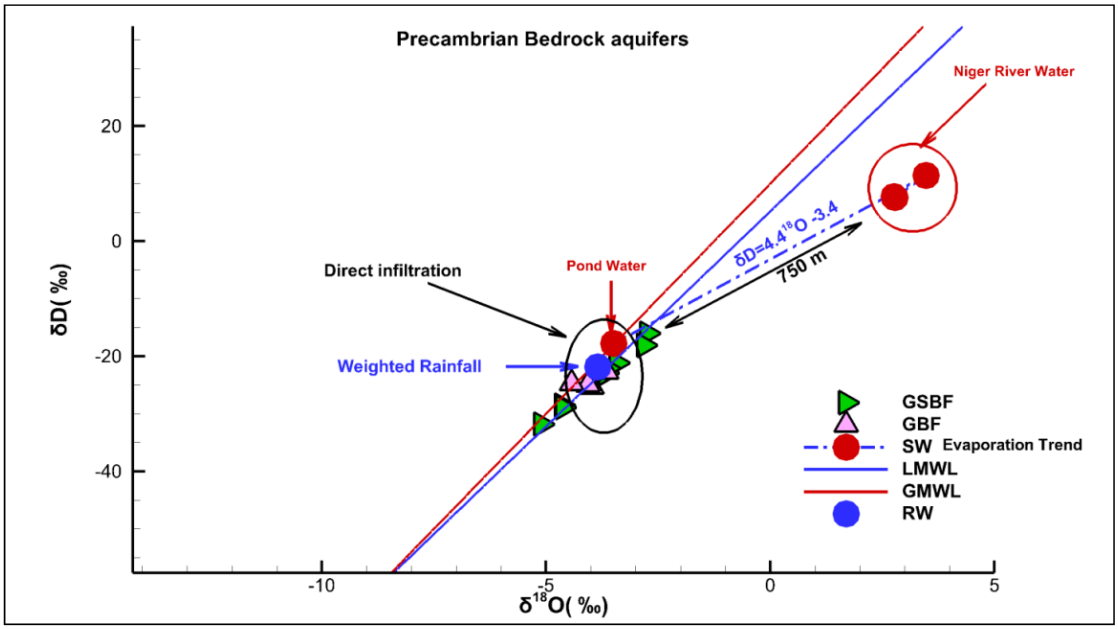

Figure 33: ^{18}O and δD diagram of CT3 and Alluvial showing the sedimentary groundwater isotope composition compared to precipitation and surface water isotope signatures

The isotope composition of sedimentary (CT3 and Alluvial) and Precambrian bedrock (GBF and GSBF) aquifers do not show significant track toward the isotope signature of Niger River in exception of some localized wells and boreholes located close to the main River channel. The δ ^{18}O and δD composition of groundwater and pond water are very similar to the long term mean isotope signature of precipitation, and provide useful information on the dominant groundwater recharge process. The similarity between local precipitation and groundwater isotope signature suggests clearly that recharge is mainly due to direct infiltration. Also, the quasi absence of evaporated trend in the pond water is likely resulting from the relatively rapid infiltration during the recharge process, with minimal evaporation. However, the evaporated signature of the Niger River is retained in some wells, and show the localized influence of River water infiltration within few distance (200 m to 1 Km), from the main river channel. The absence of evaporated trend in groundwater in the CT3 aquifer in the region was interpreted as a result of rapid and valley focused recharge in the east of the study area (Favreau, 2000).

Furthermore, the evidence of the dominance of rapid and direct infiltration recharge process over the indirect infiltration provide additional constraint on the cluster and PCA analysis performed in the previous section. It is therefore showing that the PC1 component is largely dominated by rainfall input rather than surface water influence. The previous interpretation of

the Clusters A3 and A4 as resulting from rapid and direct recharge inferred from rainfall water is therefore confirmed. Also, isotopes and PCA analysis provide significant argument to consider that the wreathing process is more enhanced in the cluster A1 and A2.

Moreover, the isotope sampling during the baseflow and due to the fact that Precambrian water sample isotopes signature track away from the signature of River water, the baseflow is likely to be primary provided by the river water.

Conclusion of the Chapter 5

The cluster analysis performed using the hydrochemicals similarities allowed to group groundwater and surface water into four distinct clusters (A1-A4). The clusters A3 and A4 are dominantly associated to SW and the CT waters with relatively few GSBF and GBF samples. The dominant water types of these clusters are of Na-Ca-HCO3 facies. The PCA analysis combined with major ions molar ratio have shown that the major sources of ions is in this group is controlled by the silicate weathering, and stable isotopes signal of water in these clusters is typical of rapid recharge due to direct infiltration with shorter residence time. This direct recharge is dominating, in increasing order of importance the CT, GBF and GSBF aquifers.

The Clusters A1 and A2 are dominated by Ca-HCO3 water type, and are composed mainly of GBF, Alluvial and GSBF aquifer samples. The PCA analysis constraint with major ions molar ratios suggested a strong silicate weathering and ion exchange process as major source of ions in these aquifers. The cation exhange process is preferentially liberating Na cation during the water rock interaction. The isotope signal of water in this group is characterized by significant recharge due to direct infiltration from rainfall, with relatively lower and localized infiltration inferred from Niger River water. The isotope signal of Niger River tracking away from the groundwater signal may also provide indication of dominance of Niger River water contribution to baseflow of the River.

Also, the combined analysis of PCA, major ions molar rations and isotopes signal shown that CT and GBF aquifers are almost exclusively recharged by rapid and direct infiltration, while alluvial and GSBF aquifers have both direct infiltration and localized evaporated river water isotopes signal.

However, the hydrochemicals and isotopes analysis only provide qualitative information on recharge process, and available data collected herein are not sufficient enough to quantify the exchange flux between groundwater and surface. Further hydrodynamic modelling will certainly provide useful quantification of groundwater recharge as well as exhange flux between surface and sub-surface.

Chapter 6: Integrated hydrological modelling of groundwater –surface water interactions

In this chapter, the watershed scale integrated surface-subsurface modelling results will be discussed. The hydrogeological parameter estimation as well as calculation of the magnitude and direction of the exchange of water between the surface water system and complex groundwater aquifer systems will be performed. Also, the water balance components considering different land use types, groundwater systems, as well as surface water bodies will be calculated.

6.1 Model Discretization and Boundary Conditions

The boundary conditions specified to the hydrological HydroGeoSphere (HGS) model are presented in Figure 34. As detailed in the methodological section, the types of boundary conditions are as follow: No flow boundary conditions were assigned to all outer subsurface model domain boundaries, precipitation, potential evapotranspiration (PET), critical depth and surface water flux assigned at the top surface model domain (Figure 34 a). The spatial horizontal resolution corresponds to triangular mesh elements with a resolution ranging from 300 m on average to 70 m near surface flow features (Figure 34 b). The subsurface model consists of triangular prism-shaped elements which are each defined by 6 nodes. The model has eleven layers with a total of 516,901 nodes, and 927,030 elements.

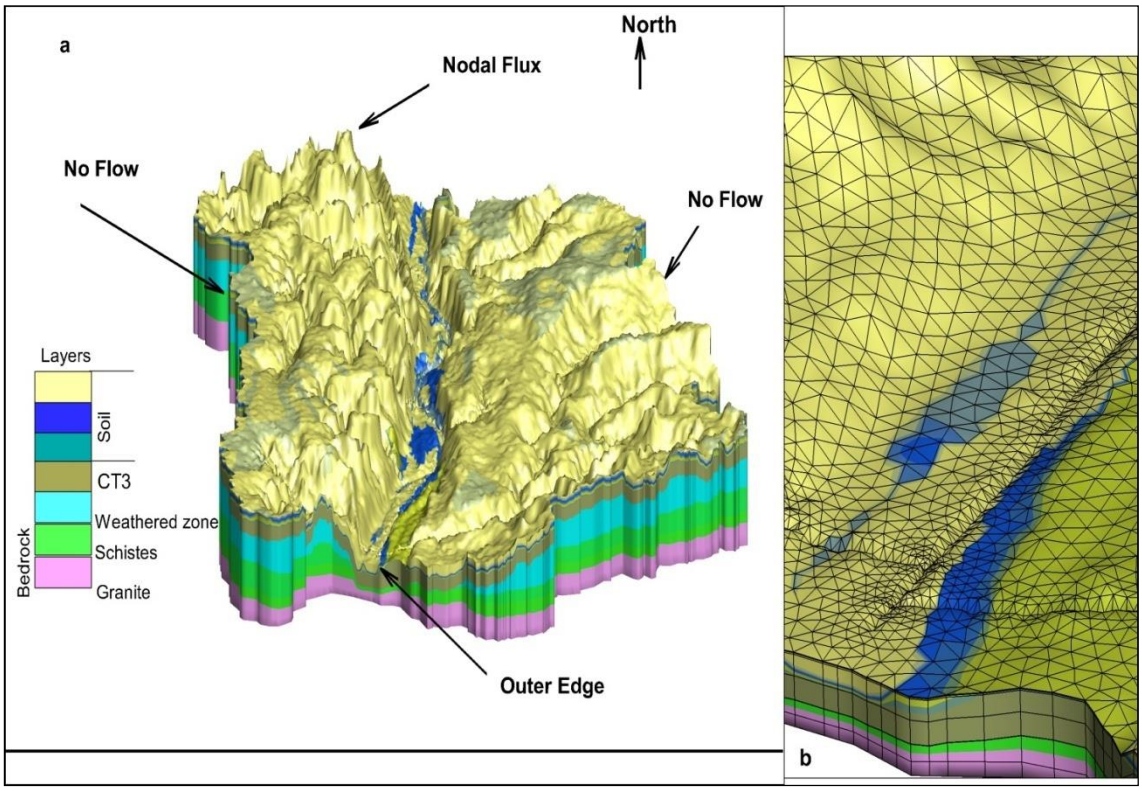

Figure 34: Boundary conditions of the model (a) and view of the spatial discretization at the outer edge boundary of the model (b).

6.2 Parameter estimation

6.2.1 Land Use and Soil parameters

The recent land use map (CILSS, 2016) at 2 Km resolution was reclassified at 30 km resolution into six main land use classes (Figure 35). The mapping results indicate that agricultural land covers 11 % of the watershed, natural vegetation of Sahelian savanna and steppe cover 32% and bare and sandy soil cover 45% of the watershed. The main city and surrounding village occupy approximately 8 %, and water bodies cover the remaining are 4 %.

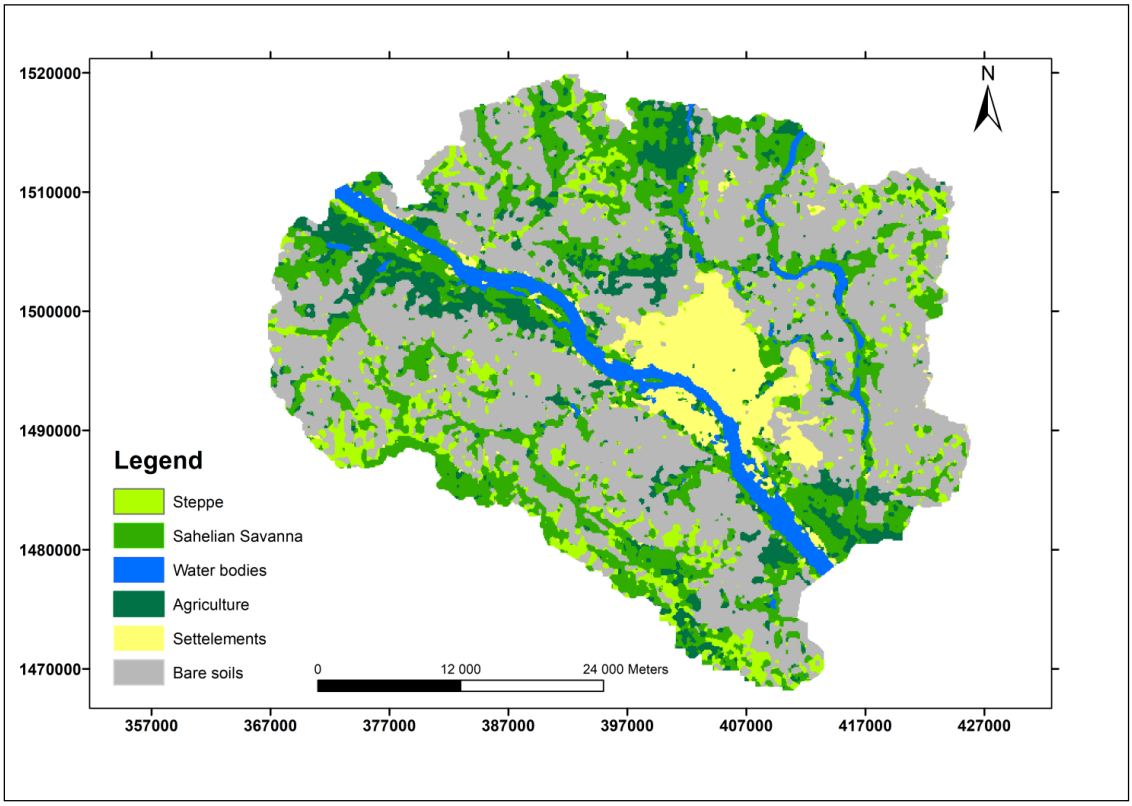

Figure 35: 2013 Land Use map of the study area (reclassified from CILSS, 2016)

The unsaturated soil zone hydraulic conductivities values *K* are presented in Figure 36. The soil *K* values range from 0.2 10^{-3} m/s to 8.7$10^{-3}$ m/s, with high *K* values located in sandy soil while lower *K* values are common in most clayey soils. The hydraulic conductivities of ephemeral stream alluvium are greater than Niger River alluvial (Figure 36). This has an interesting implication regarding the focused groundwater recharge through surface water features. Also, Table 6 provides the full hydraulic parameters required for the calibration of the model. The appendix 2 presents the calibrated hydraulics parameters values for the 41 unsaturated soil zone discretized in this study.

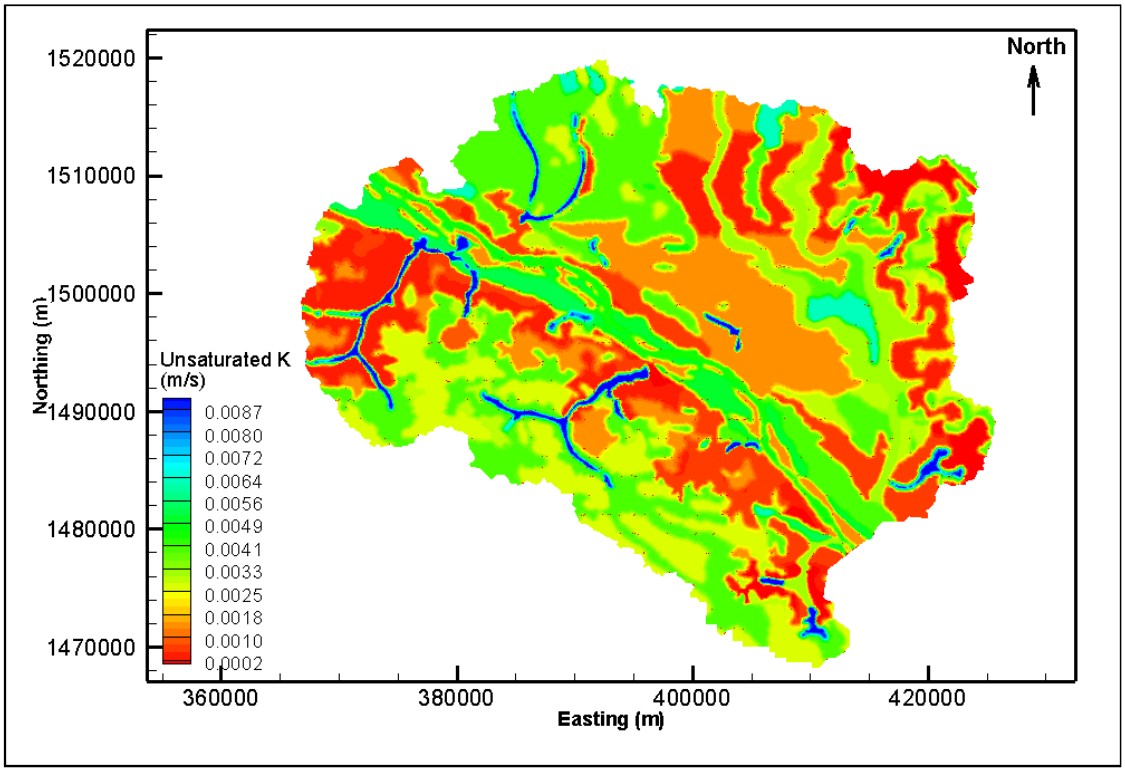

Figure 36: Saturated soil hydraulic conductivities values (K)

Table 6: Required hydraulic parameters for the model calibration

Parameters	Symbol	Units
Saturated hydraulic conductivity	K	[m/s]
Total porosity	n	[-]
Specific storage	S_s	[m^{-1}]
Van Genuchten parameter	α	[-]
Van Genuchten parameter	β	[m^{-1}]
Residual water saturation	S_{wr}	[-]
Coupling length	L_c	[m]
Manning roughness coefficient	n_x	[$m^{-1/3}$ s]
Manning roughness coefficient	n_y	[$m^{-1/3}$ s]
Evaporation depth	L_e	[m]
Evaporation limiting saturations	θ_{e1} θ_{e2}	[-]
Leaf Area Index	LAI	[-]
Root depth	L_r	[m]
Transpiration fitting parameters	C1, C2, C3	[-]
Transpiration limiting saturations	θ_{t1} θ_{t2}	[-]
Canopy storage parameter	C_{int}	[m]

6.2.2 Evapotranspiration and overland flow parameters

Calibrated actual evapotranspiration and overland flow parameters are presented in Table 7, for each land use type. Maximum Leaf Area Index values range from 0.01 for urban area, to 1.25 for Savanna, with Agriculture and Steppe having the same maximum LAI values of 1.2. Root depth values for Savanna (4.5 m) are three times more than for agriculture (1.5m), with steppe having a root depth value of 1 m. Root depth of urban and bare soil land use are respectively of 0.1, and 0.01 meters. The calibrated root depth values of savanna and agricultural land are in good agreement with values presented in Ibrahim et al. (2014). Calibrated Manning friction coefficients for overland flow range between 0.016 to 0.43 (s. $m^{-1/3}$) for different land use types, and coupling length values range from 0.01 to 0.1 m (Table 7).

Table 7: Calibrated Transpiration and Overland flow parameters

Parameters	Agriculture	Savanna	Steppe	Urban	Bare soil
Max Leaf Area Index [-]	1.2	1.25	1.2	0.2	0.01
Root depth [m]	1.5	4.5	1	0.1	0.01
Manning friction Coefficients [m−1/3 s]	0.139	0.187	0.154	0.016	0.43
Coupling Length [m]	0.01	0.01	0.01	0.1	0.01

6.2.3 Saturated hydraulic conductivities and Van Genuchten parameters.

Calibrated hydraulic conductivity (*K*) values, residual water saturation and van Genuchten parameters for the different hydrogeological units are shown in Table 8. The CT3 aquifer, which is pinching out over the basement aquifer, has a calibrated hydraulic conductivity of 1.12 $x10^{-5}$ m/s. This value agrees well with the calibrated value from Favreau (1996) for the CT3 aquifer at the Wankama site.

No previous studies have estimated the *K* of the Precambrian basement aquifers. Calibrated *K* values (Table 8) for the Precambrian basement aquifers are generally within the literature reported range (Domenico and Schwartz, 1990). The calibrated *K* of the granitic aquifer is one order magnitude greater than the calibrated value for the schist aquifer (Table 8). The calibration process also revealed a structural control on the *K* values for different hydrogeological units. The calibration process further showed a kind of geologic and or structural control on the hydraulic conductivities values for different hydrogeological units. Although this control depends on very localized geologically phenomenon (fracture density, weathering process), the granitic aquifer, when altered mechanically and or fractured, has a higher *K* than the schist aquifer, of which the alteration products are generally composed of clayey materials, and are less likely to fracture.

Table 8: Calibrated saturated hydraulic conductivities and Van Genuchten parameters.

Units	K[m/s]	Residual water saturation	Van Genuchten parameters	
Continental Terminal	$1.12 .^{10-5}$	0.023	0.088	1.113
Weathered zone	$1.24 .^{10-6}$	0.042	0.166	1.128
Schistes	$6.36 .^{10-9}$	0.042	0.100	1.153
Granites	$9 .^{10-8}$	0.079	0.134	1.34

6.3. Calibration of hydraulics heads and surface water flow rates

Long term steady state calibrated groundwater heads for 25 observations wells are plotted against available long term measured groundwater heads for both the CT and Fractured aquifer (Figure 37 a).

The long-term average period considered is 1980-2005, and simulated groundwater heads reasonably approach the observed head with an R^2 value of 0.82. The level of agreement between groundwater heads for the fractured aquifer is higher than for the CT, because a higher weighting was placed on the fractured aquifer calibration performance as it has more reliable

long-term groundwater heads measurements. The steady state calibration is the first step of the calibration approach followed by the dynamic equilibrium calibration, for groundwater heads (Figure 37 b) and surface water flow rates (Figure 37 c).

The simulated seasonal cycle of groundwater heads (Figure 37b) at Kossey Djerma observation well after 15 years of monthly normal simulations follows the measured groundwater heads reasonably well, but with a time lag bias in the simulated hydraulic heads. Calibration further showed that groundwater wells located near the river reached the dynamic equilibrium more rapidly, within 10 years simulation, more than 10 years was required for wells that are further from the river.

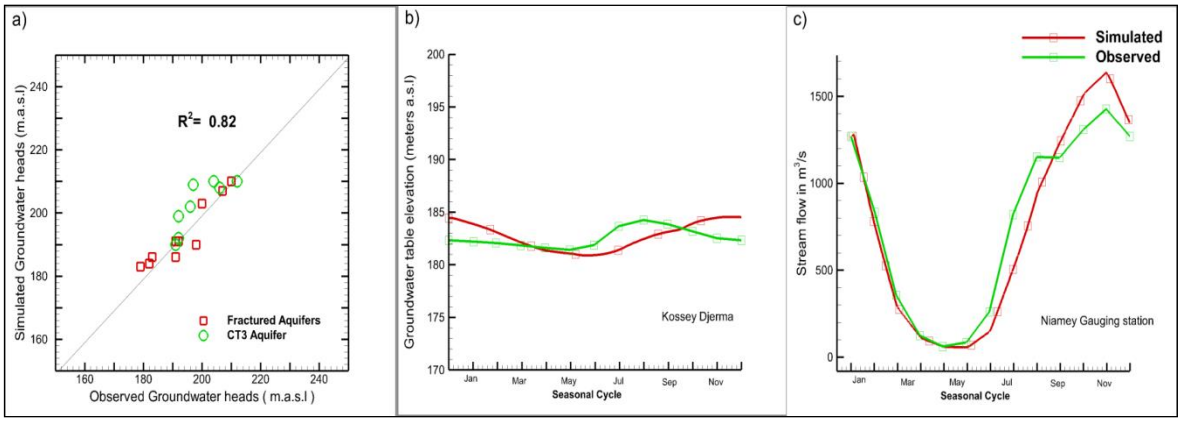

Figure 37: Steady state (a) and groundwater head calibration under dynamic equilibrium (b) and surface water flow rate calibration under dynamic equilibrium (c)

Also, surface water flow was found to stabilize in less than 2 years of simulation, similar to the findings of Goderniaux et al. (2010). The calibration of monthly normal groundwater levels shows good agreement with observed groundwater levels for both mean values and seasonal amplitude, however, a time lag bias is present in the simulated heads which is suspected to be a result of the EPM conceptualization of the fractured rock aquifer. The time lag bias between the simulated and observed groundwater levels for the Dynamic Equilibrium calibration step were not rigorously addressed to avoid overfitting, and to maintain calibrated values within physically reasonable ranges. The simulated seasonal cycle of surface water flow rates at Niamey station are in good agreement with observations (Figure 37c), with both river peaks

during the local rainy season and of the inflow from upstream well captured by the model with a slightly positive bias during the peak of September.

In fact calibrating integrated hydrological models with both surface water flow rate and groundwater wells is not a very common practice (Goderniaux et al., 2009; Jones, 2005; Li et al., 2008; Sudicky et al., 2008) in integrated hydrological model calibration, and as the calibration level will allow to reasonably reach the objective of the model development (water balance, GW-SW) considering the EPM approach, the monthly normal calibration results are considered satisfactory and are used as initial conditions for daily transient simulations (Figure 38).

Daily transient simulations results for three observations wells that have available groundwater head measurements (Figure 38) show acceptable agreement between observed and simulated groundwater heads for 5 years (2013-2017). The first two years (2011-2013) are considered as model spin up period. The three observation wells (Figure 38) are located in the fractured aquifer, because no continuous groundwater measurements heads are available for the CT aquifer. Compared to the monthly normal simulations, simulated daily transient groundwater heads have less time lag, and in all the three wells, simulated mean heads approach the measured heads very closely. The time lag bias observed from daily transient wells is different for the three observations wells, implying highly variable hydraulic conductivities in the fractured aquifer, controlled by localized geological features (fractures density, aperture, and weathered zone thickness) that the current EPM conceptualization of the model may not be able to capture. The EPM representation appears to be useful in regional groundwater flow system characterization, but may be too simple to capture the complexity of local geological conditions (Anderson and Woessner, 1992).

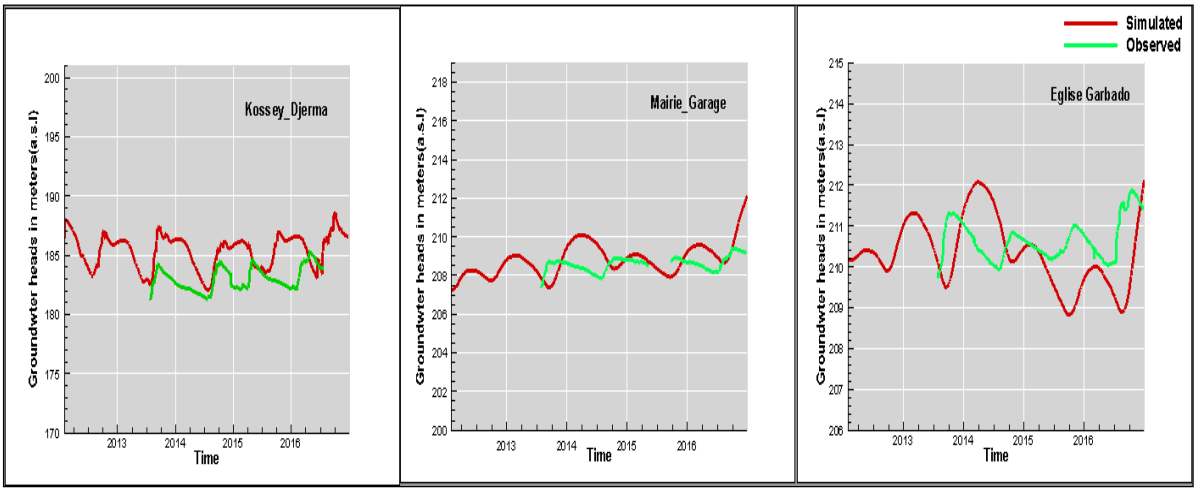

Figure 38: Comparison of simulated and observed daily transient groundwater heads

Daily transient simulated surface water flow rates at the Niamey gauge (Figure 39) are relatively well reproduced by the model, with the local flow peak (rainy season) and Guinean flow peak captured in August and December respectively.

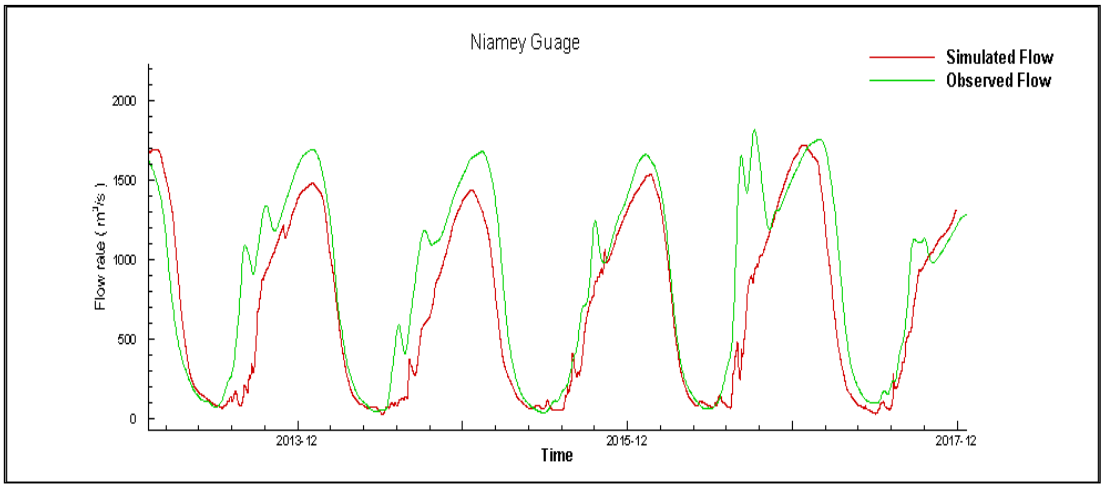

Figure 39: Comparison of simulated and observed daily surface water flow rate at Niamey gauge.

6.4. Monthly normals exchange flux between surface and sub surface

The simulated exchange flux from five years of daily transient simulation (2013-2017) has been aggregated into monthly normal exchange flux (Figure 40) in units of mm/day. Positive values (red) represent the exfiltration from the porous medium to the surface, while negative values (blue) correspond to the water infiltrating from the surface to the subsurface. The 2D spatial representation of the exchange flux is used to qualitatively characterize the process of exchange between the surface water bodies and the aquifer system. The distribution of the exchange flux values (Figure 40) shows that the model is able to reproduce the importance of the monsoonal rainfall in groundwater infiltration occurring only in the rainy season. July and August are the most important periods of infiltration with an average value of up to 8 mm/day.

In June and September, infiltration is localized at the right bank of the Niger River (upstream) where irrigation occurs. The rest of the season is dry, and there is no infiltration. Groundwater exfiltration shows different patterns depending on the surface water bodies considered. The Niger River acts as a gaining stream where groundwater exfiltrates to the river during the rainy and dry seasons. Although, it is clear that the River is gaining, the exfiltration rates are very small, relative to the total flows in the river, and the process is only important for few months of the year (August, February and March). Using a piezometric map of Niamey, Hassane et al. (2016), have already shown the CT aquifer discharges to the Niger River which agrees with this study.

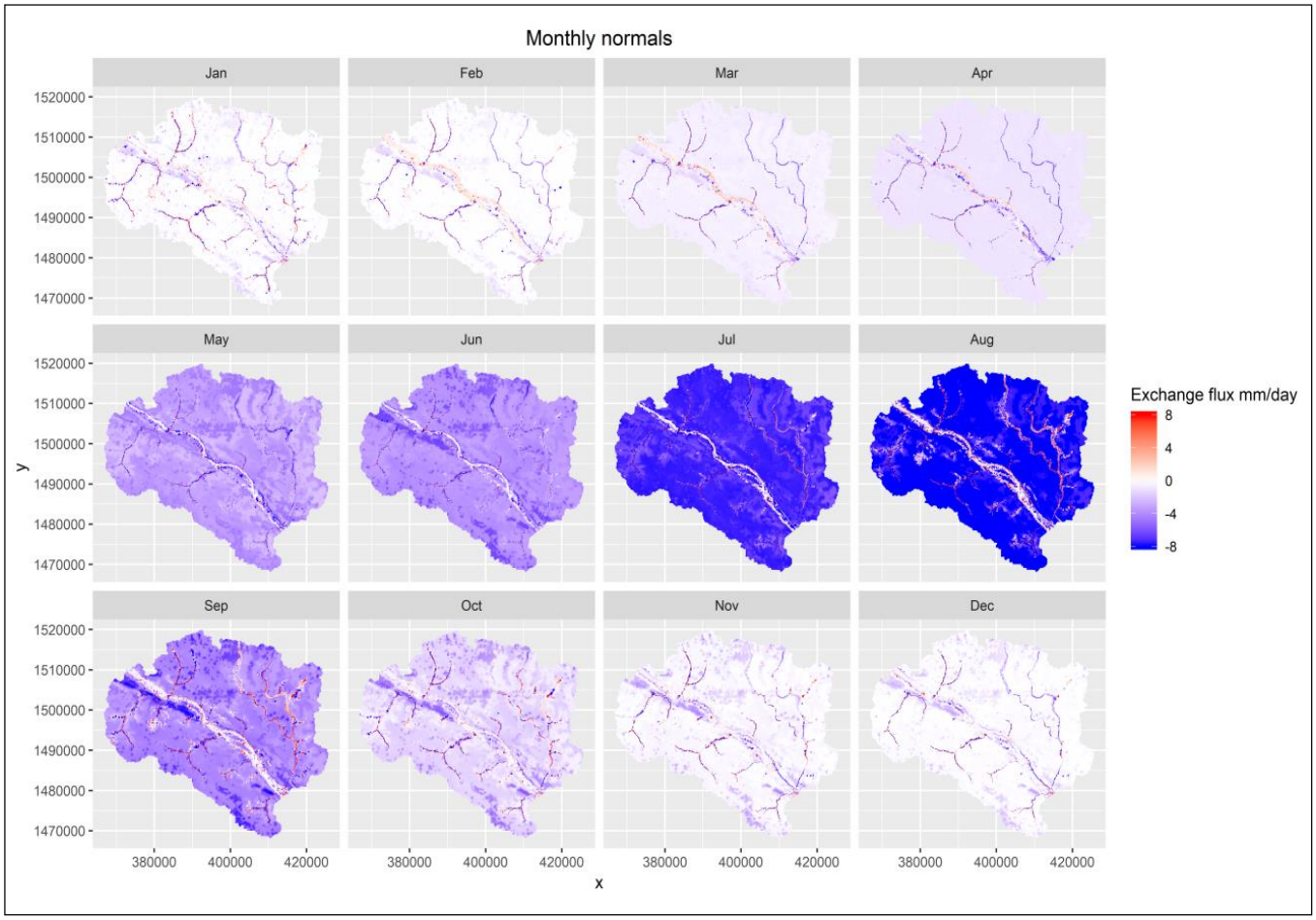

Figure 40 : 2D spatial monthly normals Exchange flux

Considering the ponds and ephemeral streams, the exchange flux processes are a bit more complex, and result from more local hydrogeological conditions (topography, hydrologic conductivities), with some ponds acting as depressions focused recharge areas and others as groundwater discharge area. The channels of the ephemeral streams are predominantly groundwater discharge areas while the main stream course is mainly a recharge area. This phenomenon of ponds and parts of ephemeral streams acting as groundwater discharge zones may be related to the recent changes of land use resulting in the creation of temporary ponds (Favreau et al., 2009; Mamoudou et al., 2015).

While monthly normal exchange fluxes provide a qualitative understating of the seasonal cycle of river-aquifer exchange (Erler et al., 2019), they do not carry sufficient temporal resolution to quantify and understand the highly transient relationship between surface and subsurface exchanges fluxes for this dry environment with intermittent precipitation. For this watershed daily exchange fluxes are required (Figure 41)

6.5. Daily transients exchange flux between surface and sub surface

Daily time series of exchanges flux have been derived at multiple locations in order to characterize the surface water groundwater interactions depending on the type of the surface water features considered (i.e., Niger River, ponds, ephemeral stream)

Figures 41a and 41b show the daily time series profile of ponds-aquifer exchange flux for the Zarmagande pond and Koungou pond respectively. Exchange flux at Zarmagande pond (Figure 41 a) is dominated by groundwater discharge during the rainy season (July to September), and by groundwater recharge in the dry season (October to June). In the rainy season, when groundwater is discharging into the ponds, the volume discharging into the pond is more important during intense rainfall events (Figure 41 a) with an exfiltration rate of up to 40 mm/day, which is considerably greater than actual evapotranspiration rate of 2 -3 mm/day. In contrast, infiltration of up to 20 mm/day may occur from pond to aquifer during the dry season, which lead to about 17 to 15 mm/ day of recharge after removing actual evapotranspiration rate (3 to 5 mm/day).

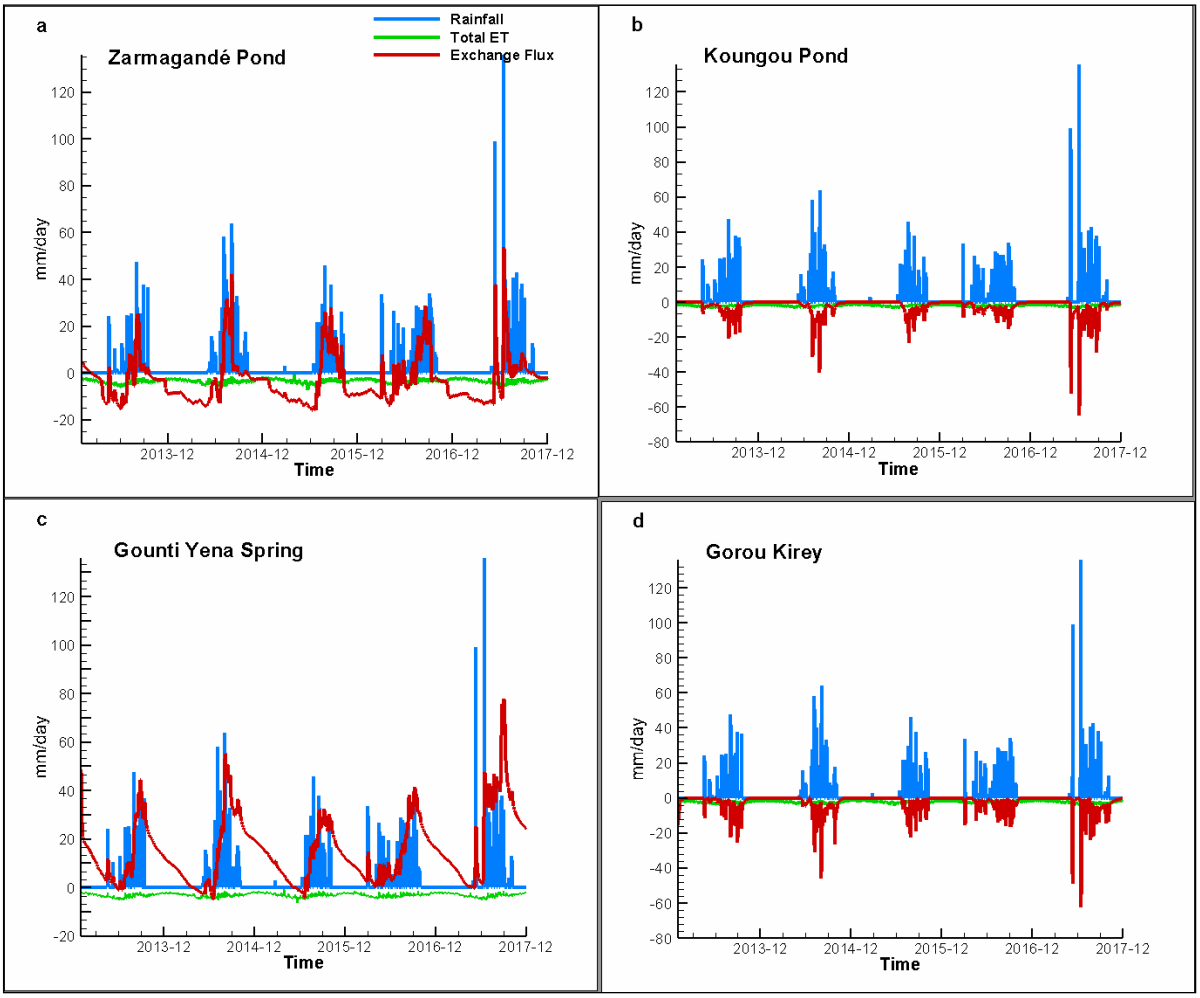

Figure 41: Exchange Flux profile for ponds (a, b) and Ephemeral Stream (c,d)

At Koungou pond (Figure 41 b), located 500 m away from Zarmagande pond, at a lower altitude, the exchange flux is exclusively characterized by infiltration of pond water into groundwater. The infiltration rate, which is dependent on rainfall intensity, can reach up to 50 mm/day during intense precipitation events (i.e., 120 mm/day). The difference in the exchange flux of the two ponds may be related to local topography, with Zarmagande pond located in a topographically low area (196 a.m.s.l), and Kongou pond, at greater elevations (201 a.m.s.l). Furthermore, the phenomenon of groundwater discharge into ponds, may be a result of recent land use change and climate induced groundwater table rise well documented in the study area from rural zones (Favreau, 2000; Favreau et al.,2009) to urban area (Hassane et al., 2016).

While there is significant groundwater recharge in the vicinity of the two ponds, there is a qualitative difference to the spring at Gounti Yena (Figure 41 c) where the exchange flux is characterized by a continuous groundwater discharge throughout the year. The main peak of the exfiltration occurs during the late rainy season and decreases during the dry season. The more intense the rainfall event is, the greater the exfiltration rate. During the late dry season (May, June) and early rainy season (July), little infiltration occurs, as evapotranspiration is the dominant process and considerably reduces the amount of water available to infiltrate. The ephemeral stream, Gounti Yena, is a groundwater discharge area, and its discharge rates can serve as a precursor to groundwater flooding especially during extreme precipitation event. Another ephemeral stream at Gorou Kirey shows a different exchange flux behavior (Figure 41 d) with surface water infiltrating into groundwater and producing a significant groundwater recharge.

Figure 42 shows exchange flux time series between the Niger River and the underlying aquifer at two locations, to characterize groundwater-surface water interactions. The time series (Figure 42) are considered to represent the main types of interactions in the vicinity of the permanent river in the study area. The simulation results further show that when there is a significant interaction between the river and underlying aquifer, the river is acting as either gaining, or losing stream depending on the zone considered. While the monthly normal exchange flux discussed earlier showed the Niger River to mainly have a gaining stream profile, the daily exchange flux time series allows for a more detailed profile.

Therefore, Niger River acts as loosing stream is some zones (Figure 42 a), and gaining stream (Figure 42 b) in others zones. In general, the losing zones are located near faults zones, where fractures are dense, and allow significant surface water infiltration into groundwater. One important aspect to notice is that no infiltration occurs during the Guinea river peak flow from November to February. Infiltration occurs only during the rainy season, during the local peak of the river, resulting in groundwater recharge of up to 50 mm/day during intense rainfall, as actual evapotranspiration (Figure 42 a) is low during these events, allowing significant groundwater recharge to occur.

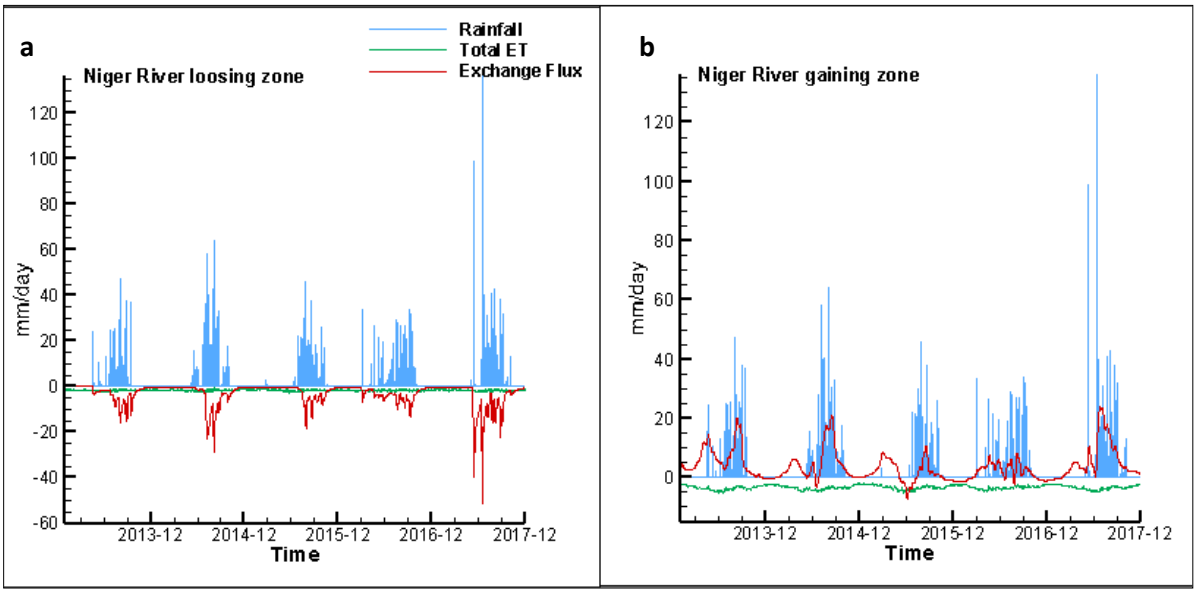

Figure 42: Exchange Flux at Niger River showing losing (a) and gaining zone (b) profiles

However, the losing zones of the river are only localized near important fractures zones, and in most area, models results do not show significant infiltration processes in other zones of the river. It is also worth noting that the infiltration rate of river water is more dependent on the intensity of individual rainfall events, than the mean monthly or annual rainfall. The importance of fractures zones in groundwater recharge has been shown by Girard (1993) for this study area using hydrochemicals and isotopes methods.

Apart from above mentioned localized fractures zones where the river water recharges groundwater, the remaining part of the Niger River is gaining from underlying aquifer (Figure 42 b). The exchange flux profile at gaining parts of the river (Figure 42 b) is dominated by groundwater exfiltration in the rainy season, with an exfiltration rate of up to 20 mm/day. This exfiltration rate results in baseflow of up to 15 mm/day when actual ET (less than 5mm/day) is considered (Figure 42 b), and shows two peaks, one at the end of the dry period (April –May), and another in the earlier rainy season (June-July). This shows that groundwater is sustaining the baseflow of the river during the dry season, and at the beginning of the rainy season. The exfiltration rate then decreases from the middle of the rainy season (August) to reach zero by the end of the Guinea high peak flow period (November-February). This is because groundwater heads are almost always above the Niger River levels (Hassane et al., 2016), and

particularly, during the dry period. Figure 42 b also shows that there is slight infiltration occurring during the high Guinea flow of the river resulting in low groundwater recharge rate (less than 5 mm/day). The Niger River peak that is generated by the Guinea flow peak upstream, in the upper Niger basin does not contribute to groundwater recharge in the study area. This may be explained by the relatively slow flow of the Guinea flow compared to the local flow peak, which is characterized by intermittent precipitation flashy stream flow behavior.

In order to confirm the relative position of the Niger River to groundwater, 3D map of the depth to groundwater table (Figures 43 a and 43 b) and groundwater heads (Figures 43 c and 43 d) are shown for different seasons of the year. During the dry season, the depth to the groundwater table ranges from less than 5 meters near the Niger River and ephemeral streams (Figure 43 a), to 65 meters in topographically high areas. In most areas the groundwater table is at a shallow depth during the rainy season (Figure 43 b).

Both depth to groundwater table and groundwater heads show the topographical control on the groundwater flow system The Niger River as well as many ephemeral streams act as natural groundwater discharge areas (Figure 44). A good illustration of the seasonal variability of groundwater flow is shown in the Figures 43 c and 43 d. Groundwater heads during the dry season (Figure 43 c) are almost always less than model calculated heads during the rainy season where many piezometric domes appeared as a combined effect of topographical control and groundwater table rise (Figure 43 d). The observed heads difference is a result of groundwater recharge occurring in the rainy season.

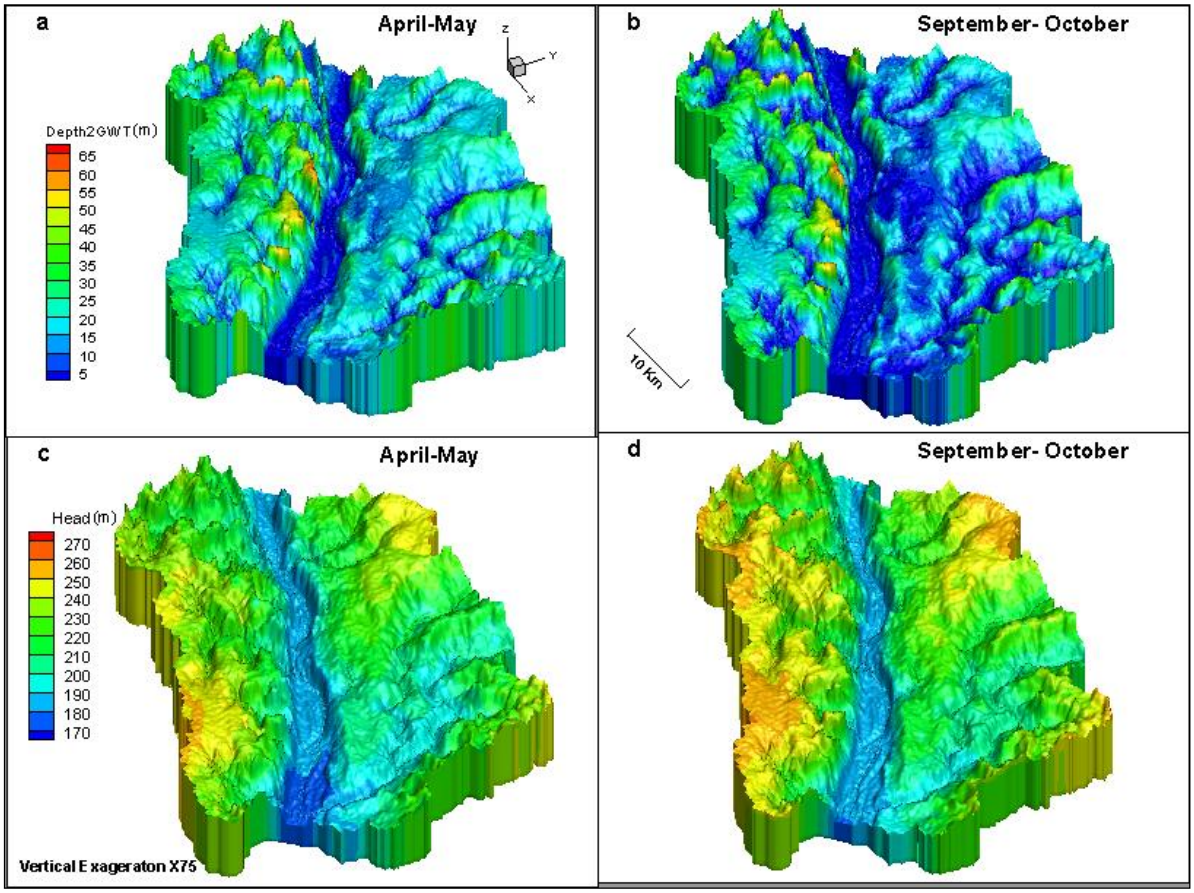

Figure 43: Simulated 3D Spatial Depth to groundwater table (a, b) and groundwater heads (c, d) at different periods.

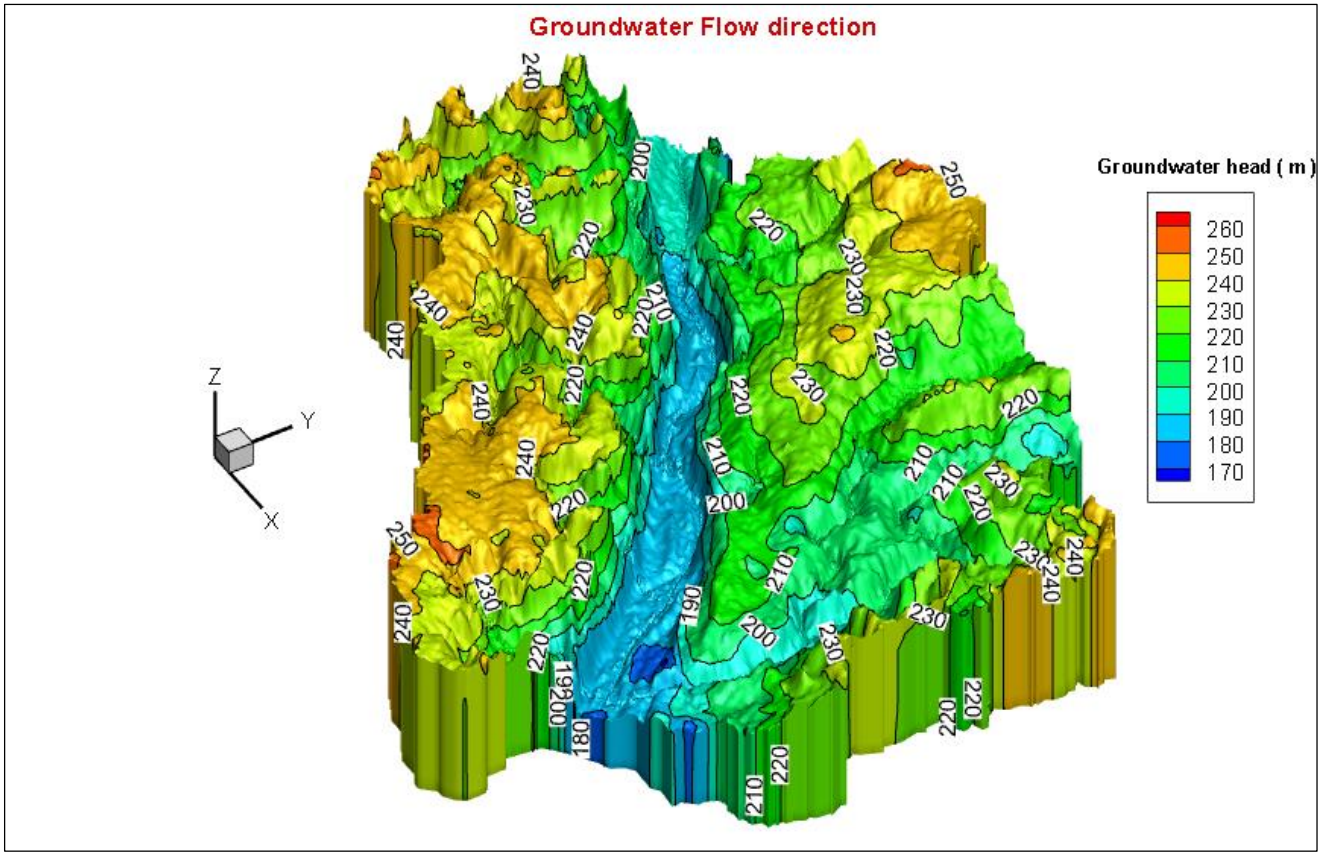

Figure 44: Groundwater flow direction in the study area (2013-2017)

6.6. Water balance

The previous section has highlighted that different surface water features (i.e., ponds, ephemeral stream, the Niger River, and springs) exhibit different type of exchange flux profiles. In this section, the water balance for different land use types will be presented as well as the basin average water balance. We also qualitatively present model calculated recharge for different land use types which is one of the most problematic parameters to estimate in semi-arid climate (Simmers, 1997).

6.6. 1 Water balance by land use type

The different land use types considered as along with relevant water balance components are presented in Table 9. Ponds that are similar to Zarmagandé pond (ponds type 1), discussed in section 3, have a recharge rate of up to 203 mm/year, and a discharge from groundwater reaching 213 mm/year. The infiltration rate calculated from the exchange flux is 203 mm/year and is assumed to represent groundwater recharge because the surface evaporation representing the main ET process is removed in the exchange flux. The total actual ET represented mainly by surface evaporation is of 101 mm/year. Groundwater recharge at the vicinity of the pond type 2 (Koungou pond) is 174 mm/year, with total actual ET (mainly surface evaporation) of 97 mm /year (Table 9).

However, the recharge values calculated here are point values (less than m^2); in order to qualitatively understand the exchange flux profile at the vicinity of the ponds. Previous studies (Favreau, 1998; Disconnets et al., 1997) have highlighted the strong spatial and temporal variability of focused recharge near ponds, depending on the size of the ponds drainage area, which is critical to exactly compute in an endoreic basin (Favreau, 2000).

Table 9: Water balance (mm/year) profiles for different land use types

Land Use	Infiltration (mm/year)	Total ET	Recharge	Groundwater Discharge
Fallow/ Agriculture	119	51	68	0
Sahelian Savanna	93	103	0	0
Pond type 1	203	101	203	213
Pond type 2	174	97	174	0
Niger River (loosing zone)	98	67	98	0
Niger River (Gaining zone)	138	112	0	138
Ephemeral Stream	70	49	70	0

Groundwater infiltration at agricultural sites is 119 mm/year, with total actual ET of 51 mm/year and groundwater recharge of 68 mm/year. In contrast, no groundwater recharge was recorded at Savanna site, where total ET is greater than the infiltrated water (93 mm/year). While, the infiltration values of agriculture and Savanna land use are in the same order of magnitude (119 and 93mm/year respectively), and consistent with measured values (160 –290 mm/year) by Rockstromet al. (1998) under millet fields at 1.8 m depths, Total actual ET of Savanna (101 mm/year) is twice the actual ET of agriculture. The main reason for this difference is probably the temporal activity of the root as well as the root depths. Agricultural land use is characterized by millet and/or maize crops, with average root ET activity lasting 3 months (only during the rainy season) and a root depth of 1.5 m, while the Savanna consist of shrubs that transpire continuously throughout the year and have a root depth of more than 5 m.

Ephemeral streams can have a groundwater infiltration rate of up to 70 mm/day, resulting in groundwater recharge of the same rate and total ET of 49 mm/year. In contrast to ephemeral streams that always act as depressions focused recharge areas (**Table 9**), ponds act either as groundwater recharge areas or groundwater discharge zones.

6.6. 2 Basin average water balance

The basin average water balance (**Table 10**) is computed from HGS water balance output file, and averaged over the study area. The calculated five years (2013-2017) basin average groundwater recharge is 28 mm/year representing 4.92 % of the total mean annual rainfall (580 mm). Total actual evapotranspiration over the basin is 386 mm/year, accounting for 66% of the total rainfall. The total ET is highly dominated by transpiration, which is 58% of the total ET, while surface evaporation is only 8.65 %. Infiltration over the basin represents 15.9 % of the water balance and overland flow constitutes 10.91%.

Simulated groundwater recharge (28 mm/year) is consistent with previous recharge rate of 36 mm/year found by Hassane et al. (2016) using a water table fluctuation method, considering a value of 1.2 m of water table rise. Favreau, et al., (2009) estimated a net groundwater recharge rate of 25 ± 7 mm/year using combined water table fluctuations and geophysical methods,50 km east of the study area.

Actual evapotranspiration as simulated by HGS is in agreement with previous measurements and modeling results, focused on millet and fallow sites with total actual ET in the range of 50 to 44% of total rainfall (Ibrahim et al.,2014), and up to 65% to 45% (Boulain et al. 2009; Ramier et al., 2009) for fallow and millet respectively.

Table 10: Basin average water balance in mm/year (5years)

Rainfall mm/year	Infiltration	Surface Evaporation	Overland Flow	Transpiration	Total ET	Recharge	Groundwater Discharge	Balance Error
580.88	92.4	139	63.4	247	386	28.6	9.66	0.82
100%	15.9	8.64	10.91	58.01	66.31	4.92	1.66	0.14

Conclusion of the Chapter 6

An equivalent porous medium approach was used to characterize groundwater surface water interaction in geologically complex fractured and sedimentary aquifers, with a high resolution fully integrated surface-subsurface hydrological model. The finite element HydroGeoSphere model has a horizontal resolution ranging from 300 m to 70 m and eleven vertical layers resulting in a total of 516901 nodes and 927030 elements. The model was calibrated using a 3-step methodology: 1) steady state, 2) dynamic equilibrium and 3) daily transient. The model results allowed for both a qualitative and quantitative evaluation of groundwater-surface water interactions for different land uses categories. In general, the groundwater flow system is controlled by local topography, and the Niger River showed mainly a gaining stream profile with groundwater discharge rate of up to 20 mm/day in the rainy season. However, the river may act as losing stream near main faults, with an infiltration of up to 50 mm/day during intense rainfall events. Ephemeral streams occur in areas of focused groundwater discharge, while ponds exchange flow profile is controlled by local topography, and they act as groundwater recharge or discharge areas. Significant groundwater recharge occurs in agriculture /fallow land use, in contrast of Savanna where all the infiltrated groundwater are lost by intense evapotranspiration processes. The calculated 5 years average groundwater recharge over the basin is 28.6 mm/year with actual evapotranspiration accounting for 66.31% of the total mean annual rainfall (580 mm), and slight groundwater contribution to baseflow (1.66¨%).

Chapter 7: Integrated hydrological modeling of climate change impacts

In this Chapter, the previously calibrated state of the art, high resolution fully integrated hydrological model will be used to investigate integrated climate change impacts on groundwater and surface water resources. Using multiscale statistically downscaled regional climate models, potential climate change impacts will be first evaluated on groundwater resources and then the frequency and duration of the minimum environmental flows for the next coming thirty years will be determined.

7.1. Biases uncorrected and corrected historical climate simulations

The observed historical (1980-2005) rainfall and temperatures data at Niamey airport station are compared at different time scales in Figure 45 with the basin weighted average uncorrected historical precipitation simulated by the three (3) RCMs models. Rainfall biases are plotted as relative differences between historical observed and simulated data, while biases in temperatures are calculated as absolute differences averaged over different season. DJF is the December-January-February season; JJA corresponds to June-July-August and is the rainy season; MAM and SON are respectively March-April-May and September-October-November periods (Figure 45).

Considerable differences in the statistical characteristic of the mean biases at different time scales can be seen in Figure 45. The biases increase when time interval increase from daily to monthly, sub-seasonal, and seasonal (yearly) averages with increasing levels of biases. CANRCM4 and WRF present the largest biases in mean precipitation, while the RCA4 has less bias in rainfall and temperatures data. All the three regional models perform better during the Jun-July-August (JJA) period which corresponds to the rainy season, confirming therefore the ability of the selected models in reproducing the precipitation seasonal cycle (Heinzeller et al., 2018; Mascaro et al. (2016). All the three RCMs have large positive biases in mean simulated historical rainfall compared to observed historical rainfall. Rainfall biases are greater for the CANRCM4 model, followed by the WRF and RCA4 models, particularly for the March-April-May period, where the biases in mean could reach up to 300%. The observed large biases are probably to the general wet days biases of uncorrected regional climate models.

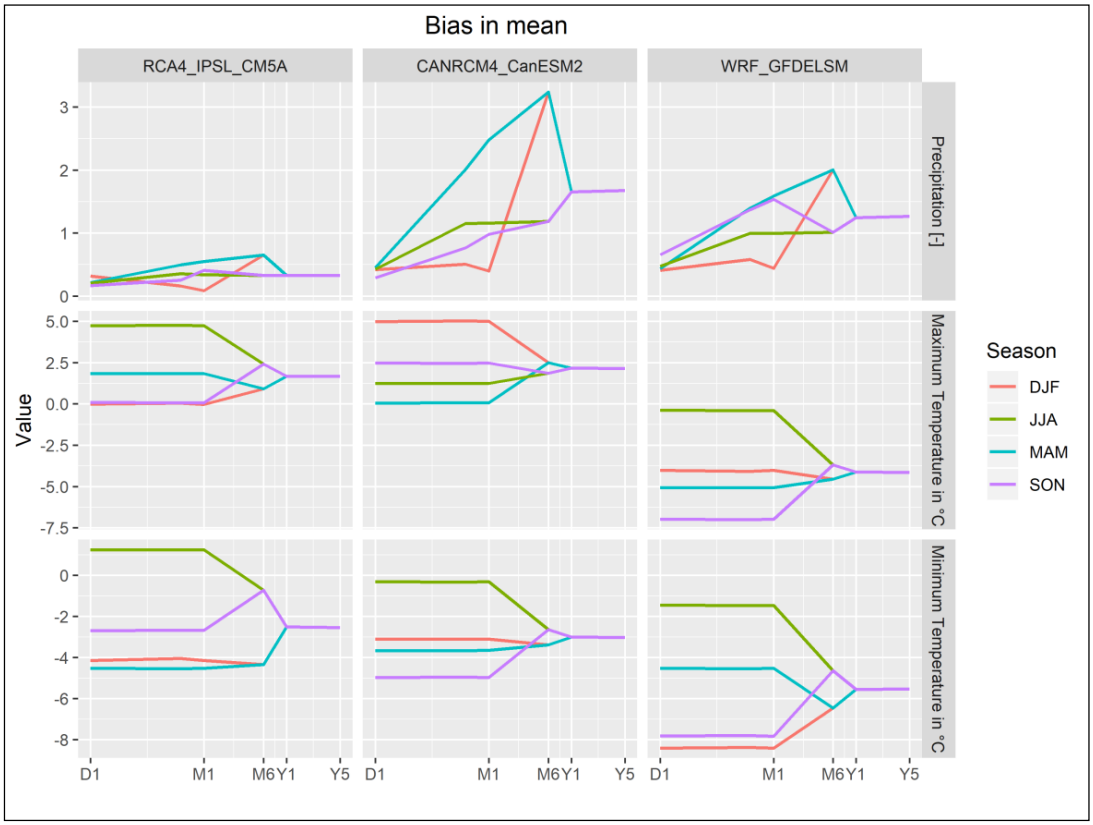

Figure 45: Bias in mean basin-average precipitation and temperature at different timescales between observed and simulated climate model data for the historical period (1980-2005).

As for the temperatures, the CANRCM4 and RCA4 models show positive maximum temperatures biases whereas the WRF model is negatively biased for all season. The 3 RCMs have negative minimum temperatures biases for all the season, except for the JJA period where they are positively biased, with the WRF recording the largest minimum temperature biases.

Biases calculated using corrected and original (uncorrected) rainfall, maximum and minimum temperatures time series for the 3 RCMs are shown in Figures 46a; 46b and 46c, for he standard and multisclae quantile-quantile mapping bias correction methods, and for different seasons of the year.

The observed historical climate data (see Figure 2) is used to evaluate the performance of the two bias correction methods for the 3 RCMs for the simulated historical period (1980-2005). In Figures 46a; 46b and 46c, residual biases are averaged and expressed as relative differences values (to observed historical) for rainfall data, and in absolute differences for temperatures data, at daily (D1), monthly (M1), and yearly (Y1) time scales.

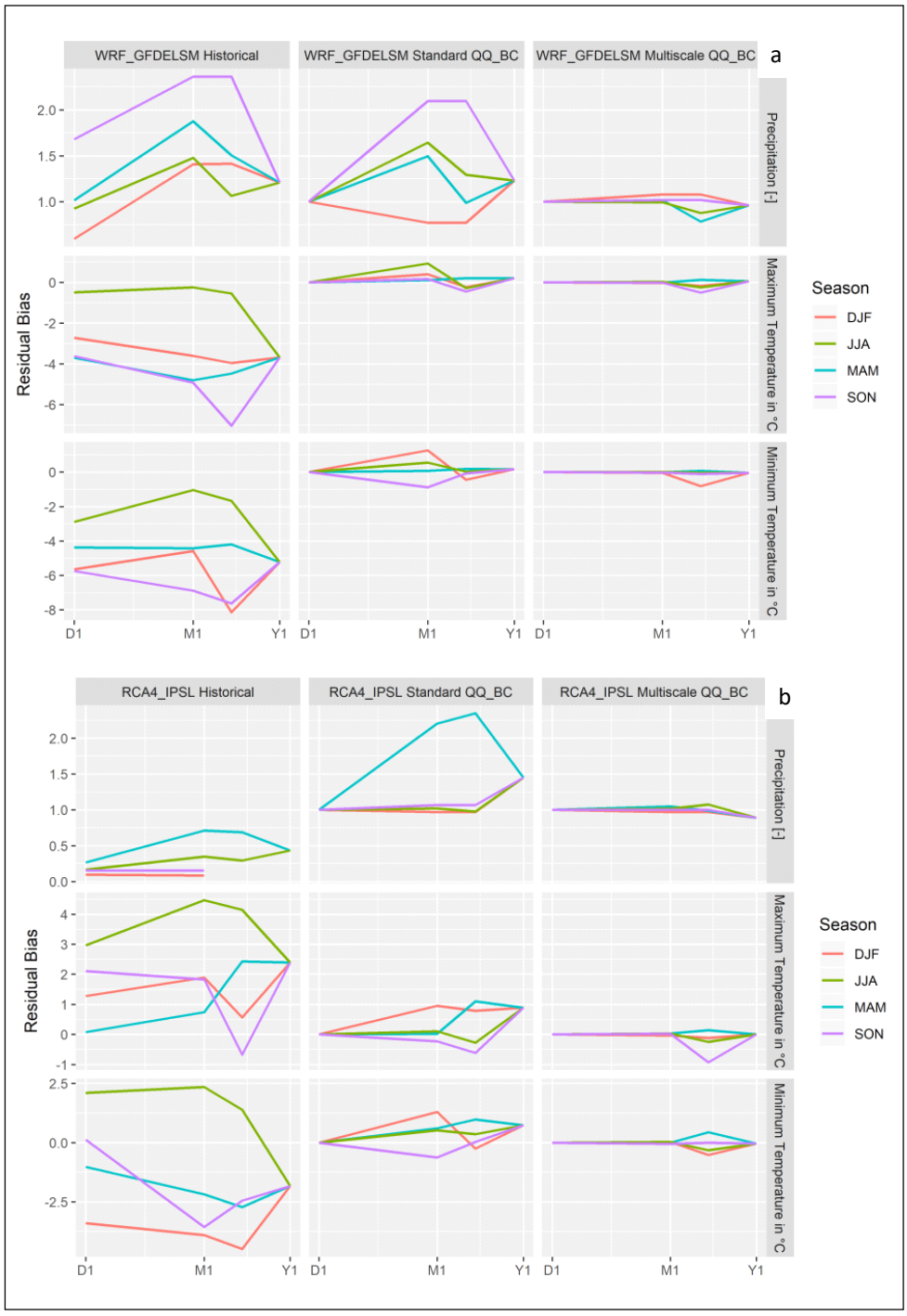

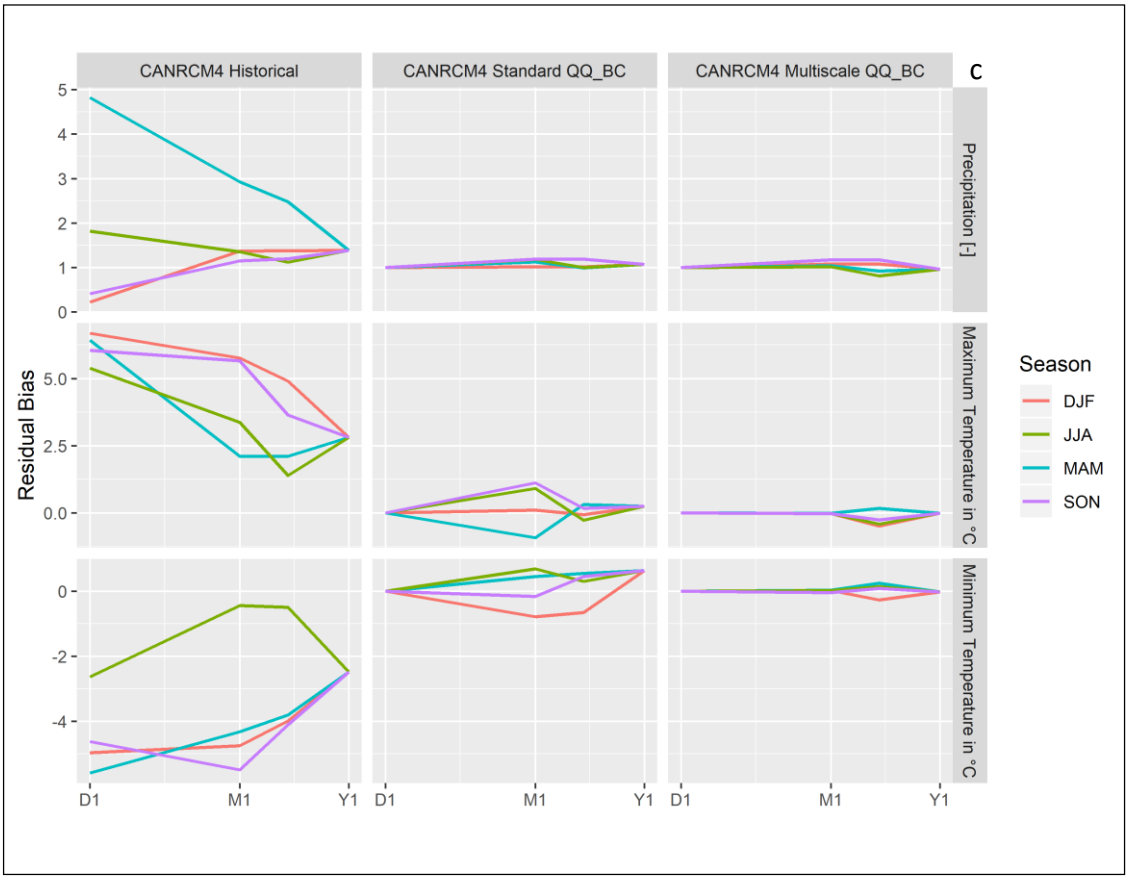

Figure 46: Standard quantile mapping and multiscale bias correction for the three RCMs: (a) WEF; (b) RCA4; (c) CANRCM4.

The bias in rainfall calculated with the uncorrected WRF historical data (Figure 46 a) vary from 50% to more than 250% across different periods, with large biases recorded for the SON period. Simulated rainfall data for the RCA4 model are relatively less biased with MAM period recording the largest bias of less than 100% (Figure 46 b). The CANRCM4 model has relative rainfall biases ranging from less than 100% to more than 450% with the MAM period having the large bias (Figure 46 c). The mean rainfall biases increase from daily to monthly temporal scale, then decrease at yearly timescale for the WRF and RCA4 models. In contrast, the biases are larger at smaller temporal scale for the CANRCM4 model. Absolute temperatures biases show different patterns for the 3 RCMs, across different temporal scales and periods. Tmin and Tmax simulated by the WRF model are negatively biased, with differences of up to -6°C for

Tmax, and up to -8°C for Tmin in the JJA period (Figure 46a). Tmax have positive biases in both RCA4 (Figure 46b) and CANRCM4 (Figure 46c) simulations across all periods except for the SON period for the RCA4 model, which has a slight negative Tmax bias. Tmin in the RCA4 and CANRCM are negatively biased across all the periods, except for the JJA period of the RCA4 that has both positive and negative Tmin biases.

The residual rainfall bias across the whole ranges of temporal scale is significantly reduced (less 100%) by the standard quantile bias correction methods at all the periods. The multiscale bias correction method produced the same performance for the CANRCM4 model. For a given model, the standard bias correction method was more efficiently at daily time scale, while biases remain large at the monthly timescale (up to 2%). The multiscale bias correction method has eliminated the residual temperatures biases across all the time scales for the all periods.

As for WRF and RCA4 models, the standard bias correction reduced slightly rainfall residual bias at daily (D1), and even increase the biases at monthly (M1). The multiscale bias correction method removed significant amount of bias at all the temporal scales. For the both models, temperatures biases were completely removed by the multisclae bias correction method at all temporal scales, while in the standard method temperatures biases still important at monthly (M1). In general, both bias corrections methods performed better for temperatures than rainfall. Standard quantile quantile mapping method proved to be more efficient at the daily time scale (D1) than at the monthly time scale (M1), while the multiscale method performs well across the all temporal scales considered. Therefore, even though WRF model has a higher spatial resolution (12 km) compared to the CANRCM4 and RCA4 models (50 km), it does not improve the model performance. Statistical downscaling appears to be necessary when using such biased models in impacts studies

7.2. Validation of historical simulations against observed groundwater levels

It was shown in the previous section that even the statistically downscaled historical climate simulations data used to force the hydrological model still have substantial biases; therefore, a validation of historical hydrological simulations is necessary before any impacts studies driven by theses climate forcing data. Depth to groundwater table and groundwater heads will be used as metrics for the validation of the subsurface component of the HydroGeoSphere model.

Depth to groundwater is a variable of great interest for water resources managers in the study area. It is crucial for drilling and managing water supply wells for both drinking and agriculture purposes. The elevation of the depth to groundwater table is calculated in HGS as a linear interpolation of the pressure head at a null pressure level. Depth to groundwater table is then derived from subtraction between the elevation of the groundwater table and surface elevations calculated from the Digital Elevation Model (DEM).

The observed and simulated depth to groundwater table corresponding to the historical period and averaged over the 1980-2005 period are mapped in Figure 47. Four groundwater observation wells locations are plotted in Figure 47 and they will be used in the next section to show the long term simulated groundwater heads transient trend (Figure 48). Across the study area, the average depth to groundwater table ranges from less than 5 m to 65 meters (Figure 47). Shallow depths to groundwater table are generally along the low topographic areas that coincide with either the Niger River, or ephemeral streams and ponds where important exchange flux processes between surface water and groundwater occurs (see Chapter 6). Depth to groundwater table are greater near high land areas and at many piezometric domes as a result of important topographic control on the groundwater flow system in the study area, as shown in previous studies (Hassane et al.,2016).

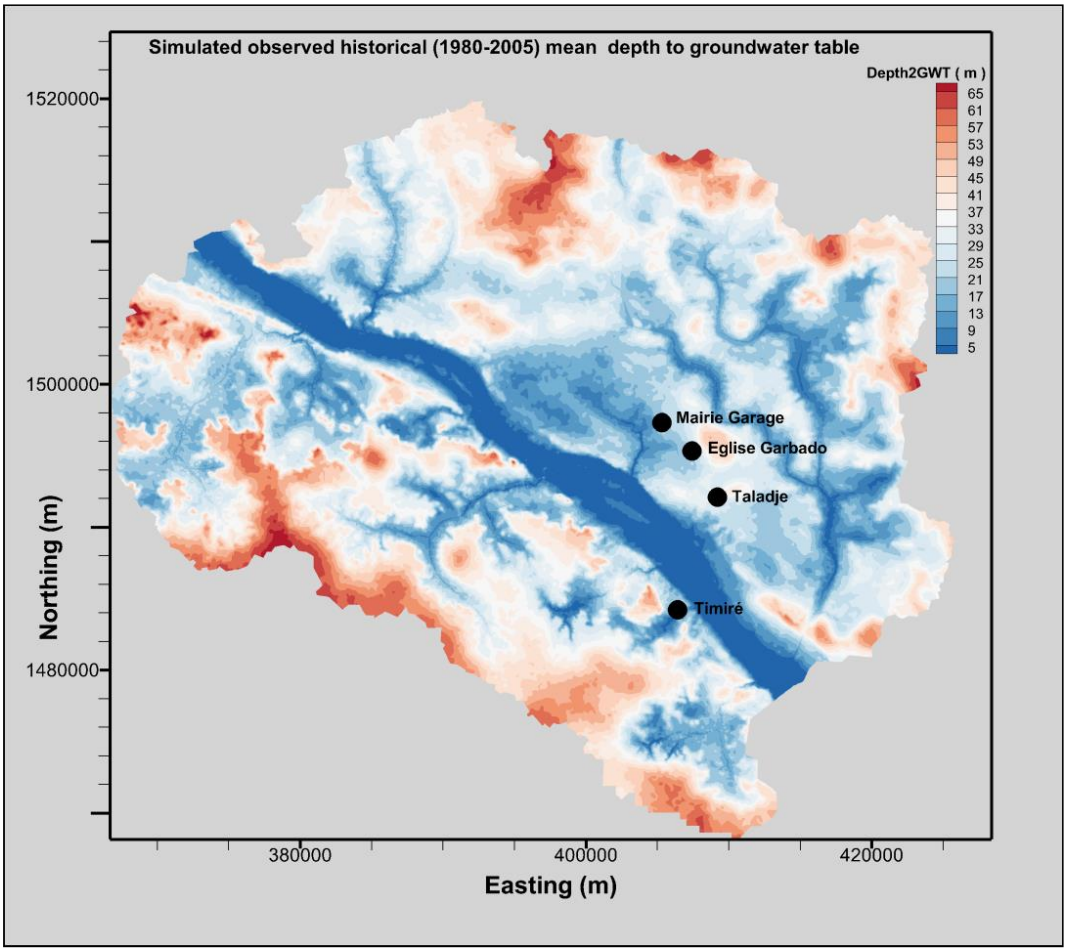

Figure 47 : 30 years (1980-2005) simulated observed historical mean depth to groundwater table

To validate historical simulations of depth to groundwater table for the three RCMs, the bias in mean depth to groundwater table is shown in Figure 48. The bias in mean depth to groundwater table is calculated as difference between simulated observed historical climate data and simulated historical climate scenario for the three RCMs considered.

Simulations with the outputs WRF and CANRCM4 models lead to a higher mean depth to groundwater table, while the RCA4 is negatively biased (Figure 48). Bias in mean depth to groundwater table ranges between 0 to +15 meters for WRF and CANRCM4; and between0 to -15 meters for the RCA4. Therefore, simulated historical climate scenarios are drier for the WRF and CANRCM4 and wetter for the RCA4; compared to simulated observed historical depth to groundwater table. This should directly be linked to residual bias of rainfall introduced by the multiscale bias correction method (see Figure 45a; 45b and 45c) where RCA4 still have

greater positive rainfall bias compared to WRF and CANRCM4 for the JJA (rainy season) period.

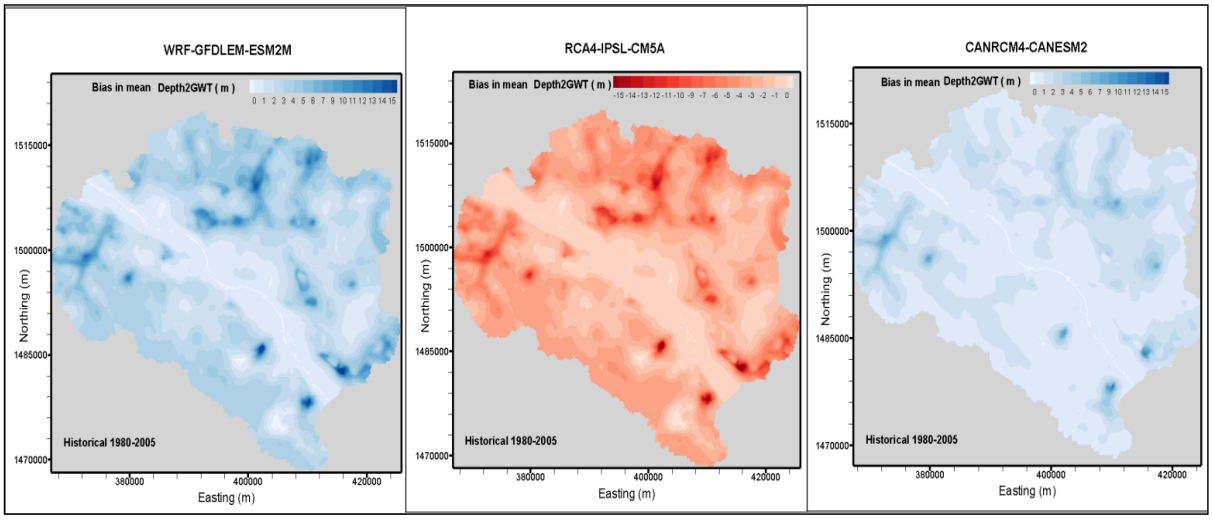

Figure 48: Bias in mean Depth to groundwater table

Also, the bias in mean depth to groundwater table is spatially different in the study area, with high topographic area having more bias than lower zones. The effect of topography on the bias will be discussed thoroughly in the section 4. However, it still important to validate simulation against the long-term transient groundwater heads, to better analyze how historical climates scenario perform in reproducing long term seasonal groundwater heads variations.

Time series of simulated groundwater heads at 4 observations wells (see Figure 47 for locations) are shown on Figure 49. **Table 11** provides information on wells altitude, distances between wells as well as simulated observed historical and simulated climate scenario heads. The 4 observations wells were chosen because they have relatively no groundwater pumping and they are located within few distances, to show the important topographical perturbation on groundwater response to climate change. They also have some historical groundwater heads measurements records.

Figure 49 shows that historical simulated groundwater heads from the climate scenario match reasonably well with the long-term seasonal variability of the observed simulated historical groundwater heads. Average (1980-2005) groundwater heads are shown as values, and groundwater heads measurements are also plotted at the bottom of each figure. Theses measured groundwater heads were reconstituted from historical measurements performed during the 1980's, at the construction of the boreholes (Figure 49). All the 3 RCMs tend to overestimate the groundwater heads for 1980-1994, and underestimate heads from 1994 to 2005. WRF shows the largest dry (wet) groundwater heads bias, and CANRCM4 the smaller dry (wet) heads bias, while the CRA4 lies in between them (Figure 49). Historical transient groundwater heads as simulated herein show a general decrease between 1980-1994 period, and an increase from 1994 to 2005. This long-term increase of groundwater heads is probably do to the recent Sahelian rainfall regime changes recorded in the central part of the Sahel (Lebel and Ali, 2009), where the 1989-2007 average rainfall exceed by 10% the average rainfall of the 1979-1990 period. The increase in groundwater heads highlights the important sensitivity of the groundwater response to rainfall pattern changes.

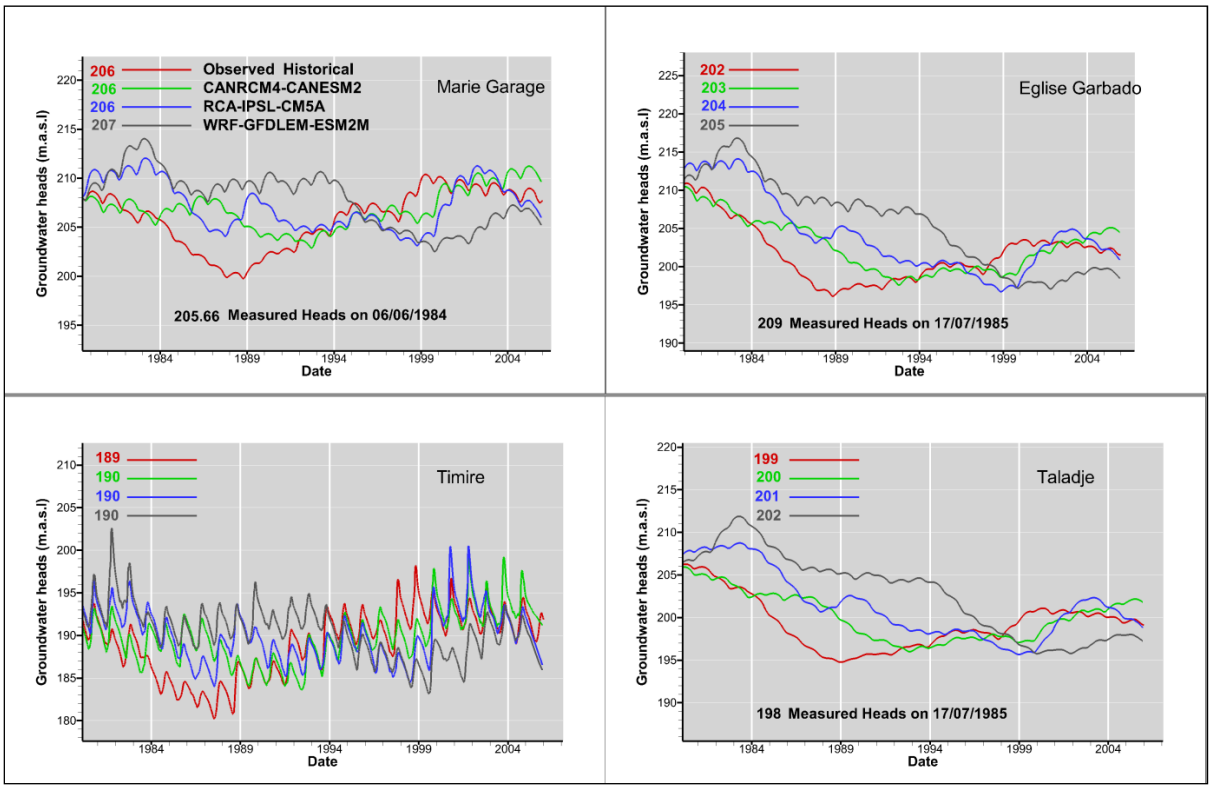

Figure 49: Simulated Historical long term (1980-2005) groundwater heads

Table 11 shows the mean absolute errors between simulated observed historical and climate scenario groundwater heads. The mean error seems to be greater at observation wells where depth to groundwater table is deep, and smaller at shallow groundwater table. This topographic perturbation of groundwater response to climate changes was recently shown by Erler et al., (2019) in the Grand River watershed, Canada. For Erler et al., (2019), the topographic perturbation is not important within few kilometers in horizontal resolution. However, Table 11 shows that in the study area, the topographic perturbation still important even for wells located within shorter distances, as soon as the altitude gradient exist, wells at high topographic positions are more biased than wells located in topographically low areas.

Table 11: Groundwater observation wells with the aquifer types; altitude, distances between wells and groundwater heads for the three RCMs.

Well name	Aquifer Type	Altitude	Simulated Observed Historical Heads	Distance (Km)	CANRCM4	RCA4	WRF
Mairie Garage	Fractured -Granites	220.56	206.0		206.7	206.8	207.4
EgliseGarbado	Fractured Schistes	221.65	201.8	3.2	202.7	203.8	205.0
Taladje	Fractured -Quartzite	225.03	199.4	3.5	200.1	201.1	202.3
Timire	CT3	210	189.2	7	189.7	189.5	189.9

7.3. Validation of historical simulations against surface flow rate

Measured Surface flow rates of Niger River at Niamey gauging station are used to validate the surface component of the Integrated HGS model. Figure 50 shows the measured and simulated historical flow rates for the 1980-2005 period. Simulated flow rate matches the measured flow well during all the simulated periods.

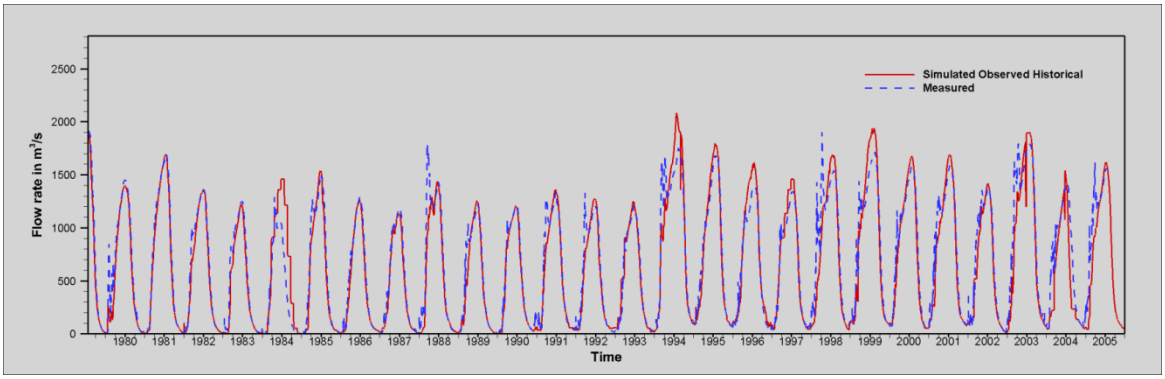

Figure 50: Validation of simulated historical surface water flow rate against measurements

7.4 Projected changes in local climate

The projected climate change scenarios are presented as relative differences for rainfall (Figure 51 A), and as absolute differences for mean temperature (Figure 51 B), between simulated historical, and mid-century periods. All the three RCMs consistently projected an increase in the mean annual rainfall, with the CANRCM4 model projecting a mean annual increase of 1.66% followed by the WRF projecting a rainfall increase of 1.35% and then the RCA4 with an increase of 1.05%. During the rainy season (JJA), WRF and CANRCM4 project a large increase in rainfall, while the RCA4 project a drier future (Figures 51A and 51B).

Similarly to rainfall, mean annual temperatures are projected to increase by +1.58°C for RCA4, 1.57°C for CANRCM4 and 1.09°C for WRF. For all the three models, greater temperatures increases are projected for the MAM period, while increases are relatively smaller for the JJA and SON periods.

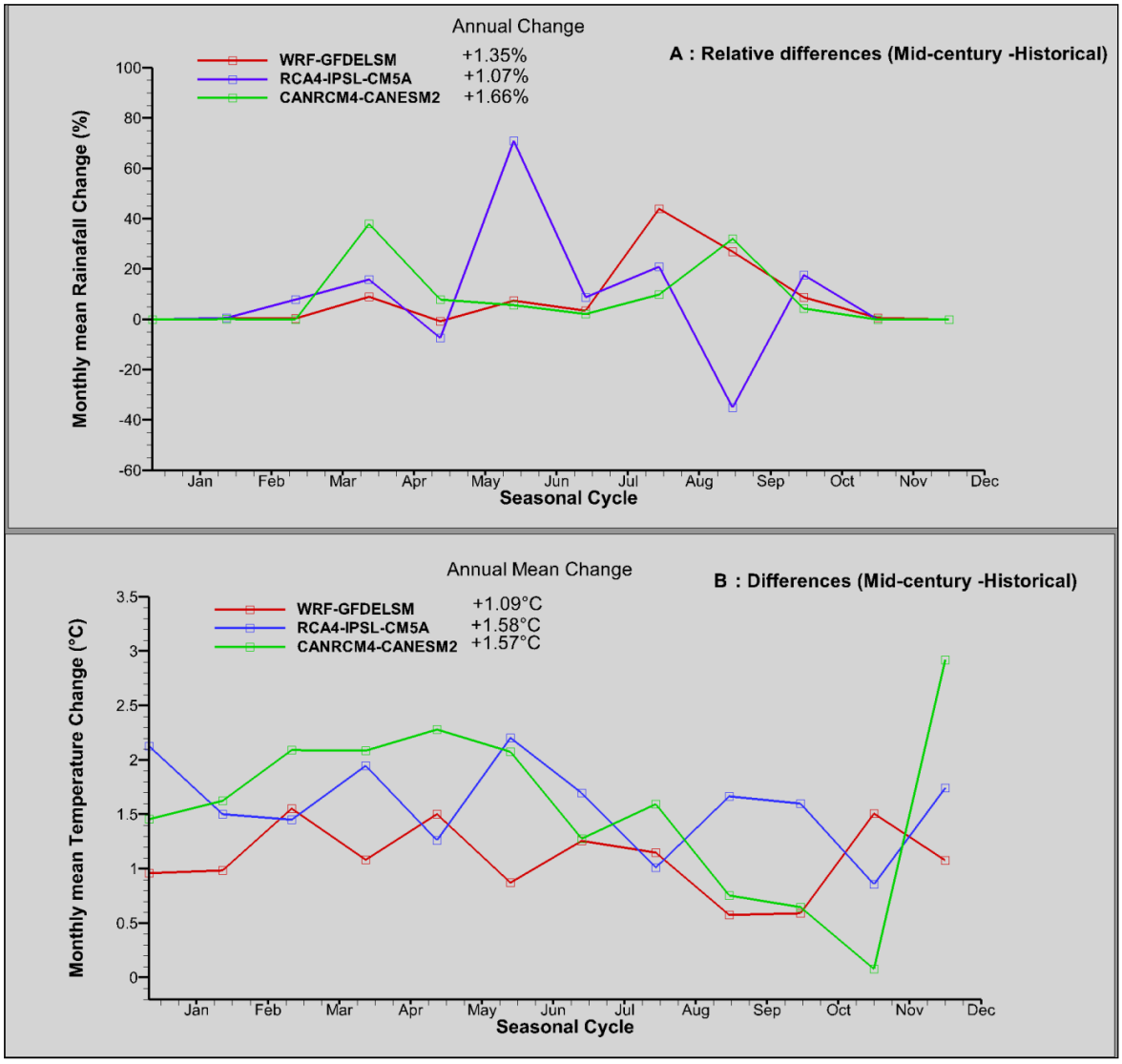

Figure 51: Rainfall and Temperatures changes between 2020-2050 (Mid-century) and 1980-2005 (Historical) at Niamey Airport Station

7.5 Changes in minimum environmental flow

MEF duration and occurrences are assessed under historical runoff (1980-2005), where the mid-century runoff conditions are kept to the historical levels (Figure 52A), and under 10 % runoff reduction scenarios (Figure 52 B) where runoff conditions are considered to be reduced by 10 % compared to historical levels. Overall, all the three model almost agree for the occurrence of the MEF, with different durations ranging between from 10 to 120 days under both historical and -10% runoff scenarios.

For the historical runoff level scenario, all the three climate models agree on the MEF occurrences for the critical duration level (shown as straight red line in Figures 52 A and 52B), defined as a period of 10 consecutive days when the minimum flow required to satisfy drinking and irrigation water demand is not meet. MEF will not be satisfied once every year from 2020 to 2025, and 3 times every five years between 2025 and 2035; then occurrences will decrease to once every 5 years from 2035 to 2049 (Figure 52 A). Obviously, conditions of MEF will be severe for the first decade (2020-2030) of the mid-century, and then they will become more favorable for the last two decades of the mid-century period. This is mostly due to the dry historical period of 1980-1990 that Niger River has experienced.

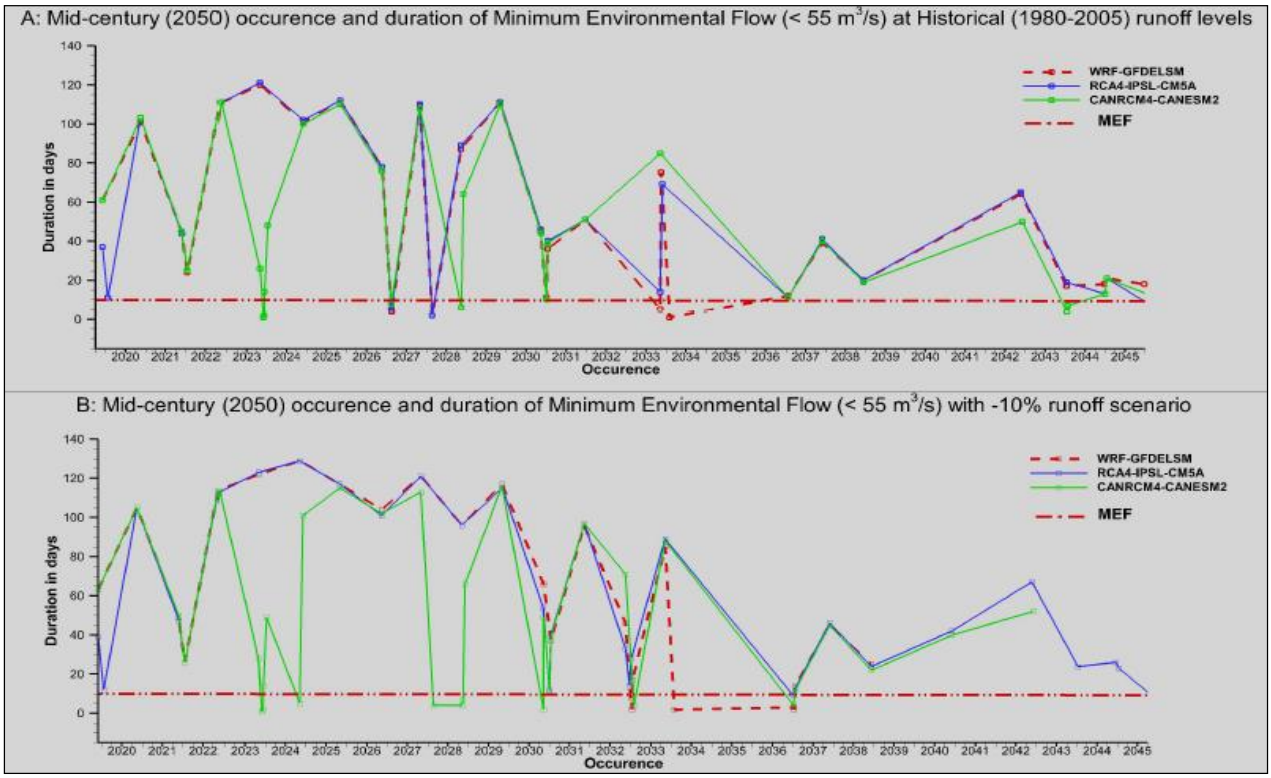

Figure 52: Projected Occurrence and duration of minimum Environmental flow at Niamey gauging station A: runoff kept at historical level; B: scenario of -10% runoff change compared to historical level

For the scenario of -10 % runoff reduction compared to historical, the occurrences of the MEF are almost the same as for the historical levels, with however different durations. Durations of MEF are shown in Table 12 for both scenarios. Average durations of the MEF ranges between 53 to 76 days for the 2020-2030 periods, and between 28 to 31 days for the 2020-2045 period under the historical runoff scenarios (Table 12). MEF average durations will increase under the -10 % flow reduction scenario, with durations ranging from 54 to 96 days for 2020-2030 period, and between 32 to 33 days for the 2030-2045 period.

Table 12: Duration of the Minimum Environmental Flow under Historical and -10% runoff scenarios

Historical Runoff Scenario	Mid-century (2020-2049) MEF Durations (days)	
	2020-2030 Period	2030-2045 Period
CANRCM4	53	30
RCA4	70	31
WRF	76	28
-10% Runoff reduction Scenario	Mid-century (2020-2049) MEF average Durations(days)	
	2020-2030 Period	2030-2045 Period
CANRCM4	54	33
RCA4	88	32
WRF	96	32

Table 12 and Figures 52 A and 52 B have shown that durations of the MEF are very sensitive to runoff reduction, with projected pattern of MEF directly influenced by the changes in net precipitation of the climate scenario models, with dry (wet) models predicting recurrent (less frequent) and high (low) MEF conditions by the end of mid-century.

MEF conditions were previously shown to also be very sensitive to runoff reduction, for two gauging station located upstream of the study area (Grijsen et al., 2013).

7.6. Changes in depth to groundwater table

Figure 53 (top panel) shows the projected mean changes of depth to groundwater table (Depth2GWT) for the three RCMs. All the three RCMs show an increase of groundwater table ranging from + 2 meters to more than +15 meters. CANRCM4 predict the greater increase of groundwater table, followed by the WRF and then by the RCA4 models. Groundwater table is likely to increase more in high topographic area, where depth to groundwater table is deep, than topographic low area with relatively shallow depth to groundwater table. For CANRCM4 and WRF models, mean groundwater table will increase by an average of 4 meters in low altitude area, and by more than 12 meters in topographic areas. While the RCA4 model predict a

maximum increase of +1 meter in shallow groundwater table area, and an increase of 3 meters in deep groundwater table area (Figure 53). Therefore, as seen for the MEF changes patterns, groundwater table response to climate change is also strongly dictated by the climate change forcing signal, particularly in mean annual net precipitation changes.

The groundwater table response to climate change is therefore more perturbed in topographically high area, than in low altitude zones (Figure 53). To illustrate the topographical effect on groundwater table response to climate change, cross section was drawn along NE-SW of the study area (Figure 53, bottom). Changes in depth to groundwater table for the CANRCM4 model are shown in colored contour, and groundwater heads are represented as line contours. It is obvious that grater changes in depth to groundwater table are located in area where the groundwater heads are also greater. The topographic perturbation is evident even within small horizontal distances (2 Km). This may be explained by the intensity of seasonal variation of groundwater table, with less variation in low topographic area that are groundwater discharge area, and where mostly exhange flux occurs with surface water, than high altitude area, that generally are direct groundwater recharge areas.

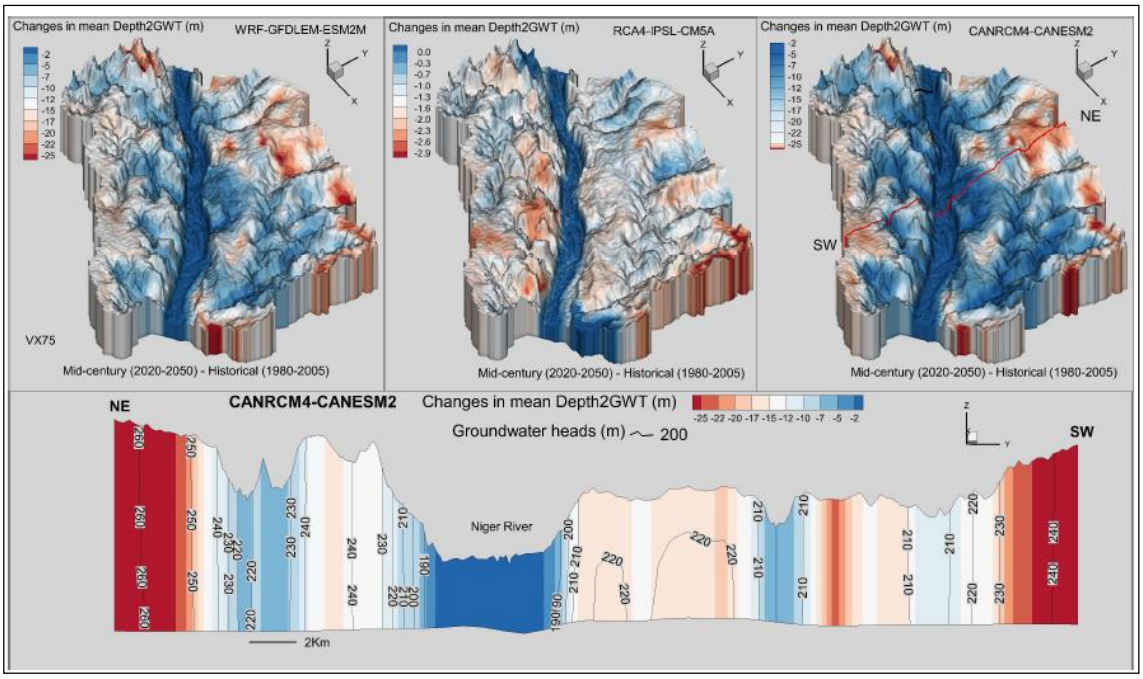

Figure 53: Changes in depth to groundwater table; top panel shows mean changes in depth 2 groundwater table by the mid-century for the 3RCMs; bottom figure shows a 2D cross section for the CANRCM

The topographical perturbation of groundwater table in response to climate change is also shown in the Grand River Watershed (Erler et al., 2019). This climate induced topographical perturbation of groundwater table in response to climate change appears to be significant even in small-scale topographic gradients as shown in Figure 53. This may result from the effect of intense monsoonal rainfall inducing a large seasonal groundwater table variation, and the local topography having a strong control in the groundwater flow system in the study area (Hassane et al., 2016).

7.7. Implications of changes in adaptation strategies

Based on the projections made on surface water response to climate changes impacts, Niamey watershed in general, and the city in particular will experience recurrent and long periods where the minimum environmental flow conditions will be under the required level. The risk level is even increased when the -10% runoff scenario is considered. However, the mid-century climate projections signal is wetter for all the three RCMs used, which means that historical runoff level reduction is less probable. But an increase in the irrigation water demand during the dry period in the upstream of Niamey will probably create a high surface water stress risk if the ongoing Kandadji dam construction, supposed to maintain the minimum environmental flow is not completed.

On the other hand, basin wide groundwater table rise is projected, with greater increase at deep water table, and relatively smaller increase at shallow water table depth. Therefore, considering the current population and urbanization rates, groundwater represents a sustainable adaptations pathway, to sustain the recurrent water stress that will be induced by the high sensitivity of the Niger River MEF to climate changes impacts.

Conclusion of the Chapter 7

The integrated hydrological response to climate change impact has been assessed on large scale, semi-arid watershed using the fully integrated HydroGeoSphere model. The model was calibrated sequentially for long term steady state (1980-2005), dynamic equilibrium and fully transient conditions. Observed historical (1980-2005) rainfall and potential evapotranspiration data have been used to force the HGS model for the calibration of surface water flow rate and groundwater heads. Three RCMs models were bias corrected at daily, monthly and yearly time scales. Performance of the HGS simulations forced by the 3 bias corrected RCMs was then evaluated against simulations forced by observed historical HGS simulations using both surface water flow rate and depth to groundwater table as metrics. Mid –century (2020-2050) climate change scenario simulations were performed with the three RCMs, and Minimum Environmental flow and groundwater table responses were evaluated under historical runoff, and – 10% runoff scenario.

Bias correction of the historical climate scenario shows that the quantile mapping correction performed better at daily and yearly time scale, than at monthly time scale. Simulations of historical depth to groundwater table by the 3 RCMs is positively biased, compared to observed historical climate simulations, with large biases at higher groundwater table depth. The resolution of the forcing RCM was found to not improve significantly its performance. All the RCMs project an increase in mean annual rainfall and in mean annual temperatures. The signal of mid-century rainfall changes is directly translated into the depth to groundwater table response to climate change showing a general groundwater table increase predicted by the three RCMs. Minimum Environmental flow durations have shown a high sensitivity to runoff reduction. The groundwater table is also found to increase more at higher altitude than at low altitude areas.

Chapter 8: General Conclusions and Perspectives

This research was carried out to evaluate the integrated hydrological response of groundwater and surface water under current and future climate change conditions. This general objective has been set out to address research gaps and oversimplifications associated with previously used hydrological models in climate change impacts studies. Methodological approaches employed herein have provided new outcome in hydrological modeling, groundwater surface water interactions in fractured aquifers, climate change modelling.

8.1 Conclusions

8.1.1 Hydrogeological conditions

An Equivalent Porous Medium approach was applied to simulate groundwater flow in intensely fractured aquifers context. This approach was employed to overcome the issue of data lack required to account for individual fractures effect in the model. It this study, we have demonstrated that an EMP model is appropriate for application in fractured system using fully integrated 3D hydrological model, HydroGeoSphere for water balance and climate change impacts studies.

8.1.2 Hydrochemicals and isotopes conditions

A sequential statistical approach including Cluster Analysis, Principal component analysis was used to investigate the origin of groundwater and surface water chemistry as well as the recharge process. This approach was also constrained with stable isotopes and ions ratio methods. Both groundwater and surface water are mainly dominated by Na-Ca-HCO3 chemical facies with the silicate weathering controlling the major source of ions. However, important cation exchanges preferentially liberating Na+ ions are shown to occur during the silicate wreathing process.

The isotopes signals of water are exempt from strong evaporation influence and implying therefore that groundwater recharge process is mainly dominated by rapid and localized infiltration.

The isotope signal of Niger River tracking away from the groundwater signal indicates that the Baseflow of the Niger River is mainly constituted with the river water. Also, and GBF aquifers are almost exclusively recharged by rapid and direct infiltration, while alluvial and GSBF aquifers have both direct infiltration and localized evaporated river water isotopes signal. However, the major drawback of the hydrochemicals approach was the lack of data that could valuably be used to quantify the recharge as well as the exchange flux between aquifers and surface water features.

8.1.3 Integrated hydrological modeling

A fully integrated 3D hydrological model was applied to first investigate groundwater surface water interaction, and then evaluate climate change impacts. The advantage of a fully integrated hydrological modeling is the better representation of the hydrological cycle which flow components are solved simultaneously in the surface, fully and partially saturated subsurface domains. It is also providing more reliable calibration using both groundwater and surface water in the objective functions. The physic-based integrated hydrological model used herein allows also providing water balance calculation by land used types.

The model was calibrated using a novel, straightforward 3-steps methodology: 1) steady state, 2) dynamic equilibrium and 3) daily transient. The model results allowed for both a qualitative and quantitative evaluation of groundwater-surface water interactions for different land uses categories. This new method provides a significant input for using integrated hydrological model in data scared arid climatic conditions. Because the scientific research literature in integrated hydrological modeling is a relatively growing area.

The calibrated finite elements model, HydroGeoSphere for the Niamey watershed has shown that the groundwater flow system is controlled by local topography, and the Niger River showed mainly a gaining stream profile with groundwater discharge rate of up to 20 mm/day in the rainy season. However, the river may act as losing stream near main faults, with an infiltration of up to 50 mm/day during intense rainfall events.

Ephemeral streams occur in areas of focused groundwater discharge, while ponds exchange flow profile is controlled by local topography, and they act as groundwater recharge or discharge areas. Significant groundwater recharge occurs in agriculture /fallow land use, in contrast of Savanna where all the infiltrated groundwater are lost by intense evapotranspiration processes. The calculated 5 years average groundwater recharge over the basin is 28.6 mm/year with actual evapotranspiration accounting for 66.31% of the total mean annual rainfall (580 mm), and slight groundwater contribution to baseflow (1.66¨%).

Large scale integrated hydrological models have attracted considerable interest over the past 10-15 years, largely due to better availability of input data and high-performance computing capacity. The study described here confirms that the application of fully integrated hydrological models to address real world problems is feasible, even with modest computing resources and in regions where less data is available. While most developing countries are facing challenges in water resources management, due to high population growth combined with climate change, we have demonstrated that integrated hydrological models help to address some of these water management challenges. Integrated hydrological models constitute a useful tool for helping developing countries achieve successful integrated water resources management.

8.1.4 Integrated hydrological modeling of climate change impacts

The climate change scenario used in this study included three regional climate models with different spatial resolution ranging from 50 to 12 Kilometers. The multiscale statistical downscaling methods employed herein represent state of the art downscaling technics that allow correcting climate models bias at daily, monthly and yearly time scales. While the resolution of the forcing RCMs was found to not improve significantly their performance, the multiscale statistical downscaling has allowed to strongly reducing potential errors associated with the stationary assumption stationarity bias in the climate change scenario. The 3 RCMs predict an increase of up to 1.6% in annual rainfall, and of 1.58°C for mean annual temperatures between period 2020-2050 and the historical period 1980-2005.

To evaluate climate change impacts on the water resource in the study area, two new metrics namely depth to groundwater table and Minimum Environmental Flows (MEF) conditions were used. The depth to groundwater table has a great interest for water resources managers in the study area. It is crucial for drilling and managing water supply wells for both drinking and agriculture purposes and the MEF provides the potential water stress due to surface water (river) baseflow.

The mid-century predicted rainfall increase by the RSMs is directly translated into the depth to groundwater table response to climate change, with a general groundwater table increase. The groundwater table is also found to increase up to 10 meters in topographically high zones while an increase of 2 meters in predicted in the shallow groundwater table more at low altitude areas. This depth to groundwater table is likely to balance the recurrent and long MEF conditions predicted by the three RCMs models.

This study has demonstrated that development and application of fully integrated hydrological can provide reliable guidance and directions in addressing concern about the combine response of surface water and groundwater to future climate change impacts. It is therefore, possible even with modest computing resources and sparse data, to provide to water resources managers in developing countries, decision making tools to define integrated climate change adaption strategies.

However, the application of theses integrated models is computationally expensive, and highly data consuming. That should probably be the reason of few published application of integrated hydrological models at large scale. For example, a single 30 years daily simulation for a typical modern computer (12 Gb Ram, core i7 and 2.5 GHz) can take up to 2 months depending on the resolution.

While acknowledging the data challenge for model validations, the use of higher mesh resolution seems to improve simulations quality, and in some extent compensate the spare data issue.

8.2 Perspectives

The fully integrated 3D hydrological model HydroGeoSphere, calibrated in this study can provide more application apart from water balance, depth to groundwater table changes and Minimum environmental flow conditions.

8.2.1 Climate change

Although in the present research work, the limited computational resources available has constrained to use only the RCP4.5 scenario, it is strongly recommended to consider at least an additional climate change scenario such as RCP8.5 to force the hydrological simulations.

8.2.2 Soil moisture

One important output HydroGeoSphere provides is the soil saturation in the partially saturated subsurface domain. This variable could be valuably used to inform decision makers for agriculture application as the soil saturation is crucial for irrigation as well as rained agriculture.

8.2. 3 Land use changes

The integrated hydrological model developed herein could also be used to evaluate land use changes under historical and futures climate change, as well as their impacts on the hydrological cycle. It can serve to verify and constraint the land use changes impacts for groundwater recharge, exchange flux, as well as soil moisture and surface water flow rates.

8.2. 4 Water quality and pollution control

This research work has provided insights on groundwater and surface water interaction process in a semi-urban watershed. It is therefore, a first order priority to consider protecting water sources quality, as important exchange between surface water and groundwater are shown. This can be effectively be achieved through a sustainable sanitation and environmental friendly urban waste management practices.

8.2. 5 Real time flood and drought forecasting

The HGS model calibrated in this study can further be trained to forecast high flow periods (flood) and low flows (drought) in both the Niger River and ephemeral streams. The adaptive time steps capability of the model and the high resolution of time step (up to seconds) represent an added value of flood and drought forecasting tools. The MEF occurrences and durations predicted in this study provide a good starting example.

References

Allen, R.G., Pereira, L.S., Raes, D., Smith, M. 1998. Crop evapotranspiration-Guidelines for computing crop water requirements-FAO Irrigation and drainage paper 56. FAO, Rome, 300(9), D05109.

Amogu, O., Descroix, L., Yéro, S.K ., Le Breton, E., Mamadou, I ., Ali, A., Vischel, T., Bader, J.C., Moussa, B.I ., Gautier, E., Boubkraoui, S., And Belleudy, P 2010. Increasing River Flows in the Sahel? Water, ISSN 2073-4441

Andersson, J. C.M., Ali, A , Arheimer, B., Gustafsson, D , Minoungou, B., 2017. Providing peak river flow statistics and forecasting in the Niger Riverbasin. Physics and Chemistry of the Earth 100 3- 12

Andersen, I., O. Dione, M. Jarosewich-Holder, And J. C. Olivry., 2005. The Niger River basin: A vision for sustainable management,World Bank Publications. [Available at http://siteresources.worldbank.org/INTWAT/Resources/4602114-1206643460526/ Niger_River_Basin_Vision_Sustainable_Management.pdf.

Aquanty,Inc. 2018. HGS User Manual, available at https://static1.squarespace.com/static/54611cc8e4b0f88a2c1abc57/t/59cea371017db2ee57a6d0b0/1506714489255/HGS_Reference_Manual.pdf

Armandine Les Landes, A., Aquilina, L., De Ridder, J., Longuevergne, L., Page, C., Goderniaux, P., 2014. Investigating the respective impacts of groundwater exploitation and climate change on wetland extension over 150 years. J. Hydrol.509, 367–378.

Babaye. A M.S. (2012) : Evaluation des ressources en eau souterraine dans le bassin de Dargol (Liptako-Niger). PhD thèses Université de Liège, 244p.

Barthel, R., And Banzhaf, S., 2016. Groundwater and surface water interaction at the regional-scale–a review with focus on regional integrated models. Water resources management, 30(1), 1-32

Bastola, S., Murphy, C., Sweeney, J., 2011. The role of hydrological modelling uncertainties in climate change impact assessments of Irish river catchments. Adv. Water Resour.34, 562–576

Bates, B.C., Kundzewicz, Z.W., Wu, S., Palutikof, J.P., 2008. Climate change and water Technical Paper. Intergovernmental Panel on Climate Change, Geneva.

Berg, S.J. And Sudicky, E.A., 2019. Toward Large-Scale Integrated Surface and Subsurface Modeling. Groundwater, 57(1), pp.1-2.

Bernert G, Dehays H., Garin H., Zunino C., 1985. Programme d'urgence pour le renforcement de l'alimentation en eau potable des quartiers périphériques de Niamey (Niger): exécution de 50 forages productifs [Emergency program to strengthen the supply of drinking water in suburban areas of the city of Niamey (Niger): execution of 50 productive boreholes]. Technical report BRGM/MHE, BRGM, Orléans, France, 52 pp

Bigi, V., Pezzoli., Maurizio, R., 2018. Past and Future Precipitation Trend Analysis for the City of Niamey (Niger): An Overview. Climate, 6, 73

Bisdom, .K ., Bertotti, G ., Nick, M.H., 2016. The impacts of in-situ stress and outcrop-based fracture geometry on hydraulic aperture and upscaled permeability in fractured reservoirs. Tectonophysics, 690, 63-75,

Bonnot H., Abdou A., Daouda Bory K., Chalamet D., Saint-Martin M. Et Younfa I., 1998. Notice explicative des cartes géologiques du Liptako à 1/100 000 et 1/200 000. Rapport. MME/DRGM, Niger.

Boro, H., Rosero, E., Bertotti, G., 2014. Fracture-network analysis of the Latemar Platform (northern Italy): integrating outcrop studies to constrain the hydraulic properties of fractures in reservoir models Petroleum Geoscience, 20 pp. 79–92

Boulain, N., Cappelaere, B., Ramier, D., Issoufou, H.B.A., Halilou, O., Seghieri, J., Guillemin,F., Oï, M., Gignoux, J., Timouk F., 2009. Towards an understanding of coupled physical and biological processes in the cultivated Sahel: 2. vegetation and carbon dynamics. J Hydrol 375:190‑203

Brooks, R.H., Corey, A.T.,1964. Hydraulic properties of porous media andt heir relation to drainage design. Trans. ASAE 7 (1), 26–0028

Browne, N.A.K., Sylla, M. B., 2012. Regional climate model sensitivity to domain size for the simulation of the West African summer monsoon rainfall, International Journal of Geophysics X, 625831, https://doi.org/10.1155/2012/625831

Chardon, D., Grimaud, J.L., Beauvais, A., Bamba, O., 2018. West African lateritic pediments: Landform-regolith evolution processes and mineral exploration pitfalls. Elsevier, Earth-Science Reviews, 124–146p

Chen, J., E.A. Sudicky, J.H. Davison, S.K. Frey, Y. -J. Park, H. -T. Hwang, A.R. Erler, S.J. Berg, M.V. Callaghan, K. Miller, M. Ross, W.R. Peltier., 2019. Towards a Climate-Driven Simulation of Coupled Surface-Subsurface Hydrology at the Continental Scale: A Canadian Example. Canadian Water Resources Journal / Revue canadienne des ressources hydriques, DOI: 10.1080/07011784.2019.1671235

Chen,Z., Grasby,S.E., Osadetz, K.G.,2004. Relations between climate variability and groundwater levels in the Upper carbonate aquifer, southern Manitoba, Canada, Journal of Hydrology, 290 (1-2) 43-62

CILSS., 2016. Landscapes of West Africa – A Window on a Changing World. U.S. Geological Survey EROS, 47914 252nd St, Garretson, SD 57030, UNITED STATES

Clark, I., 2015. Groundwater Geochemistry and Isotopes, 438 p. CRC Press/Taylor & Francis Group, Boca Raton/London/New York.

Clark, P.M., Wilby, L.R., Gutmann, D.E., Vano, A.J., Gangopadhyays, W.W.A., Fowler J.H., Prudhomme, C., Arnold, R.J., Brekke,D.L..2016. Characterizing uncertainty of the Hydrologic Impacts of Climate Change. Curr Clim Change Rep 2:55‑64

Cloutier, V., Lefebvre, R., Therrien, R., Savard, M.M., (2008). Multivariate statistical analysis of geochemical data as indicative of the hydrogeochemical evolution of groundwater in a sedimentary rock aquifer system. J. Hydrol. 353, 294–313.

Colautti, D 2010. Modelling the Effects of Climate Change on the Surface and Subsurface Hydrology of the Grand River Watershed. PhD Thesis,129 p, University of Waterloo, Canada

Craig.H. 1961. Isotopes variations in meteoric waters. Science 133, 1702-1703

Dai ,A., Lamb,J.P.,Trenberth, E .K., Hulme, M., Jones, D.P., Xie, P., 2004. Comment The recent Sahel drought is real. Int. J. Climatol. 24: 1323-1331

Dakouré, D., 2003. Etude hydrogéologique et géochimique de la bordure Sud Est du bassin sédimentaire de Taoudéni (Burkina Faso-Mali) –Essai de modélisation. Thèse Université Paris VI- Pierre et Marie Curie, 223 p.

Davison, J. H., Hwang, H.-T., Sudicky, E. A., Mallia, D. V., & Lin, J. C., 2018. Full coupling between the atmosphere, surface, and subsurface for integrated hydrologic simulation. Journal of Advances in Modeling Earth Systems, 10, 43–53. https://doi.org/10. 1002/2017MS001052

Davis, C.J., 2002. Statistics and Data Analysis in geology, third edition257 p, John Wiley & Sons New York

Dehays,H., Garin, H., Zunino, C., 1986. Programme d'urgence pour le renforcement de l'alimentation en eau potable des quartiers périphériques de Niamey (Niger): deuxième phase— exécution de 68 forages [Emergency program to strengthen drinking water supply in suburban areas of the city of Niamey (Niger): second phase— execution of 68 boreholes]. Technical report BRGM/MHE, BRGM, Orléans, France, 30 pp

Desconnets, J.C, Taupin, J.D., Lebel, T., Leduc, C.,1997. Hydrology of the Hapex-Sahel Central Super-Site: surface water drainage and aquifer recharge through the pool systems. J Hydrol 188–189:155–178

Dixon, K. W., Lanzante, J. R., Nath, M. J., Hayhoe, K., Stoner, A., Radhakrishnan, A., . . . Gaitán, C. F. 2016. Evaluating the stationarity assumption in statistically downscaled climate projections: is past performance an indicator of future results? Climatic Change, 135(3-4), 395-408.

DÖLL AND FEIDLER., 2008. Global-scale modeling of groundwater recharge. Hydrol. Earth Syst. Sci., 12, 863–885

Domenico, P.A., Schwartz, F.W., 1990. In: Physical and Chemical Hydrogeology. John Wiley and sons, New York.

Droogers, P.,Allen, G., Richard.,2002. Estimating reference evapotranspiration under inaccurate data conditions. Irrigation and Drainage Systems 16: 33–45

Erler, A. R., Frey, S. K., Khader, O., D'orgeville, M., Park, Y.-J., Hwang, H.-T., Et Al. 2019. Simulating climate change impacts on surface water resources within a lake-affected region using regional climate projections. Water Resources Research, 55, 130–155. https://doi.org/10.1029/2018WR024381

Everitt, B., Hothorn, T., 2011. An Introduction to Applied Multivariate Analysis with R.289p, Springer New York Dordrecht Heidelberg London, DOI 10.1007/978-1-4419-9650-3

Favreau,G., Nazoumou,Y., Leblanc,M., Guero,A., Goni I.B.,2012. Groundwater resources increase in the Iullemmeden Basin, WestAfrica. In: Treidel H, Martin-Bordes JL, Gurdak JJ Climate change effects on groundwater resources: a global synthesis of findings and recommendations. International Contributions to Hydrogeology 27, CRC, Leiden, The Netherlands, pp 113–128

Favreau, G., 2000. Caractérisation et modélisation d'une nappe phréatique en hausse au Sahel: dynamique et géochimie de la dépression piézométrique naturelle du kori de Dantiandou (sud-ouest du Niger) PhD Thesis, Univ Paris XI, Orsay, France, 258 pp

Favreau,G., Cappelaere,B., Massuel,S., Leblanc,M., Boucher,M., Boulain,N., Leduc,C., 2009. Land clearing, climate variability and water resources increase in semiarid southwest Niger: a review. Water Resour Res 45:W00A16

Favreau, G.,(1996). Modélisation locale de la recharge de la nappe phréatique sur le site de Wankama (sud-ouest du Niger). Mémoire de 3" cycle universitaire (DEA), 75 p. Université de Paris-sud / Orsay, France.

Favreau, G., Leduc, C.,(1998). Fluctuations à long terme de la nappe phréatique du Continental Terminal près de Niamey (Niger) entre 1956 et 1997. in : "Variabilité des ressources en eau en Afrique au XXème siècle", conférence Abidjan'98, 1998. AISHPubl., 252,253-2588.

Fetter, C.W. 1994., Applied Hydrogeology. Fourth Edition. Prentice Hall, Upper Saddle River, NJ 07458. 597p

Fowler, H. J., S. Blenkinsop.,Tebaldi, C., 2007. Linking climate change modelling to impacts studies: Recent advances in downscaling techniques for hydrological modelling. Int. J. Climatol., 27, 1547–1568.

Gilbert, J. M., & Maxwell, R. M. 2017. Examining regional groundwater-surface water dynamics using an integrated hydrologic model of the San Joaquin River basin. *Hydrology and Earth System Sciences, 21*(2), 923.

Giorgi, F. 2007. Regional climate modeling: Status and perspectives. Journal de Physique IV (Proceedings), 139(1), 101-118. doi:10.1051/jp4:2006139008

Girard, P., 1993. Techniques isotopiques (15N, 18O) appliquées à l'étude des nappes des altérites et du socle fracturé de l'Ouest Africain: l'Ouest du Niger [Isotopic techniques applied to groundwaters of alterites and fractured basement aquifers inWest Africa: theWestern Niger]. PhD Thesis, Univ of Quebec at Montreal, Canada, 141 pp

Girard, P., Hillaire, M.C., Oga, M.S., 1997. Determining the recharge mode of Sahelian aquifers using water isotopes. J Hydrol 197:189– 202

Goderniaux, P., Brouyère, S., Fowler, H. J., Blenkinsop, S., Therrien, R., Orban, P., & Dassargues, A. 2009. Large scale surface–subsurface hydrological model to assess climate change impacts on groundwater reserves. Journal of Hydrology, 373(1-2), 122-138

Goderniaux, P., Brouyère, S., Blenkinsop, S., Burton, A., Fowler, .J Hayley., Orban, P., Dassargues, A., 2011. Modeling climate change impacts on groundwater resources using transient stochastic climatic scenarios. Water Resources Research, 12, 52–16 doi:10.1029/2010WR010082,

Goderniaux, P., Brouyère, S., Wildemeersch, S., Therrien, R., Dassargues, A. (2015). Uncertainty of climate change impact on groundwater reserves – Application to a chalk aquifer. Journal of Hydrology, 528, 108–121

Gosling, S.N. And N.W. Arnell, 2011. Simulating Current Global River Runoff with a Global Hydrological Model: Model Revisions,Validation, and Sensitivity Analysis. Hydrological Processes 25:1129-1145, https://doi.org/10.1002/hyp.7727.

Graef, F., Duivenbooden, N.V., Stahr, K., 1998. Remote sensing and transect-based retrieval of spatial soil and terrain (SOTER) information in semi-arid Niger. Journal of Arid Environments 39, 631–644. doi:10.1006/jare.1998.0423

Green, T.R., Taniguchi, M., Kooi, H., Gurdak, J.J., Allen, D.M., Hiscock, K.M., Treidel, H., Aureli, A., 2011. Beneath the surface of global change: impacts of climate change on groundwater. J. Hydrol. 405 (3–4), 532–560.

Grijsen J.G ,Tarhule A, Brown , C. , Ghile Y.B., Taner Ü., Talbi- Jordan. A., Doffou H. N., Guero A., Dessouassi R. Y., Kone .S, Coulibaly .B., And Harshadeep N. (2013). Climate Risk Assessment for Water Resources Development in the Niger River Basin Part II: Runoff Elasticity and Probabilistic Analysis, Climate Variability - Regional and Thematic Patterns, AondoverTarhule, Intech Open, DOI: 10.5772/56708. Available from: https://www.intechopen.com/books/climate-variability-regional-and-thematicpatterns/climate-risk-assessment-for-water-resources-development-in-the-niger-river-basin-part-ii-runoff-elas

Crosbie, R. S., B. R. Scanlon, F. S. Mpelasoka, R. C. Reedy, J. B. Gates, And L. Zhang 2013. Potential climate change effects on groundwater recharge in the High Plains Aquifer, USA, Water Resour. Res., 49, 3936–3951, doi:10.1002/wrcr.20292

Gudmundsson, L., Bremnes, J., Haugen, J., Engen-Skaugen, T., 2012. Technical note: downscaling rcm precipitation to the station scale using statistical transformationsea comparison of methods. Hydrology Earth Syst. Sci. 16, 3383e3390.

Guggenmos,M.R., Daughney, C.J., Jackson, B.M., Orgenstern, U.M., 2011. Regional-scale identification of groundwater-surface water interaction using hydrochemistry and multivariate statistical methods, Wairarapa Valley, New Zealand. Hydrol. Earth Syst. Sci., 15, 3383–3398

Güler, C., G. Thyne, J.E. Mccray, And A.K. Turner., 2002. Evaluation of graphical and multivariate statistical methods for classification of water chemistry data. *Hydrogeology Journal* 10, 455–474.

Hanel. M, Kozín. R, Hermanovský. M, Roub.R ., 2017. An R package for assessment of statistical downscaling methods for hydrological climate change impact studies. Environmental Modelling & Software 95 22-28

Harvey F.E. and Welker, J.M., 2000. Stable isotopic composition of precipitation in the semi-arid north-central portion of the US Great Plains. Journal of Hydrology, 230(1), 90-109. doi 10.1016/S0022-1694(00)00316-4

Hassane, A.B., Christian, L ., Favreau, G., Barbara,A. B., Thomas, M., 2016 . Impacts of a large Sahelian city on groundwater hydrodynamicsand quality: example of Niamey (Niger). Hydrogeology Journal,

Heinzeller. D, Dieng.D, Smiatek.G, Olusegun .C, Klein .C, Hamann.I, Salack. S, Bliefernicht.J, And Kunstmann. H 2018. The WASCAL high-resolution regional climate simulation ensemble for West Africa: concept, disseminationand assessment. Earth Syst. Sci. Data, 10, 815–835

Holman, I., Allen, D., Cuthbert, M., Goderniaux, P., 2012. Towards best practice for assessing the impacts of climate change on groundwater. Hydrogeol. J. 20 (1), 1–4.

Hornberger, M.G., Raffensperger, J.P., Wilberg, P.L., Eshleman, K.L., 1998. Elements of Physical Hydrology. JUH Press. 312 pp.

Hughes, C. E. and Crawford, J., 2012. A new precipitation weighted method for determining the meteoric water line for hydrological applications demonstrated using Australian and global GNIP data. *Journal of Hydrology*, 464: 344–351.

Hwang, H.T., Park, Y.J., Sudicky, E.A., Berg, S.J., Mclaughlin, R. And Jones, J.P., 2018. Understanding the water balance paradox in the Athabasca River Basin, Canada. Hydrological processes, 32(6), pp.729-746.

Hwang, H.T., Park, Y.J., Frey, S.K., Berg, S.J. And Sudicky, E.A., 2015. A simple iterative method for estimating evapotranspiration with integrated surface/subsurface flow models. Journal of Hydrology, 531, pp.949-959.

Hwang, H. T., Y. J. Park, E. A. Sudicky, P. A. Forsyth., 2014 A parallel computational framework to solve flow and transport in integrated surface–subsurface hydrologic systems, Environ Model Software, 61 (0), 39-58.

Ibrahim, M., Favreau , G., Scanlon, R.B ., Luc,S.J., Le Coz, M., Demarty. J., Cappelaere, B.,2014 . Long-term increase in diffuse groundwater recharge followingexpansion of rainfed cultivation in the Sahel, West Africa1293–1305 Hydrogeology Journal

INS., 2012. Annuaire statistique-démographie [Statistical demographic year book]. National Institute of Statistics of Niger, Niamey, Niger

IPCC., 2013b . Climate Change 2013: The Physical Science Basis. Contribution of Working Group I to the Fifth Assessment Report of the Intergovernmental Panel on Climate Change (T. F. Stocker, D. Qin, G.-K. Plattner, M. Tignor, S. K. Allen, J. Boschung, A. Nauels, Y. Xia, V. Bex, & P. M. Midgley Eds.). Cambridge, United Kingdom and New York, NY, USA: Cambridge University Press.

Jones, J.-P., 2005. Simulating hydrologic systems using a physically-based surface subsurface model: issues concerning flow, transport and parameterization. Ph.D. Thesis, University of Waterloo, Waterloo (Canada), 145 pp.

King, A.C., Raiber, M., Cox, M.E.,2014. Multivariate statistical analysis of hydrochemicals data to assess alluvial aquifer-stream connectivity during drought and
flood: Cressbrook Creek, southeast Queensland, Australia. Hydrogeol. J. 22, 481e500.

Kollet, S., Sulis, M., Maxwell, R. M., Paniconi, C., Putti, M., Bertoldi, G., Sudicky, E. 2017. The integrated hydrologic model intercomparison project, IH-MIP2: A second set of benchmark results to diagnose integrated hydrology and feedbacks. *Water Resources Research, 53*(1), 867-890

Kristensen, K.J., Jensen, S.E., 1975. A model for estimating actual evapotranspiration from potential evapotranspiration. Nordic Hydrology 6, 170–188.

Kueppers, L. M., & Snyder, M. A., 2012. Influence of irrigated agriculture on diurnal surface energy and water fluxes, surface climate, and atmospheric circulation in California. Climate Dynamics, 38(5), 1017–1029.

Kumar, M., Ramanathan, A., And Keshari, A. K., 2009. Understanding the extent of interactions between groundwater and surface water through major ion chemistry and multivariate statistical techniques, Hydrol. Process., 23, 297–310,

Kundzewicz Z.W, Krysanov. V, Benestad. R.E, Hov. Ø ,Piniewski. M , Otto. I. M., 2018. Uncertainty in climate change impacts on water resources. Environmental Science and Policy 79 1–8

Kundzewicz, Z. W., Mata, L. J., Arnell, N., Döll, P., Kabat, P., Jiménez, B., Miller, K., Oki, T., Şen, Z. &Shiklomanov, I., 2007. Freshwater resources and their management. Climate Change 2007: Impacts, Adaptation and Vulnerability. Contribution of Working Group II to the Fourth Assessment Report of the Intergovernmental Panel on Climate Change (ed. by M. L. Parry, O. F. Canziani, J. P. Palutikof, P. J. van der Linden & C. E. Hanson), 173–210. Cambridge University Press, UK

Kurylyk, B. L., & Mac Quarrie, K. T. B., 2013. The uncertainty associated with estimating future groundwater recharge: A summary of recent research and an example from a small unconfined aquifer in a northern humid-continental climate. Journal of Hydrology, 492, 244-253.

Laprise, R., De Elía, R., Caya, D., Biner, S., Lucas-Picher, P., Diaconescu, E., . . . Separovic, L. (2008). Challenging some tenets of Regional Climate Modelling. Meteorology and Atmospheric Physics, 100(1-4), 3-22. doi:10.1007/s00703-008-0292-9

Lebel, T., Ali, A., 2007. Recent trends in the Central and Western Sahel rainfall regime (1990–2007)Journal of Hydrology 375 52–64

Lebel, T., Taupin, J.D., D'amato, N ., 1997 . Rainfall monitoring during HAPEX-Sahel. 1. General rainfall conditions and climatology. Journal of Hydrology 74-96

Leduc, C., Favreau, G., Schroeter, P., 2001. Long-term rise in a Sahelian water-table: the Continental Terminal in south-west Niger. J Hydrol 243:43–54

Leduc, C., Bromley, J., Schroeter, P., 1997. Water table fluctuation and recharge in semi-arid climate: some results of the HAPEX-Sahel hydrodynamic survey (Niger). J Hydrol 188–189:123–138

Levy, P.E., Jarvis, P.G., 1997. Direct and indirect measurements of LAI in millet and fallow vegetationin HAPEX-Sahel . Agricultural and Forest Meteorology 97 199–212

Li, Q., Unger, A.J.A., Sudicky, E.A., Kassenaar, D., Wexler, E.J., Shikaze, S., 2008. .Simulating the multi-seasonal response of a large-scale watershed with a 3D physically-based hydrologic model. Journal of Hydrology 357 (3–4), 317–336.

Lio, A., Ito, A., (2014). A Global Database of Field-observed Leaf Area Index in Woody Plant Species, 1932-2011. ORNL DAAC doi:10.3334/ORNLDAAC/1231

Macdonald, A. et Al 2012. Quantitative maps of groundwater resources in Africa. Environ. Res. Lett. 7, 024009

Machens, E., 1973. Contribution à l'étude des formations du socle cristallin et de la couverture sédimentaire de l'Ouest de la République du Niger, 3 Mém. BRGM, Fr.,1973, n° 82, 167 pages.

Mahé, G., F. Bamba, A. Soumaguel, D. Orange, And J. C. Olivry ., 2009. Water losses in the inner delta of the River Niger: Water balance andflooded area, Hydrol. Process., 23, 3157–3160.

Mamadou, I., Gautier , E., Descroix, L., Noma, I., Bouzou, M. I., Faran, M. O., Genthon, P., Amogu, O., Malam, A.M., Vandervaere, J.P., 2015. Exorheism growth as an explanationof increasing flooding in the Sahel. Catena 131, 130-139.

Manda, K.A., Mabee, B;S., David, F.B., Cooke, L.M., 2013. A method of estimating bulk potential permeability in fractured-rock aquifers using field-derived fracture data and type curves. Hydrogeology Journal (2013) 21: 357‑369

Maraun, D., Wetterhall, F., Ireson, A. M., Et Al,. 2010. Precipitation downscaling under climate change: Recent developments to bridge the gap between dynamical models and the end user. Reviews of Geophysics, 48(3). doi:10.1029/2009rg000314

Martinez, J.L., Raiber, M., Cox, E.M., 2015. Assessment of groundwater–surface water interaction using long-term hydrochemical data and isotope hydrology: Headwaters of the Condamine River, Southeast Queensland, Australia . Science of the Total Environment 536 , 499–516

Mascaro, G., D. D. White, P., Westerhoff., Bliss, N., 2015. Performance of the CORDEX-Africa regional climate simulations in representing thehydrological cycle of the Niger River basin, J. Geophys. Res. Atmos., 120,12,425–12,444, doi:10.1002/ 2015JD023905

Massuel, S, Cappelaere, B., Favreau,G., Lebel, T., Vischel, T.,2011. Integrated surface water-groundwater modelling in the context of increasing water reserves of a regional Sahelian aquifer. Hydrol Sci J 56:1242–1264

Matiatos, I., Paraskevopoulou, V., Lazogiannis, K., Botsou, F., Dassenakis, M., Ghionis, G., Alexopoulos, J.D., Poulos, S.E., (2018). Surface – ground water interactions and hydrogeochemical evolution in a fluviodeltaic setting: The case study of the Pinios River delta, Journal of Hydrology doi: https://doi.org/10.1016/ j.jhydrol.2018.03.067

Meixner, T., Manning, H.A., Stonestrom, A. D. et Al., 2016. Implications of projected climate change for groundwater recharge in the western United States. Journal of Hydrology 534 (2016) 124–138

Mileham, L ., Taylor, G R., Todd, M ., Tindimugaya , C., Thompson J., 2009. The impact of climate change on groundwater recharge and runoff in a humid, equatorial catchment: sensitivity of projections to rainfall intensity, Hydrological Sciences Journal, 54:4, 727-738, DOI: 10.1623/hysj.54.4.727

Milly, P.C.D. Krista, A.D., 2017. A Hydrologic Drying Bias in Water-Resource Impact Analyses ofAnthropogenic Climate Change. Journal of the American Water Resources Association (JAWRA) 53(4): 822-838.

Moeck, C., Brunner, P., & Hunkeler, D., 2016. The influence of model structure on groundwater recharge rates in climate-change impact studies. Hydrogeology Journal, 24(5), 1171-1184

Nelson, R. A., 1985; Geologic Analysis of Naturally Fractured Reservoirs, Gulf Publishing, Houston, Texas, Contr. in Petrol. Geology and Eng., no. 1, 320 pp.

Niger PRSP.,2008. Accelerated development and poverty reduction strategy, 2008–2012. In: Combating poverty, a challenge for all. International Monetary Fund, Niamey, Niger

Nkhonjera, G. K., Dinka, O. M .,2017. Significance of direct and indirect impacts of climate change on groundwater resources in the Olifants River basin: A review. DOI :10.1016/ j.gloplacha.2017.09.011

Nyenje, P. M., Batelaan, O. ,2009. Estimating the effects of climate change on groundwater recharge and baseflow in the upper Ssezibwa catchment, Uganda Hydrol. Sci. J. 54(4), 713 726

Ousmane, B., 1988. Etude géochimique et isotopique des aquifères du socle de la bande sahélienne du Niger (Liptako, Sud Maradi et Zinder Est), Thèse de doctorat d'état, Université de Niamey. 175 pages

Oyarzún, R., Barrera, F., Salazar, P.,Maturana, H., Oyarzún, J., Aguirre, E., Et Al., 2014. Multi method assessment of connectivity between surface water and shallow groundwater: the case of Limarí River basin, north-central Chile. Hydrogeol. J. 1–17.

Peltier, W. R., D'orgeville, M., Erler, A. R., & Xie, F. .2018. Uncertainty in Future Summer Precipitation in the Laurentian Great Lakes Basin: Dynamical Downscaling and the Influence of Continental Scale Processes on Regional Climate Change. Journal of Climate, 31, 23.

Philip, G. M., And D. F. Watson., 1982. A Precise Method for Determining Contoured Surfaces." Australian Petroleum Exploration Association Journal 22: 205–212.

Perotti, L., Antenolla D, G., Lasgna, M., Moussa, K., Spadafora, F., Yadji, G., Tankari, A., D..,(2016). Energy Procedia 97, 37–43. doi:10.1016/j.egypro.2016.10.014.

Piper, A.M., 1944. A graphic procedure in geochemical interpretation of water analyses. Transactions of the American Geophysical Union 25, 914–923.

Ramier, D., Boulain, N., Cappelaere, B., Timouk, F., Rabanit, M., Lloyd, C.R, Boubkraoui, S., Metayer, F., Descroix, L., Wawrzyniak, V., 2009. Towards an understanding of coupled physical and biological processes in the cultivated Sahel: 1. energy and water.J Hydrol 375:204‑216

Ray, R.K., Mukherjee, R., 2008 . Reproducing the Piper Trilinear Diagram in Rectangular Coordinates. GROUND WATER 46 (6), 893–896

Reimann. C and Filzmoser. P, (2000). Normal and Log Normal data distribution in geochemistry: death of a myth, consequences of the statistical treatment of geochemical and environmental data. Environmental geology 39-(9)

Refsgaard, J. C., Sonnenborg, T. O., Butts, M. B., Christensen, J. H., Christensen, S., Drews, M., Vilhelmsen, T.N., 2016. Climate change impacts on groundwater hydrology – where are the main uncertainties and can they be reduced? Hydrological Sciences Journal, 61(13), 2312-2324.

Rockstrom,J., Jansson, P.E., Barron, J., 1998. Seasonal rainfall partitioning under runon and runoff conditions on sandy soil in Niger: on-farm measurements and water balance modeling. J Hydrol 210:68–92

Schaap, M.G., F.J. Leij, And M.T. Van Genuchten., 2001. ROSETTA: A computer program for estimating soilhydraulic parameters with hierarchical pedotransfer functions. Journal of Hydrology 251, no. 3: 163–176.

Scibek, J. , Allen, D., 2006. Modeled impacts of predicted climate change on recharge and groundwater levels. Water Resour Res 42. Doi: 10.1029/2005wr004742

Shen, M., Chen, J., Zhuan, M., Chen, H., Xu,. C-Y., Xiong, L.,2017. Estimating uncertainty and its temporal variation related to global climate models in quantifying climate change impacts on hydrology. Journal of Hydrology (2017), doi: https://doi.org/10.1016/j.jhydrol.2017.11.004

Simmers I., 1997. Recharge of phreatic aquifers in (semi-) arid areas. IAH, ICH 19, 1-18. Balkema ed., Rotterdam, Netherlands. 277 pp.

Soumaïla, A., 2000. Etude structurale, Pétrographique et Géochimique de le ceinture birimienne de Diagorou-Darbani, Liptako, Niger Occidental (Afrique de l'Ouest). Thèse, 253 p. Université de Franche-Comté, France.

Soumaïla,A,. Konate, M., 2005. Caractérisation de la déformation dans la ceinture birimienne (paléoprotérozoïque) de Diagorou-Darbani (Liptako nigérien, Afrique de l'Ouest). *Africa Geoscience Review*, 2005, Vol. 12, No. 3, pp. 161-178.

Stoll, S., Hendricks Franssen, H.J., Butts, M., Kinzelbach, W., 2011. Analysis of the impact of climate change on groundwater related hydrological fluxes: a multimodel approach including different downscaling methods. Hydrol. Earth Syst. Sci. 15 (1), 21–38.

Sudicky, E.A., Jones, J.-P., Park, Y.-J., Brookfield, E.A., Colautti, D., 2008. Simulating complex flow and transport dynamics in an integrated surface-subsurface modeling framework. Geosciences Journal 12 (2), 107–122.

Sulis, M., Paniconi, C., Marrocu, M., Huard, D., Chaumont, D., 2012. Hydrologic response to multimodel climate output using a physically based model of groundwater/surface water interactions. Water Resour. Res. 48 (12).

Tarhule, A ., Lamb, J. P., 2003. Climate Research and Seasonal Forecasting for West Africans: Perceptions, Dissemination, and Use?: Perceptions, Dissemination, and Use? .

Taupin, J.D, Gallaire, R., Arnaud, Y., 1997. Analyses isotopiques et chimiques des précipitations sahéliennes de la région de Niamey au Niger: implications climatiques In: Hydrochemistry, Rabat Symposium, 1997, IASH Publ. 244, IAHS, Wallingford, UK, pp 151−162

Taupin, J.D., 2003. Interprétation paléoclimatique et paléohydrologique de l'origine des nodules carbonatés des terrasses du Niger aux environs de Niamey (Niger) au moyen des outils isotopiques et géochimiques. Hydrological Sciences Journal, 48(3): 16 pp.

Taupin, J-D, Gaultier, G., Favreau, G., Leduc, C., Marlin, C., 2002. Variabilité isotopique des précipitations sahéliennes à différentes échelles de temps à Niamey (Niger) entre 1992 et 1999 : implication climatique C. R. Geoscience 334 43–50

Taylor, R. G., Koussis, A. & Tindimugaya, C. 2009. Groundwater and climate in Africa: A review. Hydrol. Sci. J. 54, 655–664

Therrien, R., Mclaren, R.G., Sudicky, E.A., Panday, S.M.,2005. HydroGeoSphere. A three-dimensional numerical model describing fully-integrated subsurface and surface flow and solute transport, 5, 343 pp

Teutschbein, C., & Seibert, J., 2012. Bias correction of regional climate model simulations for hydrological climate-change impact studies: Review and evaluation of different methods. Journal of Hydrology, 456-457, 12-29. doi:10.1016/j.jhydrol.2012.05.052

Toure, A., Diekkrüger, B., Mariko, A., 2016. Impact of Climate Change on Groundwater Resources in the Klela Basin, Southern Mali. Hydrology 2016, 3, 17

United Nations Framework Convention On Climate Change (UNFCC) 2009. Climate Change: Impacts, Vulnerabilities and Adaptation in Developing Countries ***(****www.unfccc.int)*

Van Genuchten, M.Th., 1980. A closed-form equation equation for predicting the hydraulic conductivity of unsaturated soils, Soil Sci. Soc. Am. J., 44, 892{898.

Van Roosmalen, L., Sonnenborg, T.O., Jensen, K.H., 2009. Impact of climate and land use change on the hydrology of a large-scale agricultural catchment. Water Resour. Res. 45 (7).

Warner, T.T., 2011. Numerical Weather and Climate Prediction, Cambridge University Press, Cambridge, UK. 550 p, ISBN: 978-0-521-51389-0.

Wiltshir, E.,2013. Climate Change Impact on Available Water Resources Obtained Using Multiple Global Climate and Hydrology Models. Earth System Dynamics 4:129-144

Zhang ,Y., Xu, M., Li, X., Qi,J., Zhang, Q., Guo, J., Yu, L., Zhao, R., 2018. Hydrochemical Characteristics and Multivariate Statistical Analysis of Natural Water System: A Case Study in Kangding County, Southwestern China. *Water* **2018**, *10*(1), 80 doi.org/10.3390/w10010080

APPENDIXES

Appendix 1: Field Fractures data

Fractures on Schistes Outcrops		
number	azimuth	dip/plunge
1	235	85
2	250	85
3	65	90
4	240	40
5	238	50
6	54	80

7	55	80
8	240	83
9	40	82
10	210	35
11	35	60
12	40	62
13	60	55
14	55	50
15	60	65
16	55	80
17	225	50
18	340	60
19	250	78
20	80	65
21	135	35
22	290	35
23	320	40
24	270	20
25	280	30
26	275	25
27	260	20
28	263	20
29	70	25
30	76	55
31	55	50
32	35	45
33	45	45

Appendix 1: Continued Field Fractures data

Fractures on Schistes Outcrops		
number	azimuth	dip/plunge
36	252	70
37	68	80
38	250	65
39	263	55
40	253	70
41	235	80
42	100	80
43	60	80
44	210	75
45	45	85

46	330	30
47	315	35
48	235	60
49	95	83
50	255	65
51	250	70
52	315	55
53	320	50
54	323	50
55	225	35
56	245	80
57	74	65
58	71	80
59	250	72
60	68	55
61	154	27
62	240	45
63	355	45
64	350	55
65	165	50
66	340	45
67	255	65
68	345	70
69	350	80
70	352	80
71	350	80
72	315	80
72	300	65

Appendix 1: Continued Field Fractures data

Fractures on Granites Outcrops		
number	azimuth	dip/plunge
1	105	55
2	95	75
3	290	25
4	100	85
5	80	84
6	85	80
7	195	30

8	25	45
9	63	50
10	110	90
11	180	78
12	310	85
13	340	75
14	320	80
15	330	72
16	340	75
17	100	70
18	100	45
19	115	30
20	255	35
21	65	50
22	65	50
23	238	35
24	100	60
25	72	30
26	30	50
27	345	70
28	305	40
29	130	65
30	235	75
31	130	40
32	310	80
33	290	70

Appendix 1: Continued Field Fractures data

Fractures on Granites Outcrops		
number	azimuth	dip/plunge
1	105	55
2	95	75
3	290	25
4	100	85
5	80	84
6	85	80
7	195	30
8	25	45

9	63	50
10	110	90
11	180	78
12	310	85
13	340	75
14	320	80
15	330	72
16	340	75
17	100	70
18	100	45
19	115	30
20	255	35
21	65	50
22	65	50
23	238	35
24	100	60
25	72	30
26	30	50
27	345	70
28	305	40
29	130	65
30	235	75
31	130	40
32	310	80
33	290	70

Appendix 1: Continued Field Fractures data

Fractures on Granites Outcrops		
number	azimuth	dip/plunge
34	290	80
35	275	85
36	285	80
37	315	55
38	320	80
39	150	30
40	50	30
41	235	50

42	135	45
43	230	40
44	145	50
45	315	55
46	310	60
47	30	50
48	115	80
49	353	80
50	110	85
51	0	77
52	303	55
53	300	55
54	192	47
55	220	40
56	215	30
57	305	80
58	295	85
59	330	40
60	65	88
61	325	30
62	310	30
63	260	25
64	320	40
65	355	88
66	128	85
67	107	80
68	56	75
69	205	45
70	233	55
71	330	45
72	335	50

Appendix 2: The calibrated hydraulics parameters values for the 41 unsaturated soil zones discretized in this study.

Appendix 2: The calibrated hydraulics parameters values for the 41 unsaturated soil zones discretized in this study.

Soil zones	Ks	Theta_r	Alpha	n	Bulk_Density	Theta_s	Ss	Porosity
a1	0.0092477	0.0498	0.0434	2.5060999	1.2	0.4777	0.0094051	0.548872
a2	0.0031018	0.046	0.0368	2.6171999	1.66	0.3391	0.0031546	0.37594
a3	0.00125	0.05	0.0337	1.9302	1.64	0.3517	0.0012713	0.383459
cb1	0.0004861	0.0711	0.0231	1.4056	1.4	0.4377	0.0004944	0.473684
cb2	0.0006134	0.0729	0.0169	1.4334	1.2	0.48	0.0006239	0.548872
cc1	0.006331	0.0542	0.0395	2.2019999	1.2	0.484	0.0064388	0.548872
cc2	0.0013773	0.0535	0.0319	1.6770999	1.4	0.4241	0.0014008	0.473684
cc3	0.0003935	0.0464	0.0163	1.4672	1.4	0.3913	0.0004002	0.473684
de2	0.0001736	0.0943	0.0102	1.4543	1.3	0.4903	0.0001766	0.511278
de4	0.0049421	0.0587	0.0306	2.5272999	1.4	0.4258	0.0050263	0.473684
e1	0.0053588	0.0457	0.0664	1.9048001	0.9	0.5708	0.00545	0.661654
e2	0.0051852	0.0466	0.0665	1.9585	0.9	0.5724	0.0052734	0.661654
hb1	0.0034954	0.0487	0.0341	2.7059	1.67	0.3374	0.0035549	0.37218
hc1	0.0039931	0.0498	0.0363	2.2832999	1.4	0.4192	0.004061	0.473684
hc3	0.0070486	0.05611	0.0321	2.8838999	1.4	0.4225	0.0071686	0.473684
hc4	0.0004861	0.0593	0.0228	1.4427	1.4	0.4229	0.0004944	0.473684
hs1	0.0004167	0.0506	0.0325	1.4686	1.6	0.3685	0.0004238	0.398496
hs3	0.000706	0.0552	0.0297	1.5622	1.5	0.3985	0.000718	0.43609
hs4	0.0007986	0.0568	0.0293	1.6071	1.5	0.3995	0.0008122	0.43609
lb3	0.0009259	0.0588	0.0252	1.4689	1.3	0.4501	0.0009417	0.511278
lc1	0.0001042	0.086	0.0094	1.4809	1.4	0.446	0.0001059	0.473684
lc2	0.0001968	0.0831	0.0086	1.523	1.3	0.4587	0.0002001	0.511278
lc3	0.0004514	0.0773	0.0151	1.4392	1.2	0.482	0.0004591	0.548872
ls1	0.0000926	0.0911	0.0102	1.4469	1.4	0.4598	0.0000942	0.473684
ls3	0.0001042	0.0892	0.0113	1.4256999	1.4	0.4528	0.0001059	0.473684
p1	0.0012847	0.0455	0.0357	1.6091	1.4	0.4142	0.0013066	0.473684

p2	0.0014236	0.0448	0.0358	1.6719	1.4	0.4126	0.0014478	0.473684
p3	0.002581	0.0482	0.0377	1.5854	1.2	0.4731	0.0026249	0.548872
p4	0.0027199	0.0489	0.0381	1.6114	1.2	0.4748	0.0027662	0.548872
p5	0.0028241	0.0468	0.0394	1.6138999	1.2	0.4719	0.0028721	0.548872
p6	0.003831	0.0446	0.0448	1.5948	1.1	0.4987	0.0038962	0.586466
r1	0.0045023	0.0492	0.0642	2.0032001	0.9	0.5769	0.0045789	0.661654
t1	0.0049421	0.0474	0.0643	1.8927	0.9	0.5737	0.0050263	0.661654
t2	0.0050926	0.0465	0.0642	1.8425	0.9	0.572	0.0051793	0.661654
t3	0.0039931	0.0513	0.0552	1.6761	0.9	0.5781	0.004061	0.661654

Knowledge dissemination

Journal Articles

Abdou Boko B, Konaté, M., Nicaise, Y., Steven, J.B., Erler,R.A., Hyoun-Tae, H., Khader,O., Sudicky,E.A.(2020). Characterization of groundwater –surface water interactions using high resolution integrated 3D hydrological model in semiarid urban watershed of Niamey, Niger. Journal of African Earth Sciences. https://doi.org/10.1016/j.jafrearsci.2019.103739

Abdou Boko B, Konaté, M., Nicaise, Y et al., High-resolution Integrated Hydrological Modelling of Climate Change Impacts in a semi-arid urban watershed in the region of Niamey, Niger. Under Review in Water,

Abdou Boko B, Moussa KONATE, Rabani ADAMOU et Alassane ABDOULAYE (2017) : Influence du système de drainage sur la vulnérabilité à la pollution des aquifères du bassin de Tim Mersoï (Nord Niger). .Afrique SCIENCE 13(4) (2017) 261 – 274

Abdou Boko B, Moussa KONATE, Rabani ADAMOU et Alassane ABDOULAYE (2017) : Contribution du système de fracturation à la recharge des aquifères du bassin de Tim Mersoï (Nord Niger). Rev. Cames - Vol.05 Num.01. ISSN 2424-7235

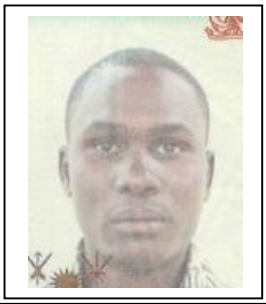

Candidate biography

Abdou Boko BOUBACAR is an Environmental and water resources expert. He holds a master degree in groundwater resource management from Abdou Moumouni University, and a Master degree in Climate Change and Sustainable Development from AGRHYMET Regional Center of Niamey. He was a fellowship of USAID West African Water Supply Sanitation and Hygiene.

Abstract: The Niger River is the sole permanent surface water used for agriculture and drinking water supply for the area of Niamey, Niger, West Africa. Given that the water distribution network does not cover the entire populated area, and because of recurrent droughts, the River cannot not cover the total water demand in the area; Groundwater is pumped through open wells and boreholes to provide water to more than 35% of 1.3 million of people of the city. The share of groundwater in water supply for drinking and agriculture purpose is increasing as a result of rapid population growth and urbanization; simultaneously, episodes of extreme low flows have become more frequent because of a combination of increasing demand, and sedimentation of the River bed, and increased variability in streamflow upstream of Niamey. The minimum environmental flow for Niamey, set to 55 m^3/s over 10 days, is therefore often violated. In this context, the main objective of this study is to investigate ground water surface interactions and the whole hydrological system response under climate change. An equivalent porous medium approach was used to define a hydrogeological conceptual model to understand the hydrodynamic of the fractured aquifer system, and quantify the integrated interaction between this system and surface water resources as well as the climate change impacts. Combined used of hydrochemicals and isotopes have shown that the major source of both groundwater and surface water is provided by silicate weathering. The isotopes signals of water are exempt from strong evaporation influence, implying that groundwater recharge process is strongly dominated by rapid and localized infiltration. A large scale, high resolution fully-integrated hydrologic model was built and calibrated using HydroGeoSphere with a sequential approach of increasing levels of temporal resolution: 1) steady state average conditions; 2) dynamic equilibrium with repeating monthly normal forcing data; and 3) fully transient conditions. Simulations results show that exchange flux between groundwater and surface water are important processes in the basin. The basin average water balance highlights the importance of plant transpiration (58 % of total rainfall) over surface evaporation (8%), with groundwater recharge of up to 5% of total rainfall. Overland flow and infiltration account for 11% and 16 % of the total annual rainfall respectively, and groundwater discharge to the river is 2% of the total rainfall. Historical (1980-2005) and projected (2020-2050) climate scenario derived from the outputs of three regional climate models (RCM), under the RCP 4.5 scenario, were statistically downscaled using the multiscale quantile mapping bias correction method. The durations of the Minimum Environmental Flow (MEF) conditions, required to supply drinking and agriculture water were found to be very sensitive to changes in runoff resulting from climate changes. MEF occurrences and durations are likely to be greater for the first decade (2020-2030) of the mid-century, and then they will be reduced for the last two decades (2030-2050) of the mid-century period. All the three RCMs consistently project a rise in groundwater table of more than 10 meters in topographically high zones where the groundwater table is deep and an increase of 2 meters in the shallow groundwater table.

Keywords: Integrated model, Groundwater, surface water, climate change, impact

PhD

ABDOU BOKO BOUBACAR

INTEGRATED HYDROLOGICAL MODELLING OF CLIMATE CHANGE IMPACTS IN SEMI-ARID URBAN WATERSHED OF NIAMEY, NIGER

GRP/CCWR/INE/WASCAL – UAC Month, Year